DEVELOPMENT OF GALLIUM-DOPED MESOPOROUS BIOACTIVE GLASS AS HEMOSTATIC AGENT

SARA POURSHAHRESTANI

FACULTY OF ENGINEERING
UNIVERSITY OF MALAYA
KUALA LUMPUR

2017

DEVELOPMENT OF GALLIUM-DOPED MESOPOROUS BIOACTIVE GLASS AS HEMOSTATIC AGENT

SARA POURSHAHRESTANI

THESIS SUBMITTED IN FULFILMENT OF THE REQUIREMENTS FOR THE DEGREE OF DOCTOR OF PHILOSOPHY

FACULTY OF ENGINEERING
UNIVERSITY OF MALAYA
KUALA LUMPUR

2017

UNIVERSITY OF MALAYA

ORIGINAL LITERARY WORK DECLARATION

Name of Candidate: **Sara Pourshahrestani**

Registration/Matric No: **KHA140044**

Name of Degree: **Doctor of Philosophy**

Title of Project Paper/Research Report/Dissertation/Thesis ("this Work"):

Development of gallium-doped mesoporous bioactive glass as hemostatic agent

Field of Study: **Biomaterials and Tissue Engineering**

I do solemnly and sincerely declare that:

(1) I am the sole author/writer of this Work;
(2) This Work is original;
(3) Any use of any work in which copyright exists was done by way of fair dealing and for permitted purposes and any excerpt or extract from, or reference to or reproduction of any copyright work has been disclosed expressly and sufficiently and the title of the Work and its authorship have been acknowledged in this Work;
(4) I do not have any actual knowledge nor do I ought reasonably to know that the making of this work constitutes an infringement of any copyright work;
(5) I hereby assign all and every right in the copyright to this Work to the University of Malaya ("UM"), who henceforth shall be owner of the copyright in this Work and that any reproduction or use in any form or by any means whatsoever is prohibited without the written consent of UM having been first had and obtained;
(6) I am fully aware that if in the course of making this Work I have infringed any copyright whether intentionally or otherwise, I may be subject to legal action or any other action as may be determined by UM.

Candidate's Signature Date:

Subscribed and solemnly declared before,

Witness's Signature Date:

Name:

Designation

ABSTRACT

Hemorrhage remains the leading cause of potentially survivable death in both military and civilian populations. Although various hemostatic products have been shown to be effective in establishing hemostasis, they remain deficient in a number of desired criteria. An alternative approach to hemostasis is through the application of mesoporous bioactive glasses (MBGs) which can provide a platform to accelerate natural hemostasis and control hemorrhage. However, the materials may not be considered as ideal hemostats since they do not offer antimicrobial activity. The gallium ion (Ga^{+3}) not only exhibits antibacterial properties but may also be effective in the early stage of hemostasis. The main objective of this study was to develop MBGs containing increasing amounts of Ga_2O_3 (1, 2 & 3 mol %) *via* the evaporation-induced self-assembly (EISA) process and investigate their potential as hemostatic systems. The physicochemical properties, hemostatic response, antibacterial effect as well as the biocompatibility of the materials were investigated. The second objective of this study was to compare the Ga-MBG determined to have greatest hemostatic efficacy with two commercial hemostats, Celox™ (CX, Medtrade Products Ltd. Crewe, United Kingdom) and QuikClot Advanced Clotting Sponge Plus™ (ACS^+, Z-Medica, Wallingford. Connecticut, USA). The results showed that the inclusion of 1 mol% Ga_2O_3 content into the MBG system not only resulted in better textural properties (*i.e.* surface area and pore volume) compared with Ga-free MBG and other substituted glasses, but also increased the release of silicon and calcium ions and degradation rates. The 1%Ga_2O_3-containing MBG (1%Ga-MBG) was also found to be more effective in inducing blood coagulation, platelet adhesion and thrombus generation as compared to the other Ga_2O_3-containing MBGs. All experimental MBGs exerted more efficient antibacterial action against both *Escherichia coli* and *Staphylococcus aureus* as compared with Ga-free MBG. The results also indicated that antibacterial activity of MBG increased with increase in Ga

content in its matrix. Likewise, Ga-doped MBGs showed excellent cytocompatibility with human dermal fibroblast (HDF) cells even after 3 days; particularly the 1%Ga-MBG. No significant differences were found among the 1%Ga-MBG and CX with respect to the numbers of adherent platelets to their surfaces. 1%Ga-MBG activated the intrinsic pathway of coagulation cascade, induce platelet activation, thrombin and thrombus formation more significantly than CX and ACS^{+}. In addition, the 1%Ga-MBG showed higher weight loss in comparison to the CX and ACS^{+} after 35 days. The results of the cytotoxicity assay demonstrated that all the examined materials were non-cytotoxic to HDF cells after 3 days with the 1%Ga-MBG attaining the higher biocompatibility. Overall, 1%Ga-MBG was found to be superior to CX and ACS^{+} as it possesses essential factors required for coagulation activation. The results of this study identify 1%Ga-MBG as a promising material platform for designing hemostats for clinical application.

ABSTRAK

Pendarahan masih merupakan punca utama kematian dalam populasi tentera dan awam. Walaupun pelbagai produk hemostatik telah dibuktikan berkesan dalam hemostasis, mereka tetap kekurangan beberapa kriteria yang diperlukan. Pendekatan terkini untuk hemostasis adalah melalui penggunaan bahan berasaskan kaca yang berporos (bioactive mesoporous glasses, MBG) yang menyediakan platform untuk mempercepatkan proses hemostasis secara semula jadi dan mengawal pendarahan. Walau bagaimanapun, bahan-bahannya tidak boleh dianggap sebagai hemostasis yang ideal kerana ketiadaan aktiviti antibakteria. Ion galium (Ga^{+3}) bukan sahaja mempamerkan ciri-ciri antibakteria, tetapi juga berkesan jika digunakan pada peringkat awal hemostasis. Objektif utama kajian ini adalah untuk membangunkan bahan MBG yang mengandungi Ga_2O_3 (pada jumlah 1, 2 & 3 mol %) melalui proses penyejatan kendiri yang diaruh (evaporation-induced self-assembly, EISA) dan menilai potensi setiap satunya sebagai sistem hemostatik yang baik. Sifat-sifat fizikal dan kimia, tindak balas hemostatik, kesan antibakteria, serta kesepadanan biologi (biocompatibility) bahan yang dicadangkan telah dikaji. Objektif kedua kajian ini adalah untuk membandingkan keberkesanan proses hemostatik Ga-MBG yang telah dipilih dengan dua bahan hemostat komersial, iaitu Celox™ (CX, Medtrade Products Ltd. Crewe, United Kingdom) dan QuikClot Advanced Clotting Sponge Plus™ (ACS^+, Z-Medica, Wallingford. Connecticut, Amerika Syarikat). Hasil kajian menunjukkan bahawa penambahan 1 mol% kandungan Ga_2O_3 ke dalam sistem MBG bukan sahaja menghasilkan tekstur yang lebih baik (pertambahan luas permukaan dan isipadu liang), tetapi turut meningkatkan pengeluaran ion-ion silikon dan kalsium, dan kadar juga degradasi. 1% Ga_2O_3 yang mengandungi MBG (1%Ga-MBG) juga didapati lebih berkesan dalam mendorong pembekuan darah, lekatan platelet dan penumbuhan thrombus, berbanding Ga_2O_3 yang mengandungi MBGs. Kesemua

eksperimen menghasilkan keupayaan antibakteria yang lebih cekap terhadap kedua-dua *Escherichia coli* dan *Staphylococcus aureus* berbanding MBG bebas-Ga. Hasil kajian juga menunjukkan bahawa aktiviti antibakteria MBG meningkat secara selari dengan kenaikan kandungan Ga di dalam matriks yang digunakan. Selain itu, MBGs dengan pertambahan Ga menunjukkan perbandingan sitologi yang sangat baik dengan sel-sel fibroblast kulit manusia (HDF) walaupun selepas 3 hari; terutamanya 1%Ga-MBG. Tiada perbezaan yang signifikan ditemui di antara 1%Ga-MBG dan CX untuk perbandingan bilangan platelet yang melekat ke permukaan mereka. 1%Ga-MBG mengaktifkan laluan intrinsik pembekuan darah, mendorong pengaktifan platelet dan thrombin, dan pembentukan thrombus adalah lebih ketara daripada CX dan ACS^+. Di samping itu, 1%Ga-MBG menunjukkan penurunan berat yang lebih tinggi berbanding dengan CX dan ACS^+ selepas 35 hari. Keputusan penilaian sitotoksik (cytotoxicity tests) menunjukkan bahawa kesemua bahan-bahan yang dikaji adalah bukan sitotoksik kepada sel-sel HDF selepas 3 hari, dengan 1%Ga-MBG mencapai kesepadanan biologi yang paling tinggi. Secara keseluruhan, 1%Ga-MBG didapati lebih berkesan daripada CX dan ACS^+ kerana mempunyai faktor-faktor penting yang diperlukan untuk pengaktifan proses hemostatis. Keputusan kajian ini mengenal pasti bahawa 1%Ga-MBG sebagai platform bahan yang berpotensi tinggi untuk pembangunan hemostat yang sesuai untuk aplikasi klinikal pada masa hadapan.

ACKNOWLEDGEMENTS

I would like to express my appreciation and sincere gratitude to my enthusiastic supervisors, Assoc. Prof. Nahrizul Adib Kadri and Prof. Mark Towler for the immeasurable amount of support during my study as well as intellectual guidance they have provided throughout this study. It has been a pleasure and honour to work under their supervision, and in which I could broaden the horizon of my knowledge in the fields of biomaterials.

I would also like to thank the members of the National Orthopaedic Centre of Excellence in Research and Learning (NOCERAL), Dr. Sangeetha Naveen Sundar, Shani Samuel and Prof. Tunku Kamarul, for providing me with feedback and support throughout my research.

Moreover, my sincere gratitude goes to all of my sponsors, the Ministry of Higher Education (MOHE), Government of Malaysia, under the High Impact Research (UM.C/625/1/HIR/MoE/ENG/58) scheme, the University of Malaya Research Grants scheme (RP038A-15HTM) and Postgraduate Research Grant (PPP: PG077-2015B) for providing me sufficient financial support.

Last but by no means least; I would like to convey my heartiest thanks to my loving mom and sisters for their support, encouragement and love during my stay in Malaysia. My deepest love and gratitude goes to my husband and colleague Ehsan Zeimaran, his endless support, humor, love and patience made it feasible for me to go through the ups and downs of my PhD journey.

TABLE OF CONTENTS

LIST OF FIGURES

LIST OF TABLES

LIST OF SYMBOLS AND ABBREVIATIONS

%	:	Percentage
mol%	:	Mole percent
wt%	:	Weight percent
g	:	Gram
mg	:	Milligram
µg	:	Microgram
µm	:	Micrometer
nm	:	Nanometer
SD	:	Standard deviations
°	:	Degree
°C	:	Degree Celsius
h	:	Hour
min	:	Minute
s	:	Second
cm	:	Centimetre
ml	:	Millilitre
µL	:	Microliter
kV	:	Kilovolt
rpm	:	Revolutions per minute
Ɵ	:	Theta
M	:	Molar
ppm	:	Part per million
m^2	:	Square meters
k	:	Kelvin

N_2	:	Nitrogen
MBGs	:	Mesoporous bioactive glasses
Ga-MBG	:	Gallium-containing mesoporous bioactive glass
EISA	:	Evaporation-induced self-assembly
CX	:	Celox
ACS^+	:	QuikClot Advanced Clotting Sponge Plus
DFSD	:	Dry Fibrin Sealant Dressings
QC	:	QuikClot
QCG	:	QuickClot Combat Gauze
WS	:	WoundStat
HC	:	HemCon
ACS	:	Advanced Clotting Sponge
QCX	:	QuikClot Combat Gauze XL
QCTP	:	QuikClot Combat Gauze Trauma Pad
QCI	:	QuikClot Interventional
RDH	:	Rapid Deployment Hemostat bandage
TDEX	:	TraumaDEX
FSD	:	Fibrin sealant dressing
AFB	:	Army Field Bandage
SD	:	Standard dressing
ND	:	Non-dressing
RL	:	Lactated Ringer's solution
QCX	:	QuikClot Combat Gauze XL
TMS	:	TraumaStat
PG	:	Placebo QuikClot gauze
SG	:	Standard gauze

CTG	:	Celox Trauma Gauze
HCG	:	ChitoGauze
CXG	:	Celox Gauze
CG	:	Cotton Gauze
HCG	:	HemCon ChitoGauze
G	:	laparotomy gauze
SQR	:	Super Quick Relief
AFD	:	Standard army field dressing
GZ	:	Gauze
FAST	:	fibrinogen-based dressing
KX	:	Kerlix
FDA	:	food and drug administration
CoTCCC	:	Committee on Tactical Combat Casualty Care
TCCC	:	Tactical Combat Casualty Care
TEG	:	Thrombelastograph
POI	:	Point of injury
RAO	:	Radial artery occlusion
NP	:	Negative pressure
Ga^{+3}	:	Gallium
Ca^{2+}	:	Calcium
Ti^{+4}	:	Titanium
Ce^{3+}	:	Cerium
Zn^{2+}	:	Zinc
Ag^{+}	:	Silver
Na^{+}	:	Sodium
Fe^{3+}	:	Ferric iron

SiO_4^{4-}	:	Silicate
PO_4^{3-}	:	Phosphate
NaCl	:	Sodium chloride
Ba $(NO_3)_2$	:	Barium nitrate
$AgNO_3$	:	Silver nitrate
$Ga(NO_3)_3$	:	Gallium nitrate
$CaCl_2$	:	Calcium Chloride
$Ca(NO_3)_2.4H_2O$	:	Calcium nitrate tetrahydrate
$Ga(NO_3)_3.$ xH_2O	:	Gallium (III) nitrate hydrate
TEOS	:	Tetraethyl orthosilicate
TEP	:	Triethyl phosphate
EtOH	:	Ethyl alcohol
HNO_3	:	Nitric acid
TMOS	:	Tetramethyl orthosilicate
HMWK	:	High-molecular-weight-kininogen
HDF	:	Human dermal fibroblast
VWF	:	Von Willebrand factor
GP Ib	:	Glycoprotein Ib
TXA2	:	Thromboxane A2
ADP	:	Adenosine diphosphate
TF	:	Tissue factor
RBCs	:	Red blood cells
SMMs	:	Silica-based ordered mesoporous materials
SDA	:	Structure directing agent
TLCT	:	True-liquid-crystal template

CLCT	:	Cooperative liquid crystal template
cmc	:	Critical micellar concentration
SGGs	:	Sol-gel derived bioactive glasses
CTAB	:	Cetyltrimethyl ammonium bromide
MSN	:	Mesoporous silica nanoparticles
CBT	:	Clotting blood tests
MSX	:	Mesoporous silica xerogels
PT	:	Prothrombin time
APTT	:	Activated partial thromboplastin time
MBGMs	:	Mesoporous bioactive glass microspheres
MSS	:	Mesoporous silica spheres
E. coli	:	Escherichia coli
S. aureus	:	Staphylococcus aureus
LB	:	Lysogeny broth
CFU	:	Colony-forming unit
BGS	:	Non-porous bioactive glass
n-BGS	:	Nanoporous bioactive glass
CS	:	Chitosan
CSSX	:	Chitosan-silica xerogel hybrids
HA	:	Hydroxyapatite
PPP	:	Platelet poor plasma
PRP	:	Platelet rich plasma
DT	:	Degree of thrombogenicity
HMDS	:	Hexamethyldisilazane
LDH	:	Lactate dehydrogenase
OD	:	Optical density

ELISA	:	Enzyme-Linked Immunosorbent Assay
TAT	:	Thrombin–antithrombin complex
UV	:	Ultraviolet
DMEM	:	Dulbecco's modified Eagle's medium
DMSO	:	Dimethyl sulfoxide
FBS	:	Fetal bovine serum
PBS	:	Phosphate buffered solution
SBF	:	Simulated body fluid
NBOs	:	Non-bridging oxygen
BET	:	Brunauer–Emmett–Teller
BJH	:	Barret–Joyner–Halenda
SAXRD	:	Small angle X-ray diffraction,
WAXRD	:	Wide angle X-ray diffraction
FESEM	:	Field Emission Scanning Electron Microscopy
HRTEM	:	High-resolution Transmission electron microscopy
EDS	:	Energy-dispersive X-ray spectroscopic
FT-IR	:	Fourier transform infrared spectroscopy
MP–AES	:	Microwave plasma–atomic emission spectrometer

CHAPTER 1: INTRODUCTION

1.1 Background of study

1.1.1 Fundamentals of hemostasis

The clotting process, or hemostasis, is a physiological process that prevents blood loss through the formation of a stable hemostatic clot at the site of bleeding (Butenas *et al.*, 2002). It is a complex mechanism that involves the coordinated activation of various plasma proteins, platelets, cells and coagulation factors which are generated from the liver and enter the blood circulatory process in an inactive state (Butenas *et al.*, 2002; Esmon, 1993). These factors can activate each other when the coagulation cascade is started and according to their function, can initiate and complete each step of the coagulation process (Samudrala, 2008). Overall, hemostasis takes place *via* the synchronized action of three mechanisms: (1) vasoconstriction; (2) platelet response; and (3) blood clotting (Figure 1.1) (Casey, 2003).

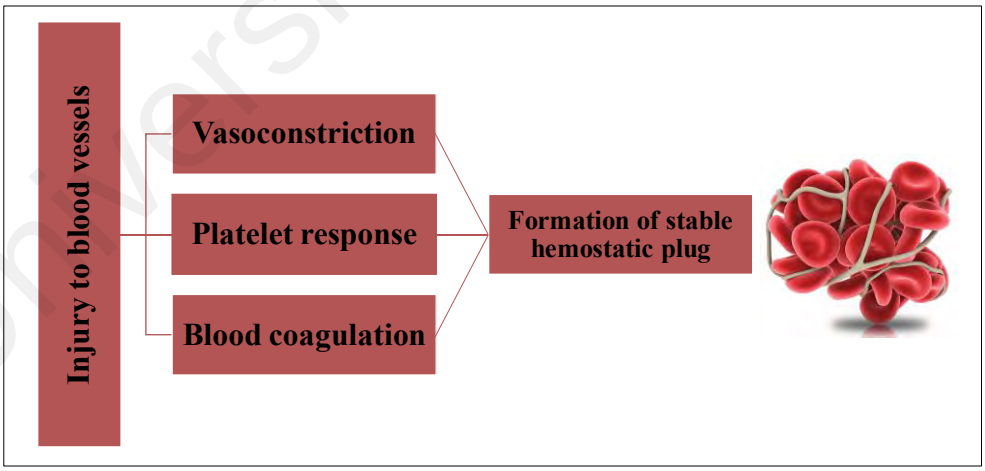

Figure 1.1: Process flow of hemostasis.

The entire process shown above proceeds in two phases: primary and secondary hemostasis (Lundblad *et al.*, 2004). Primary hemostasis initiates immediately after vascular injury and endothelial disruption and involves two processes namely

vasoconstriction and platelet plug formation. When injury to a blood vessel occurs, a reflex local contraction of vascular smooth muscle is triggered that leads to vasoconstriction. This action compresses the blood vessels, retarding blood flow and limiting blood loss. At the same time, when the blood is exposed to collagen fibers in the basement membrane of the vessel, platelets bind to von Willebrand Factor (VWF) on exposed subendothelial collagen *via* a glycoprotein Ib (GP Ib) receptor. This receptor-ligand interaction starts the process of platelet activation that leads to cytoskeletal rearrangement, shape change, and release of intracellularly stored granules by multiple signaling pathways. These granules contain substances such as thromboxane A2 (TXA2), adenosine diphosphate (ADP), and serotonin which not only enhance further vasoconstriction but also result in a conformational change in GPIIb/IIIa on platelets that allows platelets to bind to fibrinogen resulting in platelet aggregation over the injured surface (Broos *et al.*, 2011). This phase of hemostasis is short-term, and ultimately results in primary hemostatic plug formation which can easily be sheared from the injured area (Figure 1.2) (Marder *et al.*, 2012).

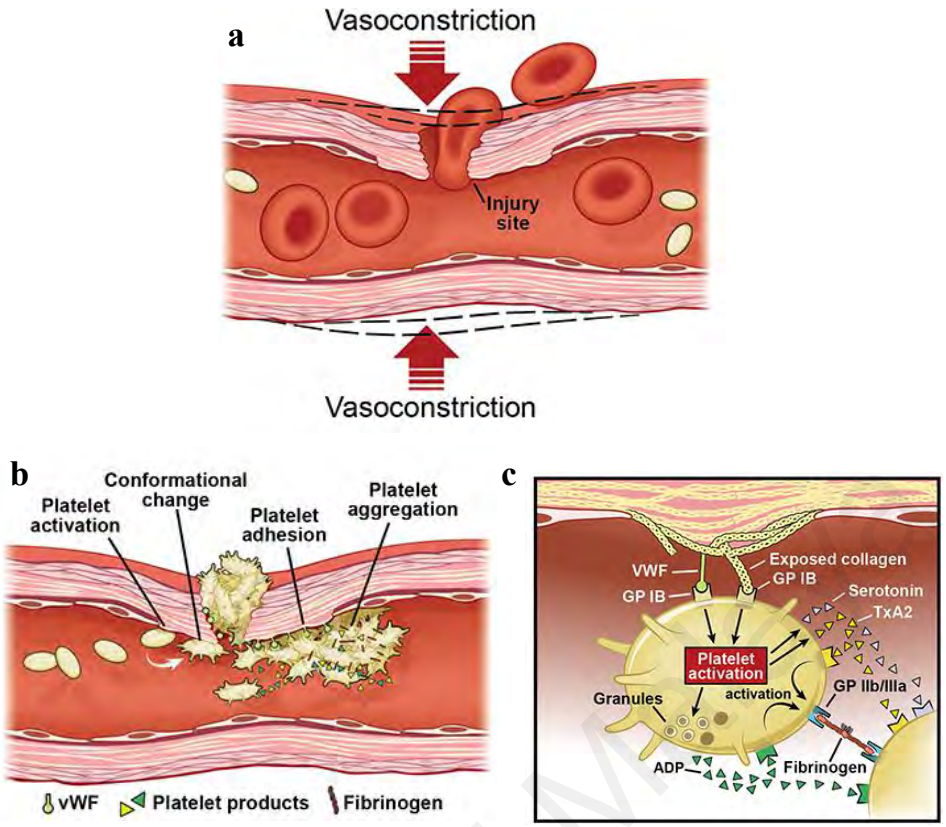

Figure 1.2: Primary of hemostasis. a) vasoconstriction, b) platelet plug formation and c) binding of platelets via the receptor GP Ib to the VWF [Reproduced with permission from (Bermudez *et al.*, 2016)].

In the next stage, secondary hemostasis, the soft platelet plugs stabilize and cross-link to form a stable and permanent plug. This occurs throughout the coagulation cascade involving a series of plasma proteins, coagulation factors, calcium ions (Ca^{2+}) and platelets that lead to the conversion of fibrinogen into fibrin. The coagulation cascade is divided into two enzymatic pathways; the intrinsic pathway (contact activation) and extrinsic pathway (tissue factor), which combine to form a common pathway. The details of the coagulation cascade are indicated schematically in Figure 1.3.

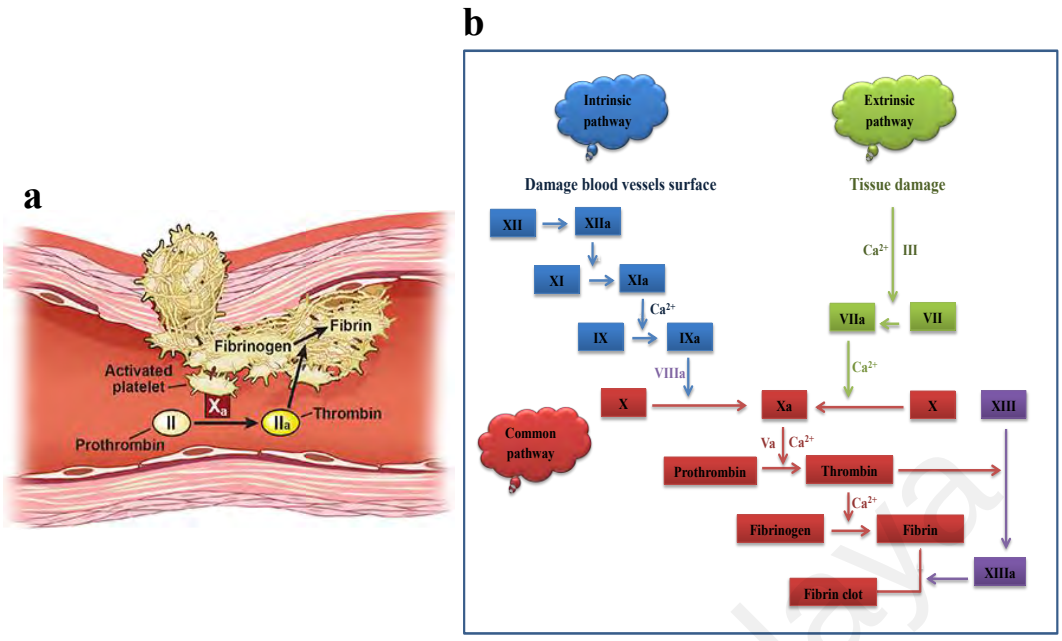

Figure 1.3: Secondary hemostasis. a) The fibrin network traps the platelets, forming the permanent plug. b) Schematic of the coagulation cascade [Reproduced with permission from (Bermudez *et al.*, 2016)].

The extrinsic pathway begins when injured vascular exposes tissue factor (TF, also identified as tissue thromboplastin, factor III) to blood, a protein that is not present in blood, but is released from vessel walls and the surrounding tissue upon vascular insult (Morrissey, 2001). In contrast, the intrinsic pathway is triggered by factor XII, an enzyme that is activated by contact of blood with a foreign surface. Ultimately, these two pathways assemble into a common pathway and lead to the activation of factor X, an enzyme that cleaves prothrombin to thrombin in the presence of Ca^{2+} and Va factor (is a cofactor that in the presence of Ca^{2+} to form the prothrombinase complex, a complex responsible for the rapid conversation prothrombin to thrombin) (Gorbet *et al.*, 2004; Samudrala, 2008). Thrombin not only transforms the soluble plasma protein fibrinogen into the insoluble protein fibrin but also activates factor XIII in the form of XIIIa, an enzyme that facilitates adherence and cross-linking of the fibrin proteins together, subsequently forming a reinforced plug (Mackman, 2004; Mackman *et al.*, 2007).

1.1.2 Importance of hemostasis

Globally, severe trauma leading to uncontrolled hemorrhage is a major public health issue. Traumatic injury accounts for one in ten mortalities, resulting in more than 5.8 million deaths worldwide annually (Naghavi *et al.*, 2015; Rossaint *et al.*, 2016), a number that is predicted to rise to over 8 million by 2020 (Insel *et al.*, 2016). Uncontrolled hemorrhage remains the greatest cause of death on the battlefield as exsanguination contributes to more than 85% of deaths from potentially survivable wounds (Kelly *et al.*, 2008). Irrepressible bleeding is also the second leading cause of civilian trauma deaths, (Evans *et al.*, 2010) and the most common cause of mortality during orthopedic, cardiovascular, hepatic and spinal surgeries (Mannucci *et al.*, 2007). Tissue trauma and hypovolemic shock caused by severe bleeding are identified as additional significant risk factors leading to the life-threatening coagulopathy, making hemorrhage control and fluid resuscitation therapy more difficult even after patient's arrival at the hospitals (Cosgriff *et al.*, 1997; Kauvar *et al.*, 2006). Coagulopathy is a condition that impairs the blood's ability to coagulate, a process needed to stop bleeding. The early coagulopathy of trauma was found to be present in 25% of civilian trauma patients admitted to Level I trauma centers as a primary response to injury (MacLeod *et al.*, 2003). Among the severely injured combat casualties who required massive blood transfusion, over one third (38%) were also diagnosed with acute traumatic coagulopathy upon arrival at a combat support hospital (Niles *et al.*, 2008).

It is reported that even when trauma victims survive the initial injury and hemorrhage is controlled, large blood loss leaves the victims more vulnerable to acidosis, hypothermia, coagulopathy, infection, acidosis, and at risk of late morbidity and mortality because of sepsis and multiple organ failure (Alam *et al.*, 2005; Holcomb, 2005; Kauvar *et al.*, 2006).

Inherited bleeding disorder such as hemophilia A (Factor VIII deficiency), hemophilia B (Factor IX deficiency) (Ferraris *et al.*, 2015) and Von Willebrand disease (Leebeek *et al.*, 2016), a genetic disorder caused by a deficient or defective VWF which plays an important role in platelet adhesion and aggregation, can also complicate the achieving and maintaining hemostasis, leading to excessive bleeding after trauma or surgery.

Despite all of these variable circumstances requiring successful hemostasis and coagulation as well as the significant mortality rates from hemorrhage, little technological progress in hemostatic materials had been made over tourniquets or standard gauze dressing until the beginning of the 21st century. Therefore, early and efficient control of the life-threatening hemorrhage by applying hemostatic agents can be of considerable use in saving lives.

1.2 Rational

Uncontrollable hemorrhage and infections poses potential fatality risks and costs in critical situations such as battlefield, emergency, and hospital settings, by which more than half of deaths are caused (Behrens, Sikorski, & Kofinas, 2014; Katzenell *et al.*, 2012; Kelly *et al.*, 2008). Immediate control of hemorrhage is therefore essential for reducing fatality rates as bleeding out can occur within 10 mins (Behrens, Sikorski, Li, *et al.*, 2014; Champion *et al.*, 2003).

Preventing the spread of infection in the wounded area is another key component of healthcare since wound infection can delay or impair healing and cause life threatening complications (Boateng *et al.*, 2008; Penn-Barwell *et al.*, 2015). In this sense, an ideal hemostatic agent should not only achieve a reliable and immediate hemostasis within minutes but should be bacteriostatic and/or bactericidal (Çinar *et*

al., 2012). The safety and biocompatibility, cost-effectiveness, approvability, ease of manufacturing on an industrial scale, degradability and minimal tissue reactivity are other parameters which should be considered when selecting an appropriate hemostatic agent (Glick *et al.*, 2013; Y. Li *et al.*, 2012).

Although several hemostats have been developed and marketed in the recent past, many of them fail to meet all of these requirements and thus hemorrhage is still a main cause of morbidity and mortality (Behrens, Sikorski, & Kofinas, 2014). For instance, inorganic hemostats based on zeolite (*i.e.* QuikClot^{TM} (QC, zeolite powder dressing, Z-Medica, Wallingford, CT) and QuikClot Advanced Clotting Sponge Plus^{TM} (ACS^{+}, Z-Medica, Wallingford. Connecticut, USA)) can result in thermal injuries and abnormal foreign-body reaction because of their highly exothermic reaction and poor biodegradability. They have also proven to be ineffective in controlling arterial bleeding (Achneck *et al.*, 2010; Granville-Chapman *et al.*, 2011).

Clay-based haemostatic agents (*i.e.* QuickClot Combat Gauze^{TM} (QCG, kaolin-incorporating gauze, Z-Medica, Wallingford, Connecticut, USA) and WoundStat^{TM} (WS, clay mineral powder, TraumaCure Inc. Bethesda, MD, USA)) as another group of inorganic hemostats, also found to be ineffective for providing immediate hemostasis, resulting in large blood loss. The materials have been shown to be less effective in coagulopathic patients and found to have significant safety issues regarding toxicity, embolization and tissue inflammation.

Chitosan-based hemostatic agents as a third generation of hemostats also have drawbacks and benefits. HemCon^{TM} (HC, chitosan standard dressing, HemCon Inc., Portland OR) whilst offering potent hemostasis in animal hemorrhage models and in some clinical trials, was later abandoned because of lack of efficacy in controlling excessive bleeding (Acheson *et al.*, 2005; Cox *et al.*, 2009; B. Kheirabadi, 2011; Rhee *et al.*, 2008); Celox (CX, chitosan powder, Medtrade Products Ltd. Crewe,

United Kingdom) has also been reported to induce a strong inflammatory response in some tissue despite possessing many of the ancillary characteristics of an ideal hemostatic dressing (B. Kheirabadi, 2011). Although newer chitosan gauzes were found to be superior to previously developed hemostats, their dressings have variable efficacy under high pressure arterial blood flow in animal studies (Gustafson *et al.*, 2007; B. S. Kheirabadi, Scherer, *et al.*, 2009). For instance, while the gauzes were able to stop low pressure bleeding, they failed to maintain hemostasis after intravenous administration of fluids to raise blood pressure back to baseline (B. S. Kheirabadi, Scherer, *et al.*, 2009). In summary, then, there are no ideal hemostatic agents.

Although many antibiotics have been developed to reduce bacteria at the wound site, the most important challenge facing caregivers is the increasing rate of antibiotic-resistant bacterial infections (Aronson *et al.*, 2006; C. K. Murray *et al.*, 2006). To address this problem, alternatives to antibiotics need to be considered for controlling infection and accelerating healing. The challenge is therefore to design and prepare fast-acting hemostatic agents that can:

i. be safer and more cost effective as compared with the previously marketed hemostatic agents.
ii. attenuate tissue burning that has been reported with other hemostatic agents without adversely affecting efficacy.
iii. exert efficient antimicrobial activity to minimize the incidence of postoperative wound infection.

Among all the new available hemostatic biomaterial technologies, mesoporous bioactive glasses (MBGs) are promising materials for facing these challenges. MBGs were first prepared by Yan *et al*. (Yan *et al.*, 2004) in 2004 using evaporation-induced self-assembly (EISA) process (Brinker *et al.*, 1999). The bioactive glasses in

the 80%SiO_2–15%CaO–5%P_2O_5 system are distinct from conventional non-mesoporous bioactive glasses developed by Hench and co-workers (Hench, 1998) since they possess well-defined mesoporous structure, controllable mesopore size ranging from 2 to 10 nm and significantly greater specific surface area and pore volume (Yan *et al.*, 2004).

Over the past decade, the interest of the scientific community in these materials as a multifunctional system for bone regeneration and controlled drug release has grown exponentially (Jiang *et al.*, 2012b; Shruti *et al.*, 2013). Recently, the porosity and textural properties of MBGs also make them good candidates to be employed in hemostatic technologies (Ostomel, Shi, Tsung, *et al.*, 2006). The *in vitro* and *in vivo* evaluation specified that they can enhance the hemostatic efficacy while overcoming the dangerous side-effects of other inorganic based hemostats (*i.e*. mineral zeolite) and thus minimizing collateral damage. However, the materials lack antibacterial activity, an essential factor which should be considered when developing a desirable hemostatic agent. Thus, this can limit the application of the MBG materials in the treatment of bleeding, especially the bleeding complicated by infection. In order to dispel this disadvantage, incorporation of therapeutic elements into their frameworks can be used to modify the MBGs so that the materials acquired antibacterial activity.

It is demonstrated that incorporation of some trace elements in the MBG matrix which can elute as ions, such as titanium (Ti^{+4}), cerium (Ce^{3+}), zinc (Zn^{2+}), silver (Ag^{+}) or gallium (Ga^{3+}) can improve the biological behaviour of MBG materials (Jiang *et al.*, 2012a, 2012b; Salinas *et al.*, 2011; Shruti *et al.*, 2013). It is surprising that only a few examples of the MBGs containing the therapeutic elements with hemostatic and antibacterial properties have been reported to date and more studies are needed to clarify their hemostatic properties.

1.3 Aims and objectives

The overall objective of the current study is to produce a series of Ga-MBGs with high accessible surface area which have the ability to release therapeutic ions from a Si-Ca-P-Ga bioglass framework and to provide an ideal surface for acceleration the blood clotting cascade, offering a better clinical outcome in controlling bleeding. To achieve this, the project has four short term objectives including:

1. To synthesize of MBGs containing various concentrations of Ga_2O_3 (1, 2 & 3 mol %) via the EISA process.
2. Investigating physiochemical properties, *in vitro* biodegradation, ion release kinetics of Ga-MBGs.
3. Assessing the role of Ga^{3+} on biological properties of MBG for better understanding of hemostatic activity, antibacterial properties and MBG-cells interactions.
4. Comparing the hemostatic response and biocompatibility of the Ga-MBG with two commercial hemostats, CX and ACS^{+}.

1.4 Thesis outline

The purpose of this research is to introduce and demonstrate a new approach to treat hemorrhage using MBG. The present thesis includes 6 chapters:

Chapter 1 Gives the background of the study, beginning with a compact coverage of the basic principles of hemostasis followed by the statement of the problem and objectives of the project.

Chapter 2 highlights a literature review summary of inorganic-based hemostats including zeolite and clay. This chapter also deals with the most recent research

progress in the field of the design and synthesis of MBG materials for hemostatic application.

Chapter 3 describes and explains the research procedures adopted for MBGs preparation. All methods used to collect both qualitative and quantitative data and generate the findings are also stated in this chapter.

Chapter 4 comprises the analysis, presentation and interpretation of the findings resulting from this study which is sub-divided into the following parts: Part I reports the development of ordered mesoporous (80-x)% SiO_2-15%CaO-5%P_2O_5 sol-gel glasses substituted with xGa_2O_3 as hemostatic agents. Part II presents the comparison of the Ga-MBG with two commercial hemostats, CX and ACS^+. Both parts deal with investigation of the physiochemical properties, *in vitro* hemostatic ability and biological characteristics of the materials.

Chapter 5 includes a comprehensive discussion of the research findings.

Chapter 6 summarizes the outcomes of the research, and provide implications and directions for future research.

CHAPTER 2: LITRATURE REVIEW

2.1 Introduction

The capability of blood to clot rapidly and seal the damaged vessels can be inadequate for controlling excessive bleeding and it may even reduce following traumatic injuries, massive blood loss as well as the development of fluid administration, metabolic acidosis and hypothermia (Dubick *et al.*, 2010). Thus, the use of hemostatic agents, devices or drugs to promote blood clotting, is essential in controlling severe hemorrhage, preventing death and increasing the survival of injured victims (Carraway *et al.*, 2008).

Although several hemostats have been developed and proved valuable for hemorrhage control in many cases, the development of an alternative effective hemostatic agent that can achieve a desirable hemostasis and minimize collateral damage is still an enormous challenge.

Over the past few years, a variety of inorganic materials including zeolites and clays have been developed that can accelerate the coagulation of the blood. Hemostats based on these materials have high utility because the materials are free of animal or human derived proteins which can lead to allergic reactions. Recently, the Committee on Tactical Combat Casualty Care (CoTCCC) has added hemostats based on these inorganic species (*i.e.* QC, QCG and WS) to the official guidelines since the products were found to be superior to other hemostatic agents. The hemostats that can stimulate the coagulation of blood, have high utility because the materials are free of animal or human derived proteins leading to allergic reactions. However, although, CoTCCC considers some of these dressings as the hemostatic agents of choice to control life-threatening hemorrhages which are not amenable to tourniquet

application (Bennett & Littlejohn, 2014), there have also been concerns related to sides effects such as thermal injury to wound tissue (Acheson *et al.*, 2005; Alam *et al.*, 2004), lack of efficacy in severe bleeding (B. S. Kheirabadi, Edens*, et al.*, 2009) and toxicity toward endothelial and macrophage-like cells (Bowman *et al.*, 2011).

Recently, a new generation of nanostructured glasses called MBGs open up new opportunities in drug delivery, implanting, and as coating-materials for tissue engineering applications. There is also a recent interest in these materials that can interface with soft biological tissue or fluid for instance, blood (Ratner *et al.*, 1996).

MBGs, due to many features including their inherently polar surface, high surface area and high porosity are candidates for hemostatic applications. The materials are able to stop bleeding quickly at the wound sites with a lower rate of complications associated with some inorganic hemostats including zeolite and clays based hemostats (Dai *et al.*, 2009; Hu *et al.*, 2012).

This chapter highlights recent advances in the development of zeolite and clay based hemostats. A critical overview of their mechanisms of action is discussed as well as the structural features that are believed to stimulate hemostasis. This chapter also collates the findings on the most effective inorganic hemostatic agents in both human and animal trials. This chapter also deals with the most recent research progress in the field of the design and synthesis of MBG materials for hemostatic application and the reasons why these materials can be a promising candidate to control blood clotting are explained.

As will be shown in the following sections, inorganic hemostats perform their actions through enhancing one or more of the above processes. Specifically, they work through three mechanisms (Table 2.1):

1. Absorbing water from blood and concentrating the blood components at the hemorrhagic site: materials with this ability are called factor concentrators.
2. Activating the blood coagulation cascade: materials with this ability are called pro-coagulants.
3. Providing a physical barrier to blood flow by cross-linking cellular blood components: materials with this ability are called mucoadhesives.

Table 2.1: Mechanism of action of inorganic hemostats according to the literature.

Inorganic hemostats	Factor concentrator	Pro-coagulant	Mucoadhesive
QC	✓		
Advanced Clotting Sponge (ACS)	✓		
ACS^{+}	✓		
QCG		✓	
QuikClot Combat Gauze XL (QCX)		✓	
WS		✓	✓

Table 2.1 summarizes which of these phenomena are contributed to the hemostatic action of zeolites and clay-based hemostats, described in the following section.

2.2 Zeolite

Zeolites, microporous crystalline aluminosilicate minerals, are found in nature and are considered "molecular sieves" a family of porous solids (Maesen, 2007). The structural framework of a zeolite is based on tetrahedral units of $[SiO_4]^{4-}$ and $[AlO_4]^{5-}$ that are co-ordinated *via* shared oxygen atoms (Figure 2.1).

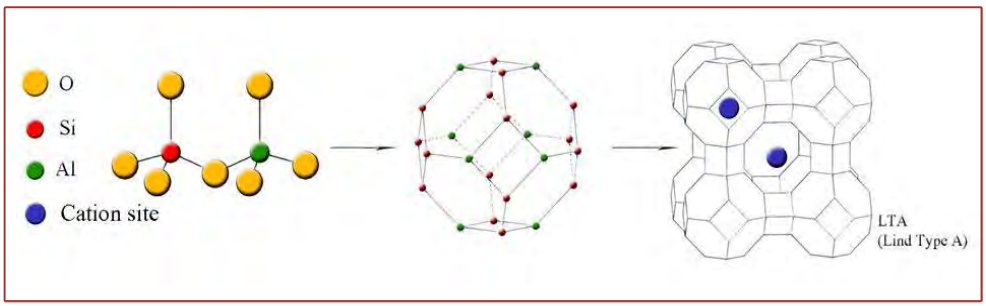

Figure 2.1: The zeolite structure.

Zeolites possess cage-like cavities that can accommodate both water molecules and a variety of positively charged ions such as $Ca^{2+}$and sodium (Na^{+}). The cations are relatively loosely held, so that they can exchange with other cations in contact with physiological solutions (SM Mortazavi *et al.*, 2009). Zeolites are chemically similar to clay-based minerals (both are aluminosilicates) but they are structurally different. Clay minerals with a layered crystalline structure can shrink and swell as water is eliminated and absorbed, respectively, between the layers. By contrast, zeolites contain interconnected channels in a rigid, 3-dimensional crystalline structure which facilitates the movement of water molecules in and out of their pores whilst remaining rigid (Warren, 2016). Zeolites offer long-term physical and chemical stability, an ability to exchange ions with surrounding solutions; they have no biological toxicity and are capable of absorbing high amounts of water. These features make the materials valuable candidate for hemostatic applications (Katic *et al.*, 2006; J. Li *et al.*, 2013; Mumpton, 1999; Pavelić *et al.*, 2001; Rimoli *et al.*, 2008; Rodriguez-Fuentes *et al.*, 1997). Zeolites can entrap large volumes of water within their pores due to the electrostatic interaction between water and the Ca^{2+} ions that reside in open porous internal space. As a result, they concentrate coagulation factors and platelets in the hemorrhaging blood (Figure 2.2) (J. Li *et al.*, 2013; SMJ Mortazavi *et al.*, 2013).

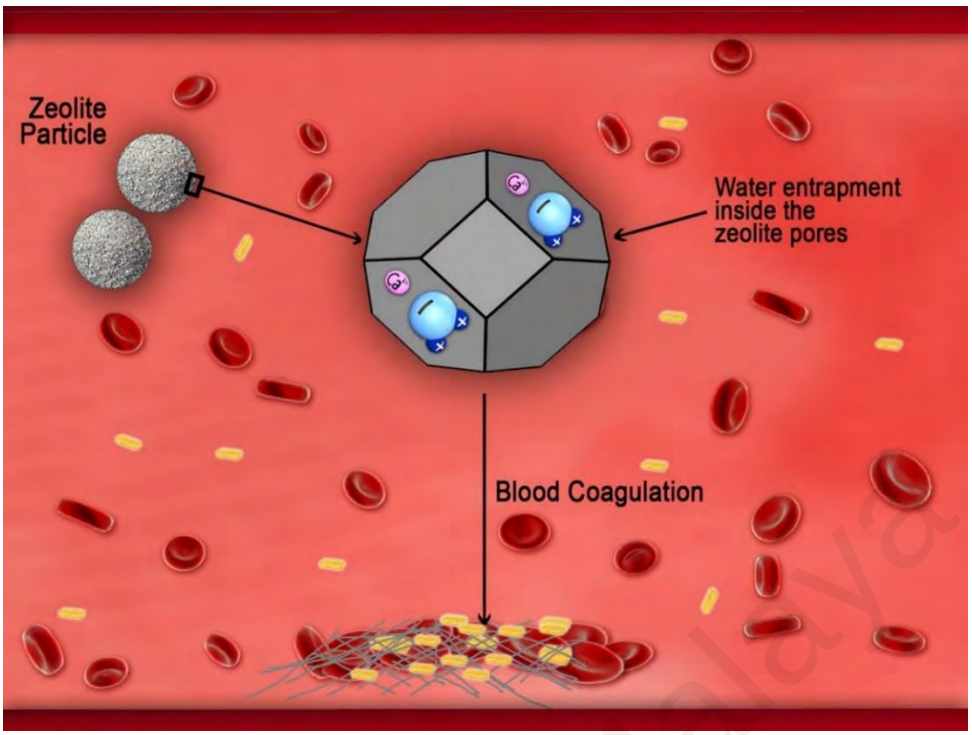

Figure 2.2: Summary of the potential hemostatic effects of zeolite. This schematic captures the effects of zeolite on the blood coagulation through absorption of water molecules into its pores resulting from the interaction with Ca^{2+} ions resided into zeolite pores. The interaction leads to concentrating the blood cells and clotting factors and promoting hemostasis.

Zeolite is marketed as QC (Z-Medica Corporation, Wallingford, CT), Advanced Clotting Sponge^{TM} (ACS, Z-Medica, Newington, CT, USA) and ACS^{+} (Z-Medica, Newington, CT, USA) (Figure 2.3).

Figure 2.3: a) The QC granules poured directly into wound. b) ACS^{+}, in which zeolite is packaged into porous bag [Reproduced with permission from (Cox *et al.*, 2009)].

2.2.1 QuikClot^{TM} granular (QC)

QC was approved by the FDA for external application in 2002 (Palm *et al.*, 2008). This product consists of granular zeolite powder with 1% residual moisture. QC as a factor concentrator that works *via* rapid absorption of the water content of blood, concentrating platelets, blood cells, and clotting factors at the site of injury, thereby promoting coagulation (Alam *et al.*, 2004; Granville-Chapman *et al.*, 2011; Schreiber *et al.*, 2011). QC is biologically inert and sterile and so the possibility of allergic reactions or viral infection transmission is minimal (Margulis *et al.*, 2005).

QC can be applied as a first aid kit to arrest bleeding from injuries within both combat and noncombat field operation, where other conventional treatments have failed (Achneck *et al.*, 2010; Alam *et al.*, 2005).

2.2.1.1 QC *in vivo* animal tests

Alam *et al.* assessed the hemostatic performance of QC in a groin injury porcine model against other hemostats, Rapid Deployment Hemostat bandage (RDH, polysaccharide, Marine Polymer Technologies, Cambridge, MA), TraumaDEX (TDEX, polysaccharide, Medafor Inc, Minneapolis, Minnesota) and a control (no dressing) (Alam *et al.*, 2003). QC had superior efficacy compared to the other dressings; it was the only agent that resulted in 0% mortality (Alam *et al.*, 2003). QC was also tested in a liver injury swine model and produced the lowest blood loss compared with gauze (1,397 mL versus 5,338 mL respectively) (Pusateri *et al.*, 2004). Seven out of eight QC-treated animals survived, whereas the number of survived subjects in the gauze group was one out of eight. Margulis *et al*. employed QC in a laparoscopic partial nephrectomy porcine model (Margulis *et al.*, 2005). In this study, QC conferred an immediate and continuous hemostasis (Margulis *et al.*, 2005). A comparative study performed by Kozen *et al*. to evaluate the efficiency of

QC in a fatal hemorrhagic groin injury (Kozen *et al.*, 2008) found that QC was more effective in cases of moderate bleeding than HC (HemCon Inc., Portland OR) and standard gauze (control) (Kozen *et al.*, 2008). QC improved survival significantly compared with these dressings. The failure of HC was attributed to its adhesion to the soft tissue surrounding the vessels so that it was not capable of sealing the actual vascular injury. However, Acheson *et al.* tested three different hemostatic products, QC, HC and fibrin sealant dressing (FSD, Fort Detrick, MD) as compared with Army Field Bandage (AFB, control) in a porcine arterial hemorrhage model and identified FSD as the superior hemostatic agent. QC was ineffective in controlling hemorrhage because it was washed away from the wounded area resulting in unopposed bleeding (hemostasis rate was 0%) (Acheson *et al.*, 2005).

2.2.1.2 QC in Humans

Wright *et al.* has described the hemostatic ability of QC in a multiple gunshot victim who suffered from hypothermia, acidosis, and coagulopathy which were not amenable to conventional treatment (F. L. Wright *et al.*, 2004). QC achieved hemostasis with no evidence of hypothermic injury. One case study considering treatment of an uncontrollable pelvic bleeding with QC was reported by Shanmugam *et al.* (Shanmugam *et al.*, 2009). Here, QC resulted in complete hemostasis where other measures such as packing, drawing pins, stenting and embolization failed to control bleeding. A comprehensive analysis on the effectiveness and suitability of QC was also reported by Rhee *et al.* in 103 patients sourced from US military and civilian personnel (Rhee *et al.*, 2008). QC was used in both external (head, neck, buttock, groin) and intracorporeal (chest, abdomen, pelvis) locations (Figure 2.4).

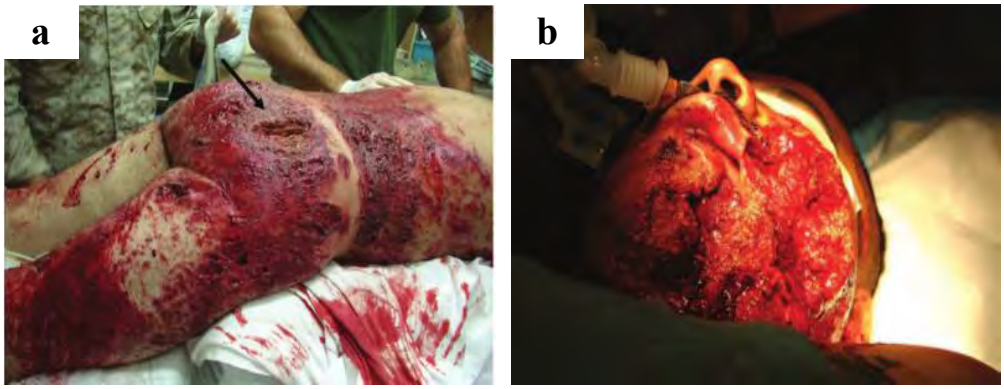

Figure 2.4: QC showed high hemostatic performance (a) in a soldier who suffers from a severe gluteal wound caused by improvised explosive devices in the military and also (b) in a sailor who experienced extreme lacerations on his face *via* a rotor blade from a helicopter [Reproduced with permission from (Rhee *et al.*, 2008)].

QC controlled bleeding in 92% of cases and had 100% efficacy when applied by first responders. However, eight failures were observed and thought to be due to both inability to apply product to the wound site alongside the coagulopathy state of the patients (Rhee *et al.*, 2008). A serious adverse effect of QC is burning of surrounding tissue at the bleeding site (Acheson *et al.*, 2005; Neuffer *et al.*, 2004; Pusateri *et al.*, 2004; Rhee *et al.*, 2008; Robinson, 2004) believed to be related to QC trapping water molecules into its pores *via* an exothermic reaction which increased local tissue surface temperatures by as much as 90 °C (Plurad *et al.*, 2009; J. K. Wright *et al.*, 2004). Wright *et al.* demonstrated that QC in a swine injury model led to increased temperature at both the tissue surface and internal to the tissue, at about 95 °C and 50 °C, respectively, which caused thermal injury and necrosis to surrounding tissues alongside impairment to the wound healing process (J. K. Wright *et al.*, 2004). McManus also reported thermal injuries resulting application of QC to four patients; the partial thickness of burning was 1–2 % total body surface area (McManus *et al.*, 2007). According to evidence gathered in Iraq, another adverse effect associated with use of QC is related to its granular nature that makes it unsuitable for high pressure bleeding as it can be flushed out or blown away from the wound site through heavy

blood flow (Neuffer *et al.*, 2004). The difficulty of removing QC at the site of bleeding because of its granular nature is an additional concern that may result in inflammatory granuloma formation (Buderi, 2013). QC was removed from military inventory in 2008, but a newer generation of zeolite hemostats such as the ACS and ACS^{+} has been commercialized and these are compositionally similar to QC.

2.2.2 Advanced Clotting Sponge (ACS)

ACS received FDA approval in 2005 for external use (Buderi, 2013). ACS is similar to QC but consists of larger beads of the zeolite which are packaged in a gauze (Arnaud *et al.*, 2008). ACS is a factor concentrator and shares a similar mechanism of action to QC (Granville-Chapman *et al.*, 2011). It is reported to be more effective than QC, especially when it comes to irregular cavities and perfuses hemorrhage and it achieves effective hemostasis without being freely distributed into the wound. The product is also easier to remove than QC (Achneck *et al.*, 2010).

2.2.2.1 ACS in animal models

ACS was as effective as QC in prompting hemostasis and prolonging survival time (Alam *et al.*, 2004; Alam *et al.*, 2003; Arnaud *et al.*, 2007; Pusateri *et al.*, 2006). ACS controlled blood loss and improved survival in a groin injury swine model. Both agents out performed standard dressing (SD) with a 75% survival rate (Arnaud *et al.*, 2007). However, a dramatic increase in wound temperature was noted in QC and ACS treated animals (58.1 °C and 58.2 °C respectively) compared with SD-treated animals (38.8 °C) which caused some localized edema. To overcome this, the literature suggests that altering the chemical composition of zeolite may be useful (Ahuja *et al.*, 2006). Ahuja *et al.* prepared sodium-exchanged QC (Na-QC), barium-exchanged QC (Ba-QC) and silver-exchanged QC (Ag-QC) through immersion of

QC in aqueous solutions of sodium chloride (NaCl), barium nitrate (Ba $(NO_3)_2$) and silver nitrate ($AgNO_3$) respectively. The modified QC compositions were packaged in airtight mylar foil packages and their hemostatic properties were compared to ACS, HC, SD and non-dressing (ND) groups in a severe groin injury swine model (Ahuja *et al.*, 2006). Based on the results, the modified QCs were found to be more effective in inducing hemostasis and improving survival as compared with ND and SD groups (Figure 2.5). The modified materials dramatically declined the temperature peak by 5-10 °C at the wound site in comparison with ACS and no evidence of tissue necrosis was observed (Ahuja *et al.*, 2006). Nevertheless, the peak temperatures in these groups were still significantly higher compared with the ND, SD, and HC groups.

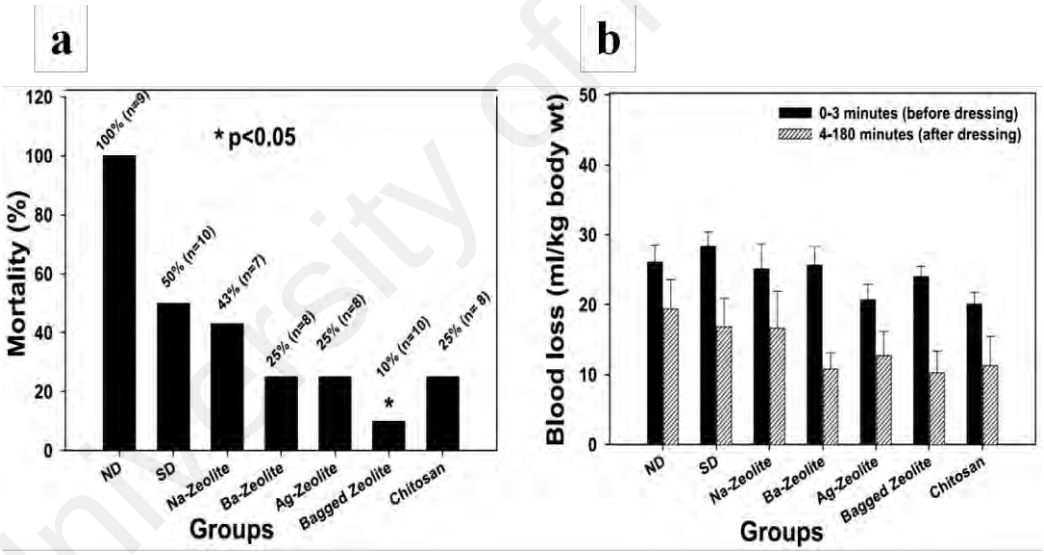

Figure 2.5: (a) mortality rate and (b) blood loss in different groups. All dressing groups reduced the mortality and blood loss rate compared with ND and SD [Reproduced with permission from (Ahuja *et al.*, 2006)].

However, Alam *et al.* claimed that, when the zeolite beads are packaged into a loose mesh bag, as with ACS, efficacy may be decreased since the bag acts as a barrier against achieving hemostasis (Alam *et al.*, 2004). Although ACS was superior to QC in controlling hemorrhages, there was still heat generation at the bleeding site

which led to tissue damage (Alam *et al.*, 2003; Arnaud *et al.*, 2007). This problem was addressed by pre-hydrating the zeolite so that it could absorb water less exothermically. The modified formulation was commercialized as ACS^+.

2.2.3 Advanced Clotting Sponge plus (ACS^+)

ACS^+ gained FDA approval for external usage in 2006. It consists of synthetic zeolite beads packaged into loose mesh bags similar to that of ACS, the difference being that the zeolite is preloaded with some water (hydration) (Clay *et al.*, 2010). Similar to ACS and QC, ACS^+ has no intrinsic hemostatic property and works as factor concentrator (Alam *et al.*, 2004; Inaba *et al.*, 2011). ACS^+ does not have the damaging thermal profile of QC and ACS, and is easier to handle and remove (Alam *et al.*, 2003; Arnaud *et al.*, 2007). However, it is no more effective than QC and ACS in management of arterial haemorrhage (B. S. Kheirabadi, Edens, *et al.*, 2009).

2.2.3.1 ACS^+ in animal models

Arnaud *et al.* compared the temperature change and the hemostatic efficacy of ACS^+ with ACS and SD in a swine model of lethal groin injury and concluded that ACS^+ is superior to ACS as it was less exothermic at the site of injury. Compared with SD, it exhibited comparable efficacy in arresting hemorrhage (Arnaud *et al.*, 2008). ACS^+ outperformed SD in a femoral arterial injury model in terms of controlling bleeding and improving survival (60 % versus 13 %) (Arnaud *et al.*, 2009). Although, ACS^+ is only FDA approved for external use, it has shown promise in a Grade IV liver injury swine model where it resulted in significantly mean lower total blood loss than using standard gauze (4.6 mL/kg compared to 8.3 mL/kg) (Inaba *et al.*, 2011). Histopathological findings also did not reveal any significant difference in the amount of necrosis between the groups (Inaba *et al.*, 2011). Eryilmaz *et al.*

demonstrated the beneficial effect of ACS^+ in a extremity arterial injury swine model in providing hemostasis in comparison with the SD (control group) (Eryilmaz *et al.*, 2009). However, Kheirabadi *et al.* examined ACS^+ in an extremity arterial hemorrhage swine model and found that although the application of ACS^+ resulted in no thermal injury at the bleeding site, it was found to be ineffective for hemostasis (B. S. Kheirabadi, Edens, *et al.*, 2009). Rhee *et al.* in their studies concerning 103 documented military and civilian cases, reported that ACS^+ failed to control hemorrhage in a patient who suffered a fracture at the femoral neck resulting from a high-velocity bullet (Rhee *et al.*, 2008). The ineffectiveness of ACS^+ was attributed to the nature of the wound which make the product unable to reach the source of hemorrhage (Rhee *et al.*, 2008).

2.2.4 Other zeolite based hemostats

Other commercial zeolite-based hemostats include QuikClot 1st Response™, QuikClot Sport™ and QuikClot Sport Silver™, which reportedly have less side-effects than QC. Their active ingredients are placed inside a porous mesh bag resulting in a cleaner application and the ability to apply direct manual pressure to the dressing and wound. QuikClot Sport Silver™ offers antibacterial activity for external applications and does not cause burning to the wound site (Suh *et al.*, 2009). As stated previously, when zeolite-based hemostats come into contact with blood, positively charged Ca^{2+} ions in the powder are released immediately in blood stream and the electrostatic attraction between water molecules in blood and the Ca^{2+} ions which reside in open porous internal space result in heat generation (Ahuja *et al.*, 2006). Replacing some of the Ca^{2+} ions with some ions such as Ag^+ not only decreases heat generation at the wound area but offers anti-bacterial activity. Studies relating to zeolite-based agents are shown in Table 2.2.

Table 2.2: Studies relating to zeolite-based hemostatic agents.

References	Model	Hemostatic agents	Treatment groups	Survival	Blood loss	Wound Temperature (°C)	Remarks
(Mahajna *et al.*, 2007)	Massive splenic injury in 40 rats	QC	QC RL QC + RL ND	237.5min 92.2 233.3 153.9	14.1% 61.8% 27.4% 33.69%	38.7 - 39 -	QC application resulted in desirable hemostasis and improved survival. Combination of RL and QC reduced blood loss and improved survival than RL alone. However, increased body temperature was observed in the QC-treated groups.
(Alam *et al.*, 2003)	A complex groin injury in 30 Yorkshire swine	QC RDH TDEX	QC RDH TDEX SD ND	100% 33.4% 66.6% 66.6% 17%	4.4 mL/kg ~15 ~13 ~12 ~22	42-44 - - - -	Among the hemostatic agents tested QC was found to be most effective agent in this model.
(Kozen *et al.*, 2008)	A complex groin injury in 48 swine	QC CX HC	QC CX HC SD	92% 100% 67% 50%	8% 0% 33% 83%	61.0 37.6 38.2 38.8	QC achieved hemostasis with greater efficacy in comparison with HC and SD. However, thermal injury resulting from QC use was observed.
(Acheson *et al.*, 2005)	Femoral artery injury in swine	QC HC FSD	QC HC FSD AFB	0% 0% 66.6% 0%	59.7 mL/kg 86.8 40.8 64.2	70.8 37.1 36.8 36.9	No hemostatic advantage was seen for QC than AFB. In addition, the exothermic reaction of QC with blood produced high temperatures at the bleeding site causing localized tissue damages
(Arnaud *et al.*, 2007)	A groin injury in 32 swine	ACS QC	ACS QC SD ND	75% 75% 12.5% 0%	10.3% 7.4% 22.3% 31.5%	37.8 58.2 58.1 37.5	ACS was equally efficacious as QC in hemostatic properties. It offers easier application and removal compared with QC.
(Ahuja *et al.*, 2006)	A complex groin injury in 60 swine	ACS CD Na-QC Ba-QC Ag –QC SD	ACS HC Na-QC Ba-QC Ag –QC SD ND	90% 75% 57% 75% 75% 50% 0%	10.3 mL/kg ~12 ~16 ~10 ~13 ~17 ~19	55.3 ~37 ~52 ~50 49 ~37 ~37	The modifications in the chemical composition of zeolite decreased the exothermic reaction and attenuated heat induced tissue damage.

Table 2.2: Continued.

References	Model	Hemostatic agents	Treatment groups	Survival	Blood loss	Wound Temperature (°C)	Remarks
(Arnaud *et al.*, 2008)	A groin injury in 33 Yorkshire pigs, including transection of both femoral artery and vein	ACS ACS^+	Evacuated Wound: ACS ACS^+ SD Non-Evacuated Wound: ACS SD	 63.6% 134 min 100% 180 min 12.5% 97 min 67% 131 min 25% 105 min	 18.8% 18.2% 22.3% 8.7% 21.85	 61.4 40.3 38.0 50.8 -	The authors conducted 2 studies: 1 in evacuated wound (blood removed from the wound) and non-evacuated wound (blood in the wound). The lower heat release was associated with ACS^+. Wound temperature in evacuated wound was significantly lower with ACS^+ treatment with respect to ACS treatment.
(Inaba *et al.*, 2011)	A grade IV liver injury in 33 swine	ACS^+ CX	 ACS^+ CX CG ACS+ CX CG	 100% 81.8% 72.7%	Blood loss at 2 min: 4.0 3.5 4.0 Blood loss at 10 min: 4.6 mL/kg 3.7 8.3	 34.2 - -	Application of ACS^+ achieved 100% survival and no significant difference was seen between groups in the extent of necrosis. However, the body core temperature declined further from 35.0°C at the time of injury to 34.2°C on closure.
(Eryilmaz *et al.*, 2009)	Arterial injury in 16 swine	ACS+	 ACS^+ SD ACS^+ SD	 100% 100%	 1100 mL 2800	After 5 min: ~80 ~29 After 15 min: ~30 ~28	ACS^+ was found to be more effective in reducing blood loss. However, peak heat production was observed immediately after 5 minutes. In the following, the heat production significantly decreased at 15 minutes.

Agent defined: Lactated Ringer's solution (RL).

Zeolite-based hemostats, while offering improved hemostatic capability in lethal hemorrhage animal models and in some clinical studies, failed to meet all of the qualifications of the ideal hemostatic agent. The major concerns with the original QC were the difficulty in removing it and the exothermic reaction produced which led to tissue damage at the application site. Although the safety concerns were addressed by the introduction of the newer product (ACS^{+}), which produced minimum exothermic reaction and was easy to use and remove, the product has not been found to be effective against arterial bleeding. Thus, this generation of hemostats was replaced by second-generation dressings such as clay materials which are reportedly more efficient in controlling hemorrhage.

2.3 Clay-based hemostatic agents

Clay minerals are hydrous aluminum silicates consisting of tetrahedral silicates sheets and octahedral aluminate sheets (Ayadi *et al.*, 2013). Based on the ratio of tetrahedral to octahedral sheets, these clays can be classified into two groups, 1:1 clay and 2:1 clay (Rosales-Landeros *et al.*, 2013; Williams *et al.*, 2010). Clay 1:1 is comprised of one silica tetrahedral layer to one aluminum octahedral layer such as kaolin while 2:1 clay consists of an octahedral sheet sandwiched between two tetrahedral sheets such as smectite (Figure 2.6).

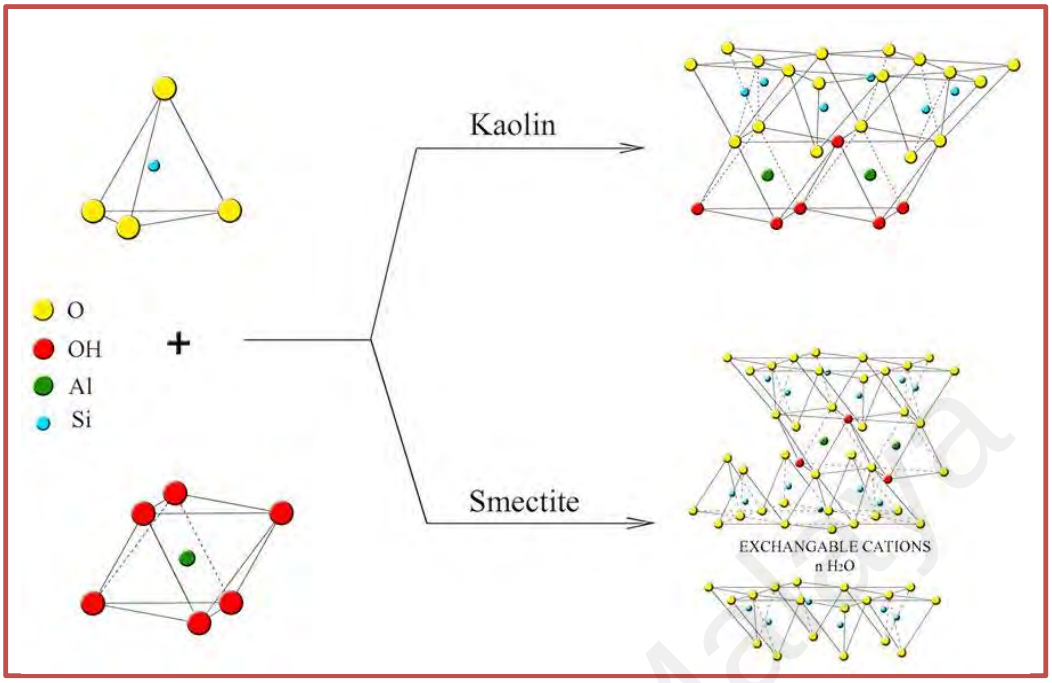

Figure 2.6: The structure of kaolin and smectite.

Clays have high thermal stability, large specific surface area, small particle size, unique crystal structures and significant surface charge as well as ion exchange capability. The materials are also expandable, due to water entrapment between the silicate sheets (Williams *et al.*, 2010). Clays can induce blood clotting and staunch blood flow when applied to a hemorrhaging wound (Bowlin *et al.*, 2012).

2.3.1 Kaolin group

Kaolin is clay consisting of the mineral kaolinite and is a 1:1 clay (Ayadi *et al.*, 2013). The characteristics of kaolin include relatively low surface area, low cation exchange capacity and a minimal charge on the layer (Hayden H Murray, 1999). The absorption property and surface charge of kaolin are low which can be associated with low surface area and substitution of other elements (*i.e.* ferric iron (Fe^{3+}) and Ti^{3+}) for Al

and Si (Hayden H Murray, 1999; Haydn H Murray, 2000). The efficacy of kaolin in the acceleration of the body's natural clotting ability was first recognized by Margolis in 1958 (Margolis, 1958). Kaolin in contact with plasma can lead to the activation of the intrinsic blood coagulation cascade. There are several factors which cumulatively contribute to this ability of kaolin. It has been proven that the polar aluminosilicate framework of the kaolin provides an ideal surface for the contact activation of the intrinsic pathway of the blood clotting cascade, referred to as the "glass effect" (where blood coagulates form quickly upon contact with polar glass-like surfaces compared with non-polar surfaces) (Ostomel *et al.*, 2007). The net negative surface charge of kaolin is also involved in triggering the intrinsic pathway of blood coagulation cascade by the autocatalytic activation of coagulation factors XII and XI along with prekallikrein and cofactor HWK-kininogen (Figure 2.7) (Gegel *et al.*, 2012; Gordy *et al.*, 2011; Griffin, 1978; Walsh, 1972).

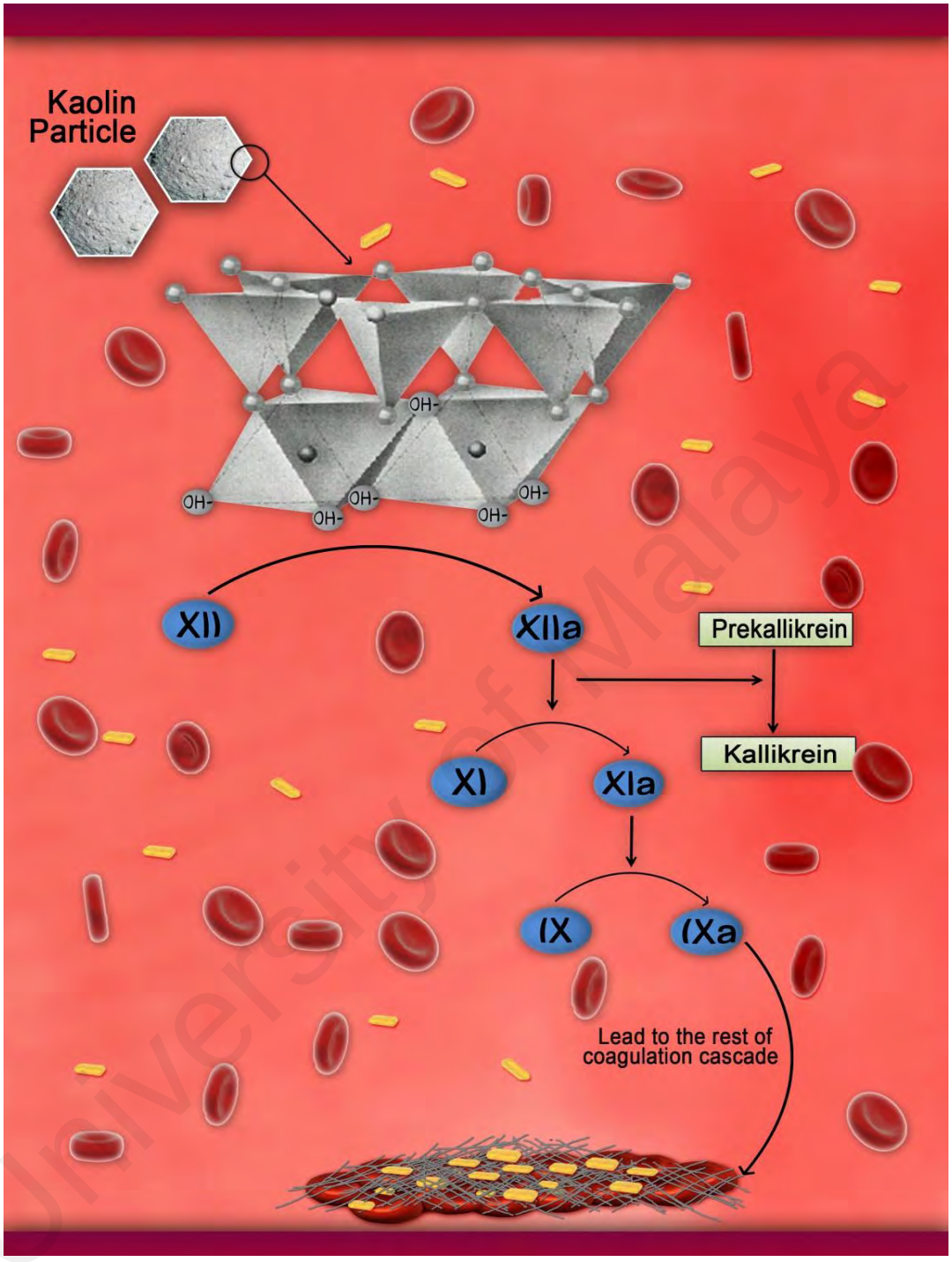

Figure 2.7: Thrombogenic potential of kaolin and its impact on the blood coagulation cascade. This schematic represents the possible effects of kaolin on the activation of intrinsic coagulation pathway through its negative surface charge leading to activation of the coagulation cascade.

The principle behind such phenomena is that factor XII binds to a negatively-charged surface *via* positively charged amino acids in its heavy chain (Colman *et al.*, 1997). The binding supposedly leads to subtle conformational changes in FXII resulting in formation of active FXIIa through auto-activation. This activated factor has been shown to directly contribute to fibrin formation (Huang *et al.*, 2014; Sperling *et al.*, 2009). Hence, the presence of the negative charge on the surfaces of kaolin is considered as a key contributor to the activation of clotting factor XII and subsequently the initiation of the intrinsic pathway of blood coagulation. Kaolin has been marketed under various names including QCG (Z-Media, Wallingford, CT), QCX (Z-Medica, Wallingford, CT) (Figure 2.8).

Figure 2.8: Quikclot Combat Gauze (QCG). The gauzes are impregnated with Kaolin [Reproduced with permission from (Castle *et al.*, 2016; Trabattoni *et al.*, 2012)].

The materials reportedly expedite hemostasis without the complications related to the previous product lines. These products will be discussed in the following sections.

2.3.1.1 QuikClot Combat Gauze (QCG)

QCG is composed of rayon/polyester gauze impregnated with kaolin (Johnson *et al.*, 2012). The dressing was approved by FDA for external application in 2013 (Sena *et al.*, 2013). QCG acts as a pro-coagulant; when it contacts blood, kaolin immediately dissociates from the gauze and activates the intrinsic clotting cascade (Margolis, 1958; Walsh, 1972). In comparison to granular agents, the application and removal of QCG are easily accomplished and require no additional procedures. As an effective, non-absorbable hemostatic dressing in the treatment of external wounds, QCG remains at the wound site for up to 24 hours until further medical care can be provided (Schreiber *et al.*, 2011; Sena *et al.*, 2013). Nonetheless, QCG, unlike other hemostatic dressings, does not provide immediate hemostasis and results in greater blood loss than many other agents (Littlejohn *et al.*, 2011; Schwartz *et al.*, 2011). The CoTCCC chose QCG for all military personal in 2008. It is also recommended as the first-line hemostatic agent for life-threatening bleeding that is not controllable by tourniquet placement (Johnson *et al.*, 2014).

2.3.1.1.1 Animal studies on QCG

The superiority of QCG over the hemostatic dressings HC, TraumaStat (TMS, OreMedix, Lebanon, OR, silica and chitosan based dressing), Celox-D (CX, SAM Medical, Portland, OR, chitosan) and placebo QuikClot gauze (PG, without kaolin) was reported by Kheirabadi *et al*. using an arterial bleeding swine model (B. S. Kheirabadi, Scherer*, et al.*, 2009). QCG increased *in vitro* clotting rate and clot strength and reduced blood loss and demonstrated the highest survival rate (80%) compared to the competitors. The authors ascribed the QCG hemostatic ability to Kaolin's high surface

area and flexibility as well as the type of gauze it was impregnated into (B. S. Kheirabadi, Scherer, *et al.*, 2009).

Johnson *et al.* assessed the efficacy of QCG in femoral artery and vein injury swine models and compared it to a control group which received a standard wound packing (Johnson *et al.*, 2012). QCG application not only markedly decreased the proportion of bleeding than control after 5 minutes (50 mL compared to 351 mL) but also provided more latitude in administration of fluid resuscitation (Table 2.3).

Table 2.3: One minute and five-minute amounts of haemorrhage [Reproduced with permission from (Johnson *et al.*, 2012)].

Group	1-minute bleed	5-minute bleed	Post hoc results
QuikClot Combat Gauze	Range = 149 to 1004 mL (mean = 654, SD ± 283 mL)	Range = 0 to 514 mL (mean = 50, SD ± 154 mL)	One-minute bleed P= 0.83
Control	Range = 100 to 992 mL (mean = 582, SD ± 259 mL)	Range = 0 to 1002 mL (mean = 351, SD ± 354 mL)	Five-minute bleed P= 0.018*

*Significant < 0.05.

The results also demonstrated that the clots formed in the QCG group were more robust than clots formed in the control group so that increased the number of animal movement (3-40 versus 0-9 respectively) with less risk of re-bleeding (Johnson *et al.*, 2012). As a result, QCG was considered an efficient hemostatic dressing.

As QCG is a pro-coagulant agent and its hemostatic function depends on the presence of inherent coagulation factors and the host clotting pathway, there remains some concern about the efficacy of the product in coagulopathic conditions (Martin, 2014). In this regard, some animal studies have been performed to examine the effectiveness of

QCG in both coagulopathy-induced animals (characterized as those that have huge hemorrhage and clotting factor depletion) and non-coagulopathy animal models. In a severe grade V liver injury swine model in which a hypothermic dilutional coagulopathy was induced, use of QCG decreased blood loss from 58 ml/kg in the standard packing group to 25 ml/kg. Based on histological examination, liver sections exposed to QCG were more likely to contain surface clots compared to those exposed to PG. There was no evidence of inflammatory response, tissue necrosis or residual material on the surface of the liver (Sena *et al.*, 2013). In a model of severe acidosis and coagulopathy, Causeys group also proved the utility of QCG, with a successful hemostasis rate of 89 % and 100 % on the first and second application, respectively (Figure 2.9). The efficacy of QCG compared to standard gauze (SG) was also confirmed by a thrombelastograph (TEG) analyzer; a medical instrument that records viscoelastic changes in blood during thrombosis and fibrinolysis. The clotting time declined in QCG-treated animals in comparison to the SG group (19.5 versus 52.33 s) (Causey *et al.*, 2012).

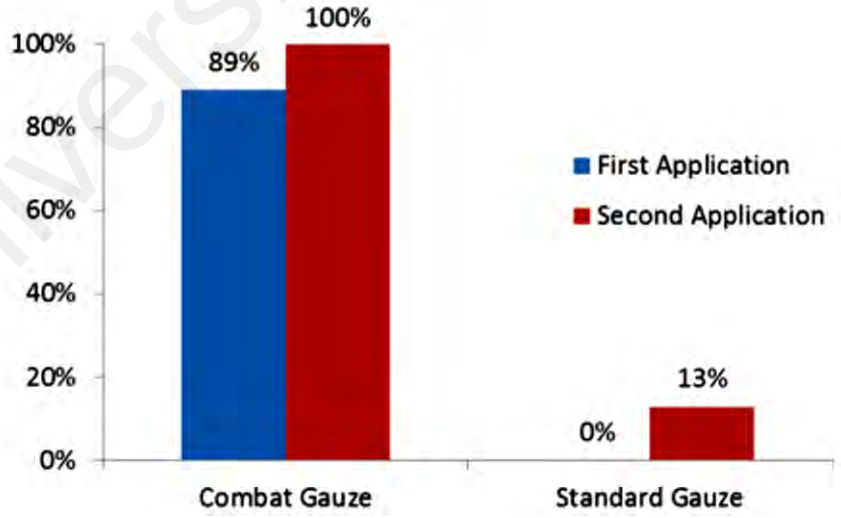

Figure 2.9: Hemostasis success rates of the QCG and SG. The was a 100% success rate with the second application of the QCG, compared with a 13% success rate with the second application of SG [Reproduced with permission from (Causey *et al.*, 2012)].

However, efficacy of QCG was contradicted by Floyd *et al.* who reported 50% animal survival in a hemodilution coagulopathic swine model. This was confirmed on histopathological examination since clotting was only seen in two of the ten QCG-treated wounds (Floyd *et al.*, 2012). The authors suggested that QCG may not be a reliable candidate for external application in coagulopathic combat casualties. However, differences in severity and mechanism of causing coagulopathy in the animals are likely to contribute to these contradictory findings (Bennett, Littlejohn*, et al.*, 2014).

2.3.1.1.2 Human studies of QCG

Ran *et al.* evaluated QCG during 'Operation Cast Lead' in the Gaza Strip in 2009 (Ran *et al.*, 2010). The dressing was used in 14 soldiers of the Israeli Defense Force (out of a total of 56 hemostatic interventions in 35 cases) who experienced injuries in their head, neck, axilla, buttocks, abdomen, back, and pelvis (Ran *et al.*, 2010). QCG achieved hemostasis with 79% efficiency (11 of 14) and a survival rate of 93%. However, it failed to achieve hemostasis in three injuries (neck, buttock, and thigh) and this was associated with the severity of injuries in the soft tissue and vascular system as well as an inability for QCG to be delivered to the bleeding site (Ran *et al.*, 2010). Fedor and coworkers also reported the influence of QCG in a patient with leech bites (Fedor, 2012), where it was found to be an efficient adjunct for treatment of bleeding. There was no evidence of re-bleeding and infection at the site of bleeding (Fedor, 2012). Another beneficial application of QCG was reported by Chavez-Delgado *et al.* (Chávez-Delgado *et al.*, 2014) in a study of 230 patients undergoing tonsillectomy. QCG was seen to be more efficient than standard surgical cotton gauze (CG) in controlling surgical bleeding after tonsillectomy. At 5 min, QCG provided rapid and complete hemostasis in 84.8%

patients compared with 34.8% in the CG group (Chávez-Delgado *et al.*, 2014). Additionally, complete removal of tonsils along with less blood loss and faster postoperative recovery was observed in QCG-treated patients compared to CG-treated patients (34.4 mL versus 54.6 mL respectively). Shina *et al*. also reported a case series of 133 QCG applications on 122 patients at the point of injury (POI). The results proved the utility of QCG, with a successful hemorrhage control in 88.6% of junctional hemorrhage applications (pelvis, shoulder, axilla, buttocks, groin, and neck) and in 91.9% of nonjunctional applications (Shina *et al.*, 2015). A case report from 1 June 2011 to 30 May 2014 by the medical department of the Paris Fire Brigade, also highlights the efficacy surrounding QCG's use in 30 cases in civil prehospital practice. The results demonstrated that the application of QCG led to complete cessations of bleeding in 22 cases, decreases of bleeding in 2 cases, and also found to be ineffectiveness in two cases (Travers *et al.*, 2016).

2.3.1.2 QuikClot Combat Gauze XL (QCX)

Similarly to QCG, QCX consists of hydrophilic gauze impregnated with kaolin. The only difference is that QCX offers a new large size gauze option (a two-ply gauze compared with single-ply gauze in QCG) with a higher kaolin content (approximately 2.7 times more kaolin than the original product) (Rall *et al.*, 2013). QCX causes hemostasis through the activation of the intrinsic clotting pathway and the production of hemostatic clots at the bleeding site (Bennett & Littlejohn, 2014). The product is pliable, conforms to any wound shape and size, is easy to remove and is hypoallergenic. QCX was produced in large samples sizes as injuries have sometimes required two packs of QCG to treat a wound (Smith *et al.*, 2013).

2.3.1.2.1 QCX in animal model

QCX has been successfully used in a swine arterial bleeding model, where it was compared with QCG and three chitosan-based gauzes namely Celox Gauze (CXG, MedTrade Products Ltd, Crew, UK), Celox Trauma Gauze (CTG, MedTrade Products Ltd, Crew, UK) and HemCon ChitoGauze (HCG, HemCon Medical Technologies Inc., Portland, OR) (Rall *et al.*, 2013). QCX and CTG outperformed QCG since they achieved immediate hemostasis in 80% and 70% of applications respectively compared to 30% with QCG (Rall *et al.*, 2013). QCX also resulted in a higher survival rate of 70% than the 60% found with QCG. The differences observed in hemostatic performance of QCG and QCX may be associated with the total mass of gauze or quantity of clotting agent (Rall *et al.*, 2013). Of particular note, however, is that both QCG and QCX did not create any significant tissue damage. The dressing demonstrated some endothelial cell loss near the injury site as well as minor necrosis of the muscle. There were no signs of lesion in any of the nerve tissue examined.

Table 2.4: Studies relating to kaolin based hemostatic agents.

References	Model	Hemostatic agents	Treatment groups	Survival	Blood loss	Remarks
(B. S. Kheirabadi, Scherer, *et al.*, 2009)	Femoral artery injury in 38 swine	QCG HC CX TMS	QCG HC CX TMS PG	167.3 min 0 0 90.0 121	37.4 mL/kg 108.2 113.8 79.8 75.5	QCG was found to be the most efficient dressing tested in this arterial hemorrhage model. The application of HC and CX discontinued after six unsuccessful tests. There was no remarkable rise in wound temperature after treatment with dressings.
(Johnson *et al.*, 2012)	Femoral artery and vein injury in 22 swine	QCG	QCG SD QCG SD	 - -	bleeding in 1 min: 654 mL 582 bleeding in 5 min: 50 351	QCG was superior over the standard pressure dressing control group at controlling hemorrhage and preventing further loss of blood when the limb was vigorously moved. There was no evidence of tissue injury.
(Arnaud *et al.*, 2011)	Femoral artery and vein transection in 12 swine and a femoral artery puncture injury in 16 swine	 QCG TMS	 QCG TMS QCG TMS	transection model: 100% 180 min 100% 180 min puncture model: 88% 174 min 50% 153 min	 0% EBV 1.3% EBV 19% EBV 31% EBV	Both QCG and TMS were found to be effective in achieving hemostasis. However, QCG had the potential to significantly reduce in vitro clotting time compared to TMS.

Table 2.4: Continued

References	Model	Hemostatic agents	Treatment groups	Survival	Blood loss	Remarks
(Sena *et al.*, 2013)	Severe liver injury in hypothermic coagulopathic swine	QCG	QCG PG	87% 50%	25 mL/kg 58	QCG was thought to be safe and effective for the treatment of liver injuries under conditions of hypothermia and coagulopathy. The resuscitation requirements were reduced in QCG group compared with PG group. However, there was no statistically significant difference in mortality since the study size was relatively small.
(Watters *et al.*, 2011)	Femoral artery punch in 24 swine	QCG XG	QCG CXG SD	100% 100% 100%	374 mL 204 260	There was no significant difference in hemostasis between groups. Both QCG and XG did not outperformed SD in this setting.
(Johnson *et al.*, 2012)	Groin injury in swine, including both femoral artery and vein transection in the presence of hemodilution	QCG	QCG SD	- -	36 mL 340	QCG was superior over SD in controlling hemorrhage and provided a more robust clot that effectively tolerates hemodilution in comparison with SD groups.
(Inaba *et al.*, 2013)	Grade IV liver injury in 48 swine	QCG CX CXG	QCG CX CXG SG QCG CX CXG SG	48hour survival: 58.3% 83.3% 41.7% 50.0% 14 days survival: 50.0% 58.3% 41.7% 41.7%	Blood loss at 15 min: 5.3 mL/kg 5.7 10.1 11.1	QCG and CX have been shown to be more effective hemostatic adjuncts than SG for providing hemostasis in this model. However, there was observed four and two deaths in CX and QCG groups respectively due to bowel obstruction.

Table 2.4: Continued.

References	Model	Hemostatic agents	Treatment groups	Survival	Blood loss	Remarks
(Sena *et al.*, 2013)	Severe liver injury in hypothermic coagulopathic swine	QCG	QCG	87%	25 mL/kg	QCG was thought to be safe and effective for the treatment of liver injuries under conditions of hypothermia and coagulopathy. The resuscitation requirements were reduced in QCG group compared with PG group. However, there was no statistically significant difference in mortality since the study size was relatively small.
			PG	50%	58	
(Rall *et al.*, 2013)	Femoral artery injury in 50 swine	QCX	QCX	70%	32 mL/kg	The outcomes with the QCX were significantly better than with QCG in this model.
		QCG	QCG	60%	62	
		CTG	CTG	50%	65	
		CEL	CEL	90%	29	
		HCG	HCG	70%,	40	
(Chávez-Delgado *et al.*, 2014)	230 patient undergoing tonsillectomy	QCG	QCG	-	34.4 mL	84.8% of QCG-treated patients experienced complete hemostasis at 5 min, while only 34.8% of CG-treated patients had partially stopped bleeding. At 10 min, hemostatic success achieved in 91.3% of the QCG group versus 51.1% of CG group.
			CG	-	54.6 mL	

In summary, with respect to outcomes from animal models and sparse clinical trial data, kaolin based hemostatic agents deliver superior hemostatic power when compared to zeolite-based hemostats. The materials can promote hemostasis without complications as gauze rolls are highly efficacious hemostatic dressings for temporary treatment of external wounds (Granville-Chapman *et al.*, 2011). Accordingly, the first kaolin based hemostat; QCG was fielded from 2008 for all U.S. military personnel and NATO militaries as a primary hemostatic dressing. Though the hemostatic abilities of these inorganic materials are more pronounced than those of other hemostats, the main disadvantage of these dressings is that they may not stop bleeding immediately after application and often require more than one application (B. Kheirabadi, 2011). Another disadvantage of the kaolin hemostats is that these dressings may be less effective in coagulopathic patients since their hemostatic function depends solely on the blood-clotting activity of hosts (B. Kheirabadi, 2011). It was also found that the QCG is not appropriate for long-term use since its long-term application might increase the risk of coagulopathy leading to the progressive stage of shock (Otrocka-Domagała *et al.*, 2016). Furthermore, with long-term use of QCG, residues from the dressing can enter systemic circulation, thereby raising the risk of embolus formation (Otrocka-Domagała *et al.*, 2016). Hence, there is still a need to produce a fast-acting hemostatic agent which can address this deficiency.

2.3.2 Smectite group

Smectite clays are 2:1 clay minerals consisting of an octahedral alumina layer sandwiched between two tetrahedral silica layers (Williams *et al.*, 2010). Smectite displays several properties including a large surface area, a large cation exchange

capacity and high viscosity resulting from their small particle sizes (Hench, 1998). They can absorb large amounts of water attributed to their structure (Hench, 1998). In comparison to kaolin, smectite demonstrates higher plasticity, absorption, swelling and viscosity making it an excellent candidate for a wide range of industrial and medical applications (Hench, 1998; Hayden H Murray, 1999; Haydn H Murray, 2000). When smectite is exposed to blood, its negative surface charge leads to the activation of the intrinsic coagulation pathway (B. S. Kheirabadi, Edens, *et al.*, 2009). Smectite has been commercialized as WS (TraumaCure, Bethesda, Maryland, USA) (Figure 2.10).

Figure 2.10: WS granules consisting of smectite minerals [Reproduced with permission from (B. Kheirabadi, 2011)].

2.3.2.1 WoundStat (WS)

WS was developed by the Virginia Commonwealth University Medical Center and consists of smectite and a super water absorbent poly-acrylic acid salt (Ward *et al.*, 2007). It was approved by the FDA in 2007 for emergency external use. This product is supplied in granular form and was added to Tactical Combat Casualty Care (TCCC)

guidelines in 2008 (Gordy *et al.*, 2011; Granville-Chapman *et al.*, 2011). WS works primarily as a mucoadhesive agent and forms a barrier to bleeding through cross-linking cellular blood components. Upon exposure to blood, WS absorbs water rapidly and swells into a clay paste with high plasticity and strong adhesiveness. Similarly to QCG, it also possesses potent pro-coagulant activity since it carries a negative charge and can activate the coagulation cascade (Carraway *et al.*, 2008; B. S. Kheirabadi, Edens, *et al.*, 2009). The main advantages of WS include its facile use (it can be poured in the wound), conformability for all kinds of wound cavities and durability (Carraway *et al.*, 2008; Schreiber *et al.*, 2011). It is also non-toxic and does not generate heat unlike zeolite-based products. However, WS is non-biodegradable and has to be physically removed from the wound area (Granville-Chapman *et al.*, 2011). Unlike QCG, WS has demonstrated faster hemostasis onset (Arnaud *et al.*, 2009).

2.3.2.1.1 WS in animals

Two studies have assessed the efficacy of WS in an arterial hemorrhage swine model (B. S. Kheirabadi, Edens, *et al.*, 2009; Ward *et al.*, 2007). In the first study, 100% survival rate in animals treated with WS was reported compared to 0% using other hemostatic agents including QC, HC, ACS^+ and AFB (control group) (Ward *et al.*, 2007). In the second study by Kheirabadi *et al.,* WS conferred considerable benefits with respect to decreased blood loss and increased survival time compared to Super Quick Relief (SQR, Biolife, LLC, Gainesville, FL, USA), CX, HC and ACS^+ (Figure 2.11). WS had a significantly higher hemostasis success rate than the SQR and CX groups (100 % in WS-treated animals versus 70 and 60 % in the SQR and CX groups respectively). However, histological examination revealed some residual particles in the arteries

treated with WS which may lead to thromboembolic complications (B. S. Kheirabadi, Edens, *et al.*, 2009).

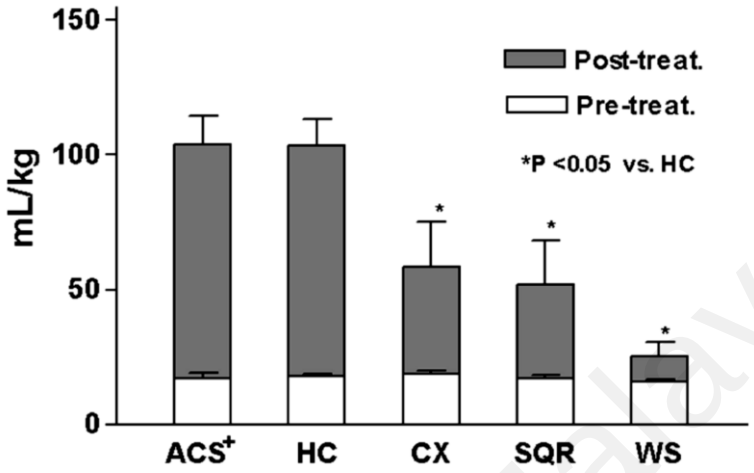

Figure 2.11: Total blood loss in pig injury models. Average values of pre-treatment and posttreatment blood losses in the ACS^{+}-, HC-, CX-, SQR-, and WS-treated pigs [Reproduced with permission from (B. S. Kheirabadi, Edens, *et al.*, 2009)].

WS has also been reported to offer 100% survival alongside reduced blood loss, compared to HC, CX and ACS^{+} in a model of mixed arterial and venous femoral injuries (Clay *et al.*, 2010). It developed a red clay-like texture that allowed the dressing to conform easily to the shape of the wound. However, the efficacy of WS in stopping bleeding was contradicted by Kheirabadi *et al.* (Bijan Shams Kheirabadi *et al.*, 2010), who reported that WS was ineffective compared to QCG and achieved hemostasis in only 2 out of 15 cases (Bijan Shams Kheirabadi *et al.*, 2010). Based on histologic examination, more damage to endothelium, smooth muscle, and adventitia experienced by WS-treated vessels compared with the other groups. WS along with some residues were also found in the lumen of arteries as well as on the adventitia of arteries and veins. Studies relating to WS are presented in Table 2.5.

Table 2.5: Studies relating to smectite-based hemostatic agent.

References	Model	Hemostatic agents	Treatment groups	Survival	Blood loss	Remarks
(Ward *et al.*, 2007)	Femoral artery vascular injury in 25 swine	WS QC ACS^+ HC	WS QC ACS^+ HC AFB	100% 0% 0% 20% 0%	1.9 mL/kg 54 62.7 76.8 59.7	WS was superior to all the other hemostatic agents tested in this study.
(B. S. Kheirabadi, Edens, *et al.*, 2009)	Femoral artery injury in 46 swine	WS CX HC ACS^+ SQR	WS CX HC ACS^+ SQR	180 min 138 83.3 0 164	9.5 mL/kg 40 85.6 86.8 34.5	WS was more efficient in treating arterial hemorrhage followed by SQR and CX powders. The application of ACS+ was stopped after 6 animals. A dramatic increase in temperature and axonal necrosis were observed in SQR group. The least and moderate tissue damage were observed with HC and with WS respectively.
(Clay *et al.*, 2010)	Femoral artery and vein injury in 30 swine	WS CX HC ACS^+	WS CX HC ACS^+ AFD	100% 83% 67% 50% 0%	4.6 mL/kg 12.9 10.0 15.8 27	Although, WS appeared more effective than other agents in providing hemostasis, it was more difficult to remove and copious irrigation was required for complete removal.
(Gerlach *et al.*, 2010)	Femoral artery injury in 21 swine	WS	WS PG	100% 100%	- -	Although, WS was an effective hemostatic agent, it revealed severe diffuse moderate myocyte necrosis and fibrogranulomatous inflammation.
(Bijan Shams Kheirabadi *et al.*, 2010)	Femoral artery injury in 55 hypothermic, coagulopathic swine	WS QCG FAST	WS QCG FAST GZ	75 min 119 145 74	- - 18.2 mL/kg 63.3	WS was ineffective under coagulopathic conditions. FAST dressing demonstrated the highest efficacy since it delivers fibrinogen and thrombin to the wound.

Agents defined: Standard army field dressing (AFD), Gauze (GZ), fibrinogen-based dressing (FAST).

The major concern with WS is the possibility of thrombosis in distal organs such as the brain and lungs (Williams *et al.*, 2010). The application of WS can also cause local inflammatory response and damage to an inner layer of blood vessels and can be accompanied by excessive clotting, traveling of the clot and its entering to the circulatory system, causing thrombosis in distal organs (Bijan S Kheirabadi *et al.*, 2010; Schreiber *et al.*, 2011). Kheirabadi *et al.* compared the safety of WS with QCG and Kerlix (KX, Covidien, Mansfield, MA, regular gauze) in an animal model with both arterial and venous injuries (Bijan S Kheirabadi *et al.*, 2010). Computed tomography angiography revealed that the majority of WS-treated vessels were occluded by the formation of a thrombus layer inside the vessel; whereas no blood clot or thrombus was seen in QCG- or KX-treated vessels. WS residues and thrombus were also found in the lungs of two subjects. As can be seen from Figure 2.12, direct observation also confirmed the occlusion WS-treated vessels by huge thrombi. Histological evidence emphasized the presence of considerable endothelial and transmural damage in subjects treated with WS. Hence, WS is considered inferior to QCG since its use can result in thromboembolic risk (Bijan S Kheirabadi *et al.*, 2010).

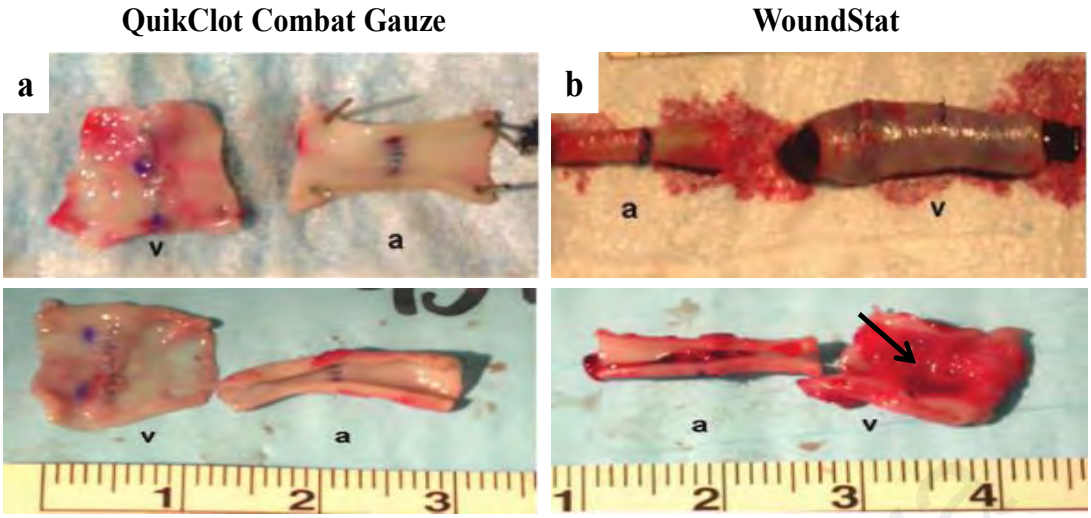

Figure 2.12: QCG- or WS-treated arteries (represented by a) and veins (represented by v) from the pigs which were taken instantly after recovery (Bijan S Kheirabadi *et al.*, 2010). Direct observation of (a) the QCG-treated vessels when the wounds were reopened indicated there is no significant thrombus or blood clot in the vessels after recovery. In contrast, direct observation of (b) both veins and arteries treated with WS represented large red clots with no blood flow *via* the vessels. As the arrow shows, a red thrombus layer covered the entire inner wall in the vein [Reproduced with permission from (Bijan S Kheirabadi *et al.*, 2010)].

There are additional safety concerns related to the cellular toxicity of WS. In a study by Bowman *et al*. the *in vitro* cellular toxicity of WS in different cell types was assessed in comparison with other minerals such as bentonite, kaolin (the principal ingredient of QCG), and zeolite (the main component of ACS^{+}) (Bowman *et al.*, 2011). Results showed that both WS and the bentonite presented higher cytotoxicity on endothelial and macrophage-like cells (are present in wounds) compared with other minerals. The authors claimed that direct contact of WS and bentonite with these cells are the principle cause of cytotoxicity. It was found that the hemostats containing kaolin and zeolite such as QCG and ACS^{+} result in lower toxicity. Indeed, since kaolin is coated on gauze (QCG) and zeolite is packaged in small porous bags, their contact with tissues is limited which may, in part, explain the lower toxicity. Although WS has been reported to be an effective hemostatic offering improved survival over standard gauze dressing (Smith *et al.*, 2013), it can cause significant

inflammatory response, neurovascular changes, necrosis and extensive bleeding (Smith *et al.*, 2013). Removal of WS also requires extensive and meticulous debridement (Bijan S Kheirabadi *et al.*, 2010). Although it was temporarily considered as a backup agent to a gauze-type hemostatic for combat medical personnel (Bijan S Kheirabadi *et al.*, 2010), based on subsequent animal safety studies, the use of WS was halted by the U.S. Army in 2009 with the FDA recommending that it should be removed from the United States market (Bijan S Kheirabadi *et al.*, 2010).

2.4 Challenges and perspective

In spite of improvements in surgical techniques and the development of various hemostatic agents, hemorrhage still remains the leading cause of morbidity and mortality. Inorganic materials have shown to be effective in arresting hemorrhage. The net negative surface charge of inorganic hemostats serves as an ideal platform for activating proteins as well as activation of the contact pathway of coagulation. Also, their structural properties allow the materials to rapidly absorb high amounts of water from the blood, and to concentrate the cells, platelets and clotting factors at the bleeding site thus promoting hemostasis. However, from this section which has assessed the *in vivo*, *in vitro* and clinical responses to applying zeolite, kaolin and smectite-based hemostats for controlling hemorrhage, it is clear that none of the agents have proven to be suitable for all trauma scenarios in normal and coagulopathic casualties. Although zeolite-based hemostatic agents were efficacious for achieving hemostasis, the materials caused thermal injury to tissue through exothermic reaction. Kaolin-based hemostats have appeared to be more efficient than zeolite hemostats, but several studies revealed that the kaolin hemostats may be ineffective to stop bleeding in patients with coagulopathy since their efficacy

depends on the individual coagulation function of the host. With regard to smectite-based hemostats, although applying and covering the wound with this agent achieves hemostasis with high survival rates, endothelial injury has been reported to occur, leading to occlusive thrombus and the absence of blood flow in the vessels.

2.5 Mesoporous SiO_2 materials

The term nanoporous materials refers broadly to materials possessing pore sizes of 100 nm or less. Depending on the characteristic pores length (d), nanoporous materials can be categorized into three groups: microporous ($d < 2$ nm), mesoporous ($2 \text{ nm} < d < 50$ nm), and macroporous ($d > 50$ nm) classes (Rouquerol *et al.*, 1994).

Silica-based ordered mesoporous materials (SMMs) has recently attracted worldwide attention because of their good biocompatibility, low cytotoxicity, thermal stability, tailorable surface charges as well as having larger pore sizes than zeolites (Gonzalez *et al.*, 2013; Rahmat *et al.*, 2010). The materials were first introduced in the early 1990s (Kresge *et al.*, 1992). These porous materials are structurally unique, exhibiting disorder on the atomic scale and well-defined order on the mesoscopic-scale (2–50 nm). In the synthesis of SMMs, organic surfactant molecules play a pivotal role to generate porosity and therefore can act as template or structure directing agent (SDA). Two different mechanisms are involved in the formation of these materials, namely true-liquid-crystal template (TLCT) and cooperative liquid crystal template (CLCT) mechanisms (Vallet-Regí, Garcia*, et al.*, 2012). In the TLCT mechanism (Route 1), the surfactant concentration is above the critical micellar concentration (cmc) so that under the prevailing conditions (temperature, pH), the surfactant molecules would aggregate themselves to form the liquid-crystalline phase without requiring the presence of the inorganic precursors

(Figure 2.13a) (Vartuli *et al.*, 1994). It is notable that this supramicellar structures can present different geometries such as cubic, laminar or hexagonal, depending on the chemical nature of the surfactant and the synthetic condition (Vallet-Regí, Garcia, *et al.*, 2012). In the following step, when silica precursors, normally tetraethyl orthosilicate (TEOS) or tetramethyl orthosilicate (TMOS), is added to the liquid crystals, a sol-gel chemistry begins to hydrolase and condensate those precursors to yield highly condensed silicon oxide around that supramicellar aggregates. After the formation of this inorganic–organic hybrid material, in order to obtaining the silica material with an ordered mesoporous framework, the surfactant need to be removed which can be carried out by thermal treatment (calcination) or solvent extraction (Beck *et al.*, 1992; Linares *et al.*, 2014; Vartuli *et al.*, 1994).

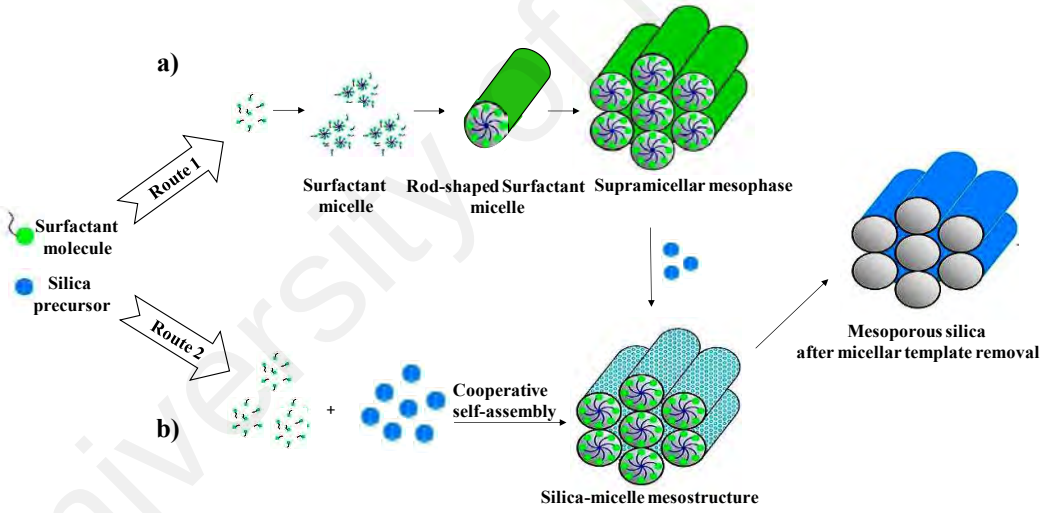

Figure 2.13: Formation of mesoporous structures: (a) via TLCT (Route 1), (b) via CLCT (Route 2).

On the other hand, in the CLCT mechanism (Route 2), in which the surfactant concentration is below the cmc, a lyotropic liquid crystalline phase can be developed *via* a cooperative self-assembly of the SDA and the already added inorganic precursors, leading to formation of ordered mesostructured with hexagonal, cubic, or

laminar arrangement (Figure 2.13b) (Vallet-Regí, Garcia*, et al.*, 2012). As explained in the TLCT mechanism, in the final step of the synthetic process, the template need to be removed resulting in the formation of a network of cavities within the silica framework. As a consequence, through these methods, SMMs are obtained with outstanding properties, such as: (i) regular and tunable meso-pore size (2–50 nm), (ii) high surface area (*ca*. 1000 m^2/g), (iii) large pore volumes (*ca.* 1 cm^3/g), (iv) homogeneous pore morphology and (v) stable mesoporous structure (Izquierdo-Barba *et al.*, 2015). These features lead to these materials being used as a suitable candidate for many potential application such as in adsorption/separation, catalysis as well as biomedicine (Huirache-Acuña *et al.*, 2013; Luque *et al.*, 2012). Over the past two decades, researches on the SMMs has demonstrated their suitability for two new applications including drug-delivery and bone regeneration applications based on their unique textural properties. The materials found to be able to load and subsequently controllably release numerous drugs and biological active molecules. (Baeza *et al.*, 2015; Slowing *et al.*, 2007; Song *et al.*, 2017; María Vallet-Regí *et al.*, 2007). Additionally, *in vitro* bioactivity of three typical SMMs including Mobil Composition of Matter No. 41 (MCM-41), Santa Barbara Amorphous (SBA-15) and Mobil Composition of Matter No. 48 (MCM-48) was investigated and the materials have shown to have the potential to form an apatite-like layer on their surfaces when soaked into a simulated body fluid (SBF), allowing their use for bone tissue regeneration (Izquierdo-Barba *et al.*, 2008).

2.6 Mesoporous bioactive glasses (MBGs)

A new generation of nanostructured bioceramics, referred to as MBGs from the 80%SiO_2–15% CaO–5%P_2O_5 system, was first developed by Yan *et.al* in 2004 by

combination of sol-gel and supramolecular routes characteristics of sol-gel derived bioactive glasses (SGGs) and SMMs, respectively (Yan *et al.*, 2004) (Figure 2.14).

In this strategy for the preparation of MBG, the incorporation of the SDAs such as Pluronic P123, F127 and Cetyltrimethyl ammonium bromide (CTAB) is vital for acquiring well-ordered structures similar to that for SMMs (Jiang *et al.*, 2012b). Under appropriated synthesis conditions, the mixture reaction system of SGGs and SDAs undergoes an EISA process. Generally, the EISA is defined as the spontaneous organization of materials via non-covalent interactions (electrostatic forces, hydrogen bonding, van der Waals forces and etc.) without any external intervention (Brinker *et al.*, 1999). The EISA process starts with a homogeneous solution of SGG precursors (Si, Ca and P elements, etc.) and surfactant prepared in ethanol/water. The concentration of the system is progressively increasing through the ethanol evaporation until it reaches the cmc which drives to self-assembly of micelles with spherical or cylindrical structure (Izquierdo-Barba *et al.*, 2013). These micelles maintain the hydrophilic components of the surfactants in contact with the SGG composition (Si, Ca and P elements, etc.) whereas shielding the hydrophobic components within the micellar interior (Jiang *et al.*, 2012b). Finally, a well-ordered mesoporous structure will be obtained after removing the surfactant by calcination or extraction methods.

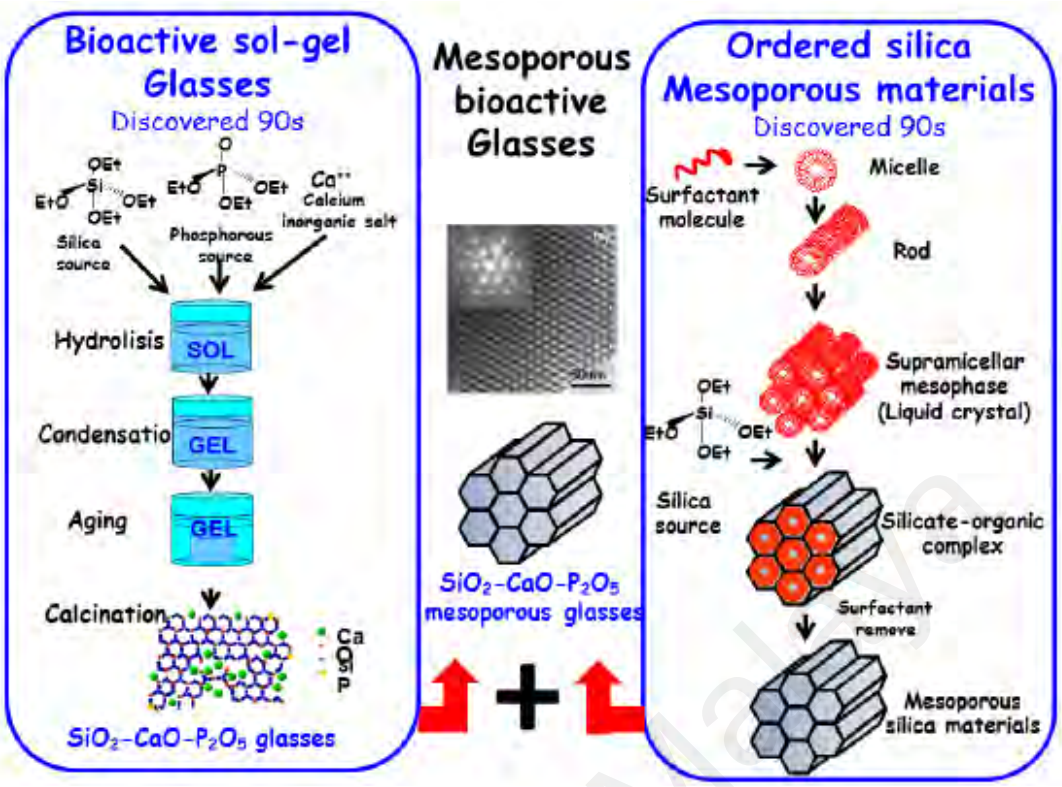

Figure 2.14: Schematic representation demonstrating the synthesis of MBGs based on the combination of sol-gel technology and the supramolecular chemistry [Reproduced with permission from (Izquierdo-Barba *et al.*, 2015)].

Similarly to conventional SGGs, MBG exhibit the amorphous atomic structure in the SiO_2-CaO-P_2O_5 system and also shares the same structural and textural properties of SMMs displaying highly ordered mesoporous arrangement with pore size ranging from 2 to 10 nm (Izquierdo-Barba *et al.*, 2015). However, the main differences between MBGs and SGGs can be summarized basically in the mesoscale which is not presented in SGGs (Figure 2.15) (Izquierdo-Barba *et al.*, 2013).

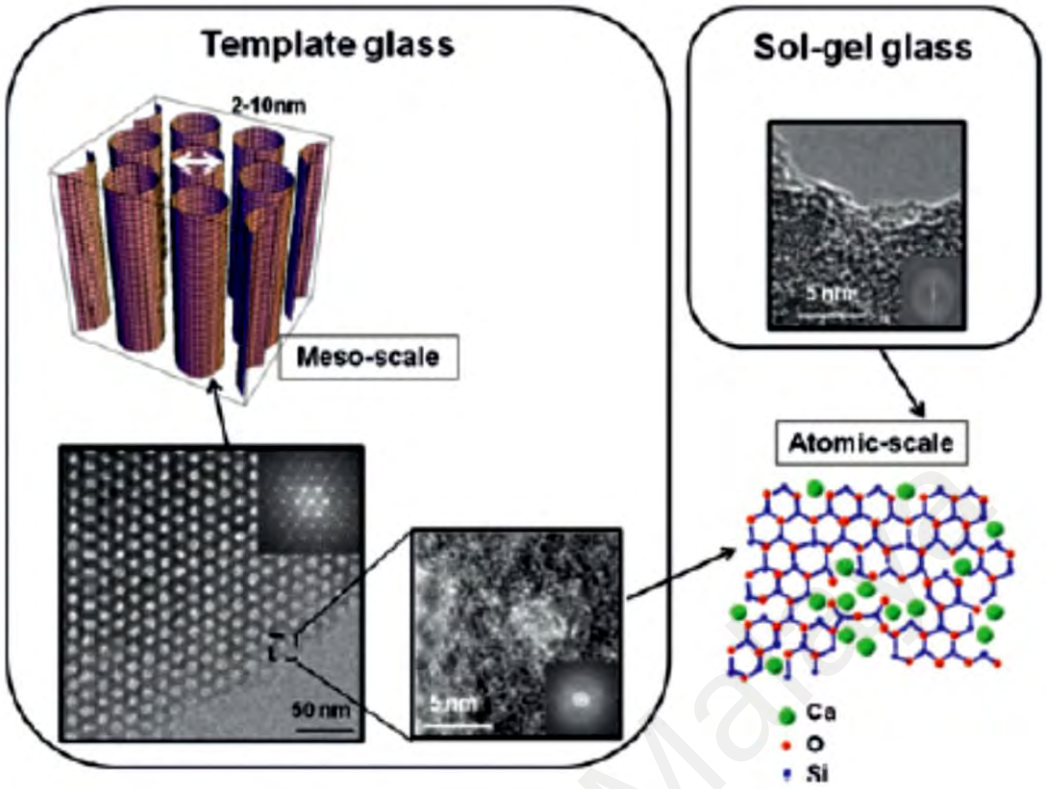

Figure 2.15: Transmission electron microscopy image of SGGs and MBGs. At atomic level, both bioglasses are similar representing a Si–Ca–P amorphous network. The main differences between the bioglasses can be attributed to presence of highly ordered mesoporous arrangement of cavities in MBGs [Reproduced with permission from (Izquierdo-Barba *et al.*, 2013)].

This ordered mesoporous arrangement in MBGs can produce surface area and pore volume remarkably larger than those obtained in SGGs (Izquierdo-Barba *et al.*, 2013; Vallet-Regí, Izquierdo-Barba, *et al.*, 2012). These outstanding features resulted in materials with improved *in vitro* bioactivity response and excellent cytocompatibility as compared with conventional SGGs thus making them attractive for bone tissue engineering applications (Yan *et al.*, 2004) (Alcaide *et al.*, 2010; Jiang *et al.*, 2012b; Philippart *et al.*, 2017; Zhang *et al.*, 2016; Y. Zhou *et al.*, 2017).

Additionally, the excellent surface properties and porosity as well as their ability to be functionalised allow the use of MBGs as local-controlled delivery systems of drugs (antibiotics and /or osteogenic agents) to treat bone pathologies (Figure 2.16)

(Izquierdo-Barba *et al.*, 2015; Y. Li *et al.*, 2013) (Xiaojian Wang *et al.*, 2016; Xiang Wang *et al.*, 2016; C. Wu *et al.*, 2012).

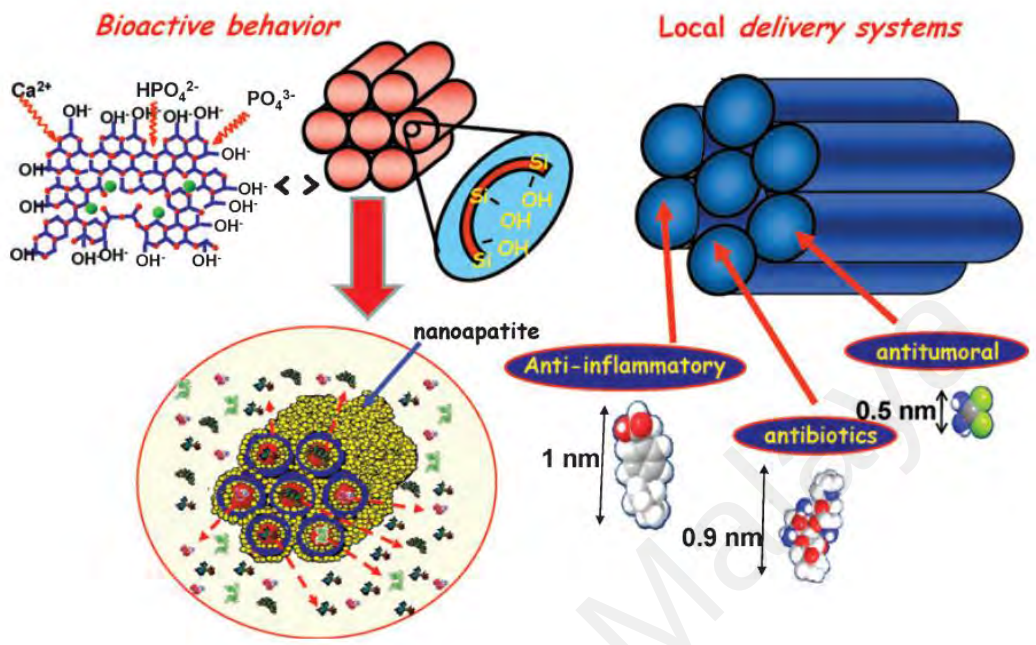

Figure 2.16: Schematic diagram depicting the application of silica-based mesoporous materials for biotechnologies [Reproduced with permission from (M Vallet-Regí, 2010)].

Recently, the studies of the applications of mesoporous materials have been expanded into another field of biomaterial science including hemostatic application. Both SMMs and MBGs produced beneficial results when exploited as hemostatic agents in cessation of bleeding. The materials provide a negative surface that promotes coagulation of blood *via* contact activation, or the intrinsic pathway (Figure 2.17); Additionally, the materials featuring high porosity and surface area can achieve a hemostatic effect by absorbing water in the blood and condensing the clotting factors and platelet, subsequently acceleration of blood clot formation.

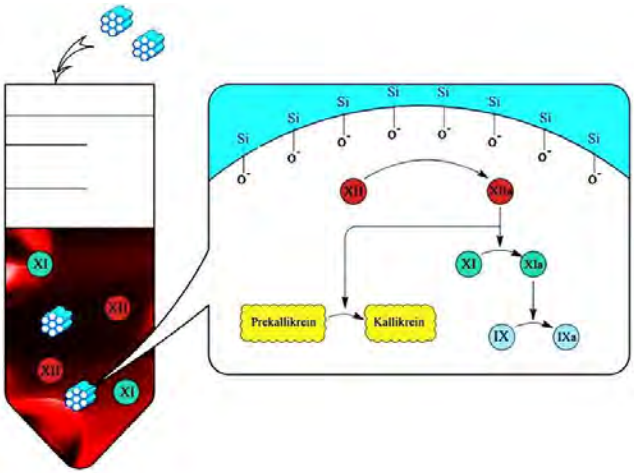

Figure 2.17: Initiation of intrinsic pathway and expected outcome with negatively charged surfaces of silica-based mesoporous materials.

In addition to available surface area and porosity in the MBGs, Si:Ca ratio and availability of Ca^{2+} ions are important parameters that contribute to hemostatic ability of MBGs (Ostomel, Shi, & Stucky, 2006). Ca^{2+} ions (known as clotting factor IV) play a key role in the immobilization and orientation of clotting enzymes on cellular surfaces, since they serve as the ionic bridge between two negatively charged residues (i.e. cellular surface and clotting factors) (Holden *et al.*, 2010). The ions are consumed within thrombosis and fibrinolysis when fibrin and negatively charged glycosylated residues are cross-linked by Factor XIII (Holden *et al.*, 2010). Hence, the presence of these ions in MBG framework can stimulate the activation of the intrinsic pathway and accelerate the generation of required thrombin for fibrin production.

Apart from this effect, the accessibility of Ca^{2+} ions can also contribute to degradability of these materials, since it increases non-bridging oxygen at the mesoporous silica network (Dai *et al.*, 2009), decreases the silica network connectivity and subsequently accelerates silica network dissolution (Dai *et al.*, 2009; X. Li *et al.*, 2007). The water adsorption ability of MBG is also improved by the Ca^{2+} ions that reside in the pores. Indeed, the electrostatic attraction between

water and Ca^{2+} ions may result in enhanced water adsorption (Halkier, 1991; Hoffman, 2003).

Although, the materials share with zeolite a similar mechanism of action, they would not cause extensive injury in tissues since exhibited very mild exothermic effects (Dai *et al.*, 2010). It is hypothesized that alumina silicate as the main component of zeolite play a fundamental role in production of heat while transitioning from dehydrated to a hydrated form (Mukherjee, 2012). On the contrary, as the mesoporous silica is comprised of amorphous silica, it can remarkably decrease the inherent exothermic reaction as well as tissue thermal injuries and thus overcoming the dangerous side effects of the zeolites minimizing collateral damage.

Therefore, the synergism of all parameters presented above, render both SMMs and MBGs as interesting candidates for hemostatic clinical application. There are some studies concerning the hemostatic efficacy of the materials which will be discussed in the following section.

2.7 The hemostatic potential of SMMs and MBGs

Chen *et al*. investigated the hemostatic ability of mesoporous silica nanoparticles (MSN) with various pore size and particle size (Z. Chen *et al.*, 2016). The results of clotting blood tests (CBT) displayed that variation of pore sizes of MSN from 5 nm to 15 nm significantly affected the blood coagulation rate of rabbit plasma, while its particle sizes varying from 60 nm to 220 nm had little influence on blood coagulation (Figure 2.18). It was found that MSN with larger pore size (15 nm) possessing the high internal surface area that is accessible to contact activation proteins, has promising ability to promote the blood clot formation. The pore size also impacted the endothelial cell viability so that the larger pore size resulted in better

biocompatibility. The superior hemostatic efficiency of MSN with pore size of 15 nm also was testified *in vivo* since the material achieved rapid hemostatis in rabbit femoral artery injury (Figure 2.18).

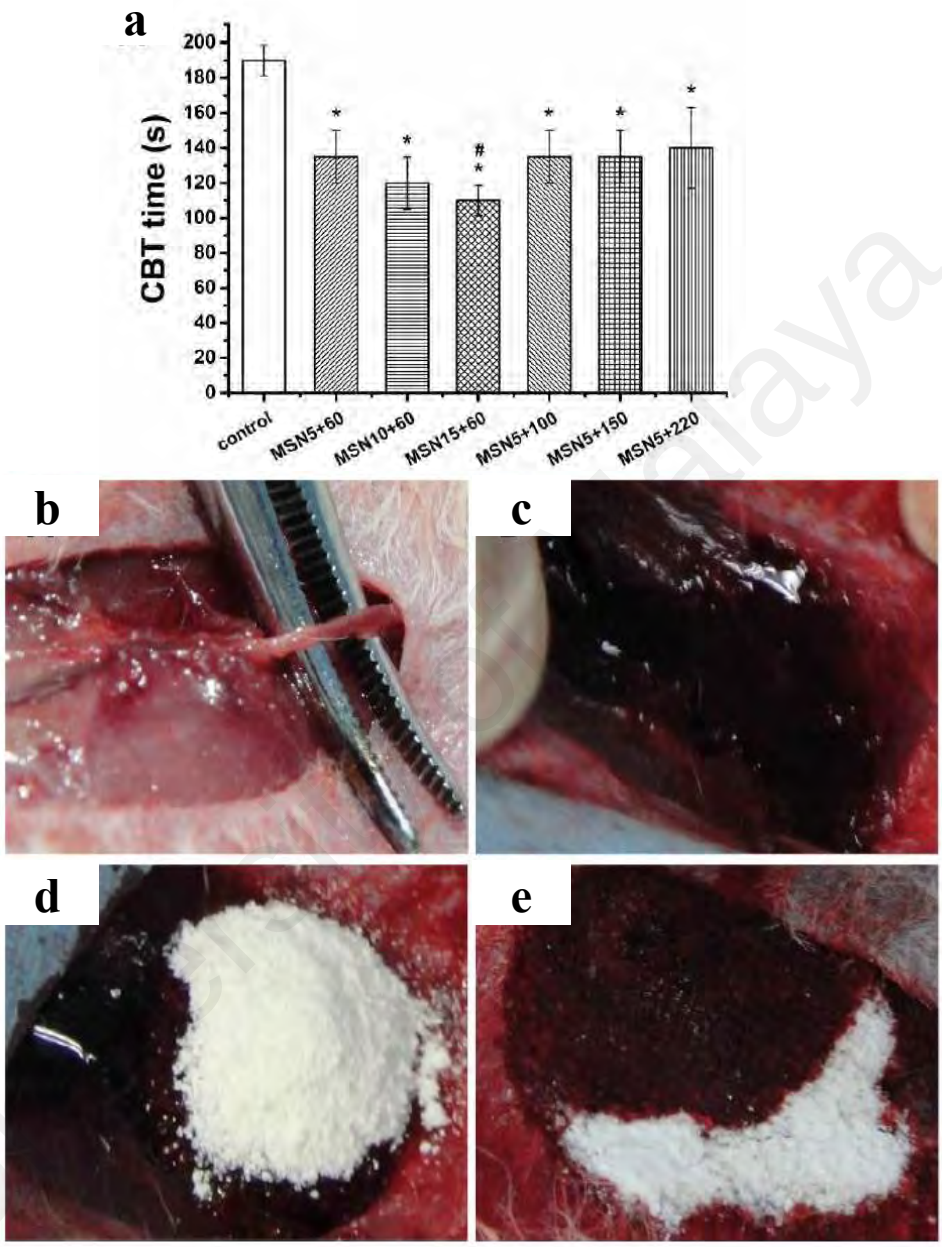

Figure 2.18: (a) CPT time for MSN. CPT time was shortened with respect to the control. The CBT results indicate that MSN with large pore size have better hemostatic performance. However, the hemostatic performance of MSN was not influenced by the particle size. Hemostasis in rabbit femoral artery injury. (b) Creation of injury in femoral artery. (c) Profuse bleeding instantly after injury creation. (d) Pouring MSN into the inguinal cavity to mask the injury completely after free bleeding for 10 s. (e) Bleeding stopped after manual pressure was applied over the injury [Reproduced with permission from (Z. Chen *et al.*, 2016)].

In a study by Wu *et al*. (X. Wu *et al.*, 2010), the influence of the surface area, mesoporous structure and Ca^{2+} inclusion on the hemostatic responses of mesoporous silica xerogels (MSX) was investigated. In this regard, MSX doped with various amounts of CaO (0, 5 and 10%) were produced and screened for their *in vitro* blood coagulation ability using prothrombin time (PT) and activated partial thromboplastin time (APTT) as compared with non-mesoporous silica xerogels (SX) (X. Wu *et al.*, 2010). The results revealed that both APTT and PT was considerably decreased by m-SXC0 (m-SX without Ca) as compared with SX (Figure 2.19).

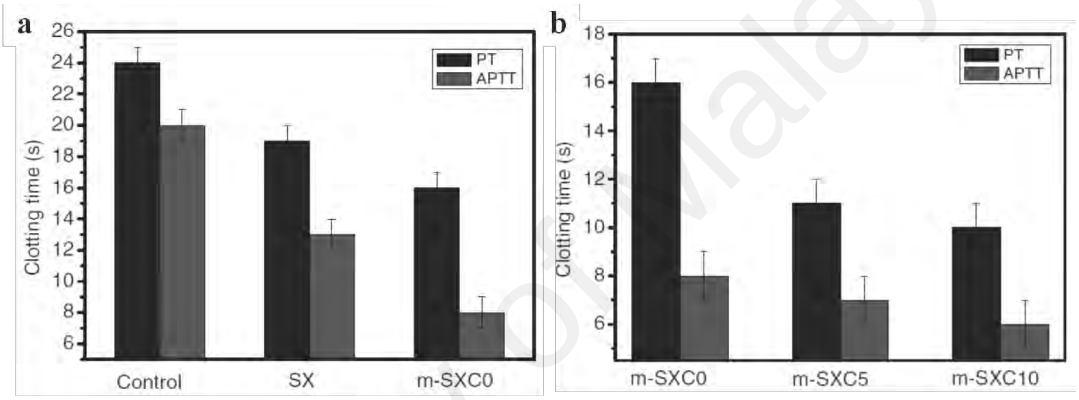

Figure 2.19: Effect of (a) mesoporous stucture and (b) Ca content on APTT and PT [Reproduced with permission from (X. Wu *et al.*, 2010)].

It was also found that the inclusion of higher Ca content in the m-SX framework (m-SXC10) resulted in a decrease of the both APPT and PT (Figure 2.19). The m-SXC samples also demonstrated greater water absorption potential (89%) in comparison with SX (31%). The results confirmed that the high surface area, meso-structure and incorporation of Ca^{+2} in the mesoporous silica network are the most important parameters affecting m-SXC's hemostatic properties.

The hemostatic efficiency of Ca/P-containing mesoporous silica-based xerogels (CaMSX) was also assessed by Li *et al.* (Lipinski & Pretorius, 2012) as compared with mesoporous silica-based xerogels without Ca/P (MSX), yuannan white medical

powder (YM) and traditional zeolite. The results obtained demonstrated that CaMSX had superior efficacy compared to the other dressings; it could significantly promote both the intrinsic and extrinsic blood coagulation processes as noticeably shortened both APTT and PT as well as induce platelet adherence. The CaMXS also demonstrated the best efficiency in promoting hemostasis in rabbit's ear side models as the time to hemostasis was significantly reduced with respect to other groups (Lipinski & Pretorius, 2012). These results were in good agreement with the previous study,(X. Wu *et al.*, 2010) confirming that the mesoporous structure and Ca amount have significant effects on hemostatic activity of the m-SX. Ostomel *et al*. compared the hemostatic response of a porous, nonporous and spherical bioactive glass with different Si:Ca ratio using the TEG (Ostomel, Shi, & Stucky, 2006). The results indicated that time until clot detection (*R*) was decreased with increasing Si:Ca ratios in all bioglasses (BGs) and minimum R time was observed for the glass with Si:Ca ratio of ~2.5. These results suggested that the hemostatic BGs not only can provide ideal surface area for thrombosis but also can supply sufficenit Ca^{2+} ions, a requieed cofactors for blood coagulation activation. Notably, the spherical bioactive glass had the tendency to induce clotting faster than that of other glasses. The authors claimed that the shape and particle morphology of spherical porous bioactive glass plays an important role in decreasing clotting time since it presents a greater surface area to blood. The coagulation rate (α) was also found to be increased with increasing Si:Ca ratios for all the tested BGs (Figure 2.20).

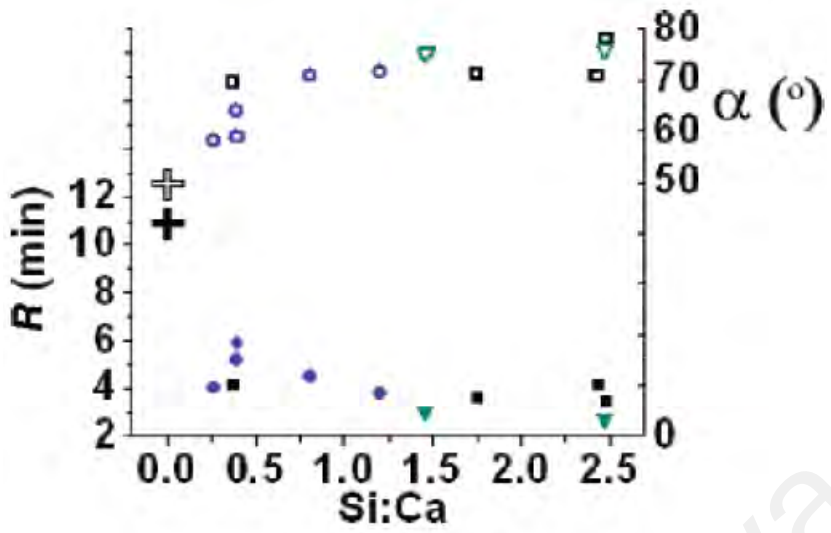

Figure 2.20: Effect of Si:Ca ratio on R time (filled shapes) and α (unfilled shapes). ▼spherical BG; ■porous BG; ●nonporous BG; + blood free sample [Reproduced with permission from (Ostomel, Shi, & Stucky, 2006).

The results also demonstrated that all blood clots induced by hemostatic BGs were more robust than natural clots, although there was no relationship between the maximum clot strength (MA) and the ratio of Si:Ca for hemostatic BGs ($MA_{BG} \geq 62$ and $MA_{Natural}$ =58 dyn/cm^2) (Ostomel, Shi, & Stucky, 2006). It is also interesting to note that although these hemostatic BGs had smaller $\Delta H_{Hydration}$ in comparison with QC (zeolite-based hemostatic agents), they could dehydrate the hemorrhaging blood without generating excessive heat. Towards a better understanding of the hemostatic effects of the BGs, the thrombotic efficacy of the constituent oxides individually as well as collectively was also investigated in this study. In this regard, the *in vitro* hemostatic property of mesoporous SiO_2 (SBA-15) and CaO as model components of hemostatic BG, as well as nonporous SiO_2 glass beads, $CaCO_3$, and hydroxylapatite [$Ca_{10}(OH)_2(PO_4)_6$] as related Si- and Ca-containing oxides were analyzed. With the exception of hydroxylapatite that revealed antithrombotic effect and delayed coagulation, all samples demonstrated a reduced *R* time. Furthermore, unlike CaO and $CaCO_3$ that resulted in the faster rates of coagulation and stronger clots, both α and MA decreased by increasing the SBA-15 content despite reducing clot initiation

time. On the basis of these results, it was speculated that the presence of calcium ions (Ca^{2+}) in both CaO and $CaCO_3$ was likely to contribute to their hemostatic actions (Ostomel, Shi, & Stucky, 2006).

The same group (Ostomel *et al.*) also investigated the hemostatic activity of ordered mesoporous bioactive glass microspheres (MBGMs) as compared with non-porous bioactive glass (MBGM-nonporous) using TEG (Ostomel, Shi, Tsung, *et al.*, 2006). MBGMs were found to be more effective in inducing hemostasis with respect to MBGM-nonporous since clot detection times and coagulation rates were reduced and increased respectively in the presence of MBGMs. The study also confirmed linear relationship between pro-coagulant activity and the ratio of Si/Ca of bioglasses, so that increased pro-coagulant activity was observed in MBGM with a higher Si/Ca ratio (80 mol % Si, $R_{MBGM-80}$). Based on the results, a significant decrease in clotting time was observed with MBGM-80 possessing lower Ca^{2+} loading with respect to MBGM with higher Ca^{2+} content (60 mol % Si, MBGM-60) and the negative control (blood without bioactive glass) (Table 2.6). Their study suggested that even the more Si-rich glass compositions can deliver sufficient amounts of Ca^{2+} species to stimulate an enhanced coagulation response. It was also demonstrated those glass compositions with higher Si/Ca, (*i.e.* MBGM-80) that reveal the most rapid contact activated clotting response found to have the least activity for bone generation than those glass compositions with lower Si/Ca ratio (*i.e.* MBGM-60).

Table 2.6: TEG analysis of MBGMs [Reproduced with permission from (Ostomel, Shi, Tsung, *et al.*, 2006)].

Hemostatic Agent	R (min)	a (°)	MA (dyn/cm^2)
Sheep Blood Alone	10.9	50.2	58
MBGM-60	15 mg: 3.9 10 mg: 4.2 5 mg: 4.3	58.6 74.1 72.4	74 70.2 74.3
MBGM-80	15 mg: 2.9 10 mg: 3.6 5 mg: 3.6	72.4 70.6 68.1	73.4 72.6 77.1
MBGM-60 Non-porous	15 mg: 3.3 10 mg: 4.3 5 mg: 5.2	69.5 67.1 62.4	68.5 73.4 74
MBGM-80 Non-porous	15 mg: 3.5 10 mg: 4.4 5 mg: 4.8	65 62.9 59.3	69 69.9 69.4

This thrombotic effect of the porous materials was ascribable to the presence of negatively charged siliceous oxide (SiOH) on their surface as well as the release of Ca^{2+} ions which make them capable of concentrating blood components through capillary absorption of fluid-phase media (Ostomel, Shi, Tsung, *et al.*, 2006). These results suggested that even the glasses with high percentage of SiO_2 have the capability to deliver sufficient amounts of Ca^{2+} ions in wounded area to induce fastest hemostatic response (Ostomel, Shi, Tsung, *et al.*, 2006).

Dai *et al.* demonstrated that chitosan-silica xerogel hybrids (CSSX) can remarkably accelerate the intrinsic pathway of coagulation cascade and achieve a desirable hemostasis. In this study, a series of CSSX beads consisted of mesoporous silica xerogel (MCX) cores and chitosan layers (CS) with macroporous structure were produced using modified sol-gel process and polyethylene glycol (PEG)

molecular imprinting technique (Dai *et al.*, 2010). The results indicated that all CSSX beads diminished APTT compared with negative controls (blood without CSSX beads), while there was no effect on the PT of CSSX beads. It was also found that APTT was not substantially affected by the chitosan coating layer on the MSX beads since it does not interfere directly with the coagulation cascade. In fact, the leading cause of shortened APTT was found to be due to negatively charged surface of MSX which resulted in activation of intrinsic pathway. The *in vitro* evaluation of thrombogenic activity also revealed that the amount of blood clot adhered on the surface of CSSX-25 (containing 2% Chitosan and 5% PEG) was much higher than pure MSX and control (Standard gauze). The superior performance of CSSX-25 was attributed to the interaction of negatively charged blood cells with positively charged chitosan which resulted in the adhesion of more blood cells on CSSX beads. The presence of large and deep pores in the surface of CSSX-25 also provided additional accessible sites for trapping the blood components. With respect to water absorption, CSSX-0 and CSSX-25 also appeared to have high water uptake potential in comparison with the gauze control (89.2 and 81.9 versus 59.0 %respectively). The *in vivo* experimental model of severe arterial bleeding was also used to test anti-hemorrhagic effects of CSSX beads. The rate of survival was 100% in the CSSX beads group when there were no survivors in the control group. There was also a significant improvement in achieving hemostasis and decreased blood loss in the CSSX-25 beads compared with CSSX-0. As an example of the results obtained, Figure 2.21 depicts bleeding control in a rabbit femoral artery injury treated with the CSSX-25 beads.

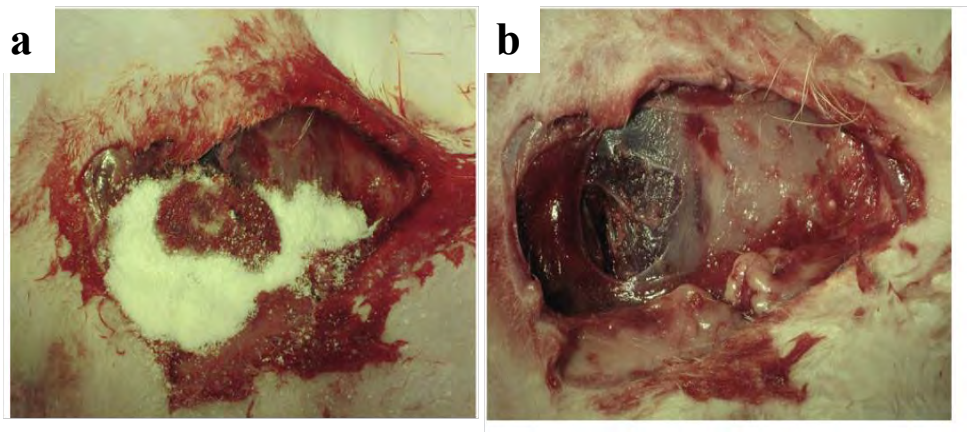

Figure 2.21: a) Treatment of a bleeding site with CSSX-25 beads, b) showing the hemostatic action of CSSX-25 beads which resulted in stop bleeding [Reproduced with permission from (Dai *et al.*, 2010)].

Notably, in contrast to zeolite, the materials produced no exothermic reaction and subsequent thermal damage. These results were confirmed by histologically, since there was no evidence of necrosis and inflammatory at the site of injury (Dai *et al.*, 2010).

Although both SMMs and MBGs demonstrated efficient hemostatic activity in both *in vitro* and *in vivo*, they lack antibacterial properties which may result in life-treating complications.

2.8 Ag_2O-doped BGs and MBGs

An efficient approach to impart antibacterial activities to the materials, can be refining their composition by incorporating the small quantity of therapeutic trace element such as Ag^+, Zn^{2+} and Ga^{3+} ions. Of those available dopants, Ag^+ specious have attracted attention due to their antimicrobial activities towards both gram-negative and gram-positive microorganisms (Balamurugan *et al.*, 2008; Bellantone *et al.*, 2002; Blaker *et al.*, 2004). The Ag^+ ions have been also demonstrated to be effective against antibiotic-resistant bacteria such as *methicillin-resistant staphylococcus aureus* (*MRSA*) and *vancomycin-resistant enterococci* (*VRE*)

(Parsons *et al.*, 2005). The antibacterial action of the ions is linked with three well-defined mechanisms: (i) leading to inactivation of bacteria proteins and enzymes through the reaction with their thiol (sulfhydryl) group, (ii) disrupting membrane permeability and leading to cell lysis and death and (iii) inhibiting the pathogen's ability to replicate by binding to bacteria's DNA and RNA (Belly *et al.*, 1982; Liau *et al.*, 1997; Matsumura *et al.*, 2003; Russell *et al.*, 1994; Thomas, 2004). Thus, these fascinating characteristics of Ag^+ persuade scientists to incorporate it into bioactive glass networks.

Bellantone *et al*. (Bellantone *et al.*, 2002) assessed the *in vitro* antibacterial properties of Ag-containing bioglass in the system of SiO_2-CaO-P_2O_5-Ag_2O (AgBG) against *Escherichia coli*, *Pseudomonas aeruginosa*, and *Staphylococcus aureus* as compared with 45S5 bioglass and bioglass in the system of SiO_2-CaO-P_2O_5 (BG). In comparison to both 45S5 bioglass and BG that exhibited no antibacterial effect, AgBG exerted an efficient anti-bactericidal property in the concentrations range 0.05-0.20 mg per ml of culture medium. The authors concluded that leaching the Ag^+ ions from the glass matrix responsible for the antibacterial action of AgBG (Bellantone *et al.*, 2002).

In another study by Bellantone *et al*., (Bellantone *et al.*, 2000) incorporation of 3 wt % Ag_2O into three-component system, SiO_2-CaO-P_2O_5, imparted antimicrobial ability to the glass without compromising its bioactivity. AgBG exhibited an efficient antibacterial activity against *Escherichia coli* (*E. coli MG1655*) in a concentration of 0.2 mg/mL (culture solution) with respect to BG which showed no antibacterial effect in the concentration range (0.1–40.0 mg/mL) (Bellantone *et al.*, 2000).

Gargiulo *et al*. (Gargiulo *et al.*, 2013) investigated the antibacterial effect of Ag-MBG against *Staphylococcus aureus* (*S. aureus*) strain, and found that the glass at 0.5 mg/mL concentration has ability to exert bactericidal activity.

The antibacterial ability of Ag-loaded MBG (Ag-MBG) powders were also evaluated against *E. faecalis* biofilm in root canal of human teeth (Wei *et al.*, 2015) compared with MBG and Ag-MBG found to exhibit significantly higher antibacterial effect than those of MBG. The results demonstrated that unlike MBG which exerted low antibacterial effect resulting from Si^{4+} ion release and pH increment, the antibacterial ability of Ag-MBG was not pH-related. The property of Ag-MBG found to be induced by the release of Ag^{+} ions from Ag-MBG framework.(Wei *et al.*, 2015)

2.9 Ag_2O-doped MBGs with hemostatic efficacy

Dai *et al*. assessed the hemostatic ability and antibacterial activity of a mesoporous silica sphere doped with Ca^{+2} and Ag^{+} (AgCaMSS) in both powder (PA) and granular (GA) forms as compared with mesoporous silica spheres (MSS), mesoporous silica sphere doped with Ca^{+2} (CaMSS) and standard gauze (positive control) in both *in vitro* and *in vivo* (Dai *et al.*, 2009). The results from *in vitro* testing showed that APTT was remarkably decreased by MSS and AgCaMSS at about 43.2 % in comparison with 100% in negative control (blood-free sample). It was found that the high surface area as well as the incorporation of Ca^{+2} and Ag^{+} into the MSS network not only resulted in more aggregation and adhesion of platelets and blood cells on the surface of AgCaMSS (Figure 2.22) but also led to the acceleration of the dissolution of the material in Tris-HCl buffer solution (more than 40 % after 42 days) compared with MSS (around 32%) (Dai *et al.*, 2009). AgCaMSS also demonstrated a potent antibacterial effect against *E. coli* and *S. aureus*. The antimicrobial activity of AgCaMSS was attributed to the presence of Ag^{+} since CaMSS and MSS did not impart an antibacterial effect. The *in vivo* study also indicated that the time to hemostasis was substantially reduced from 161.2 s in control group to 9.2 s and 10.6 s for PA and GA forms of AgCaMSS respectively

(Figure 2.22). The mortality rate for the femoral artery and liver injuries was also decreased in PA (28.6 % and 12.5 % respectively) and GA (11.1 % and 20 % respectively) groups with respect to positive control group (100 %, standard gauze) (Dai *et al.*, 2009).

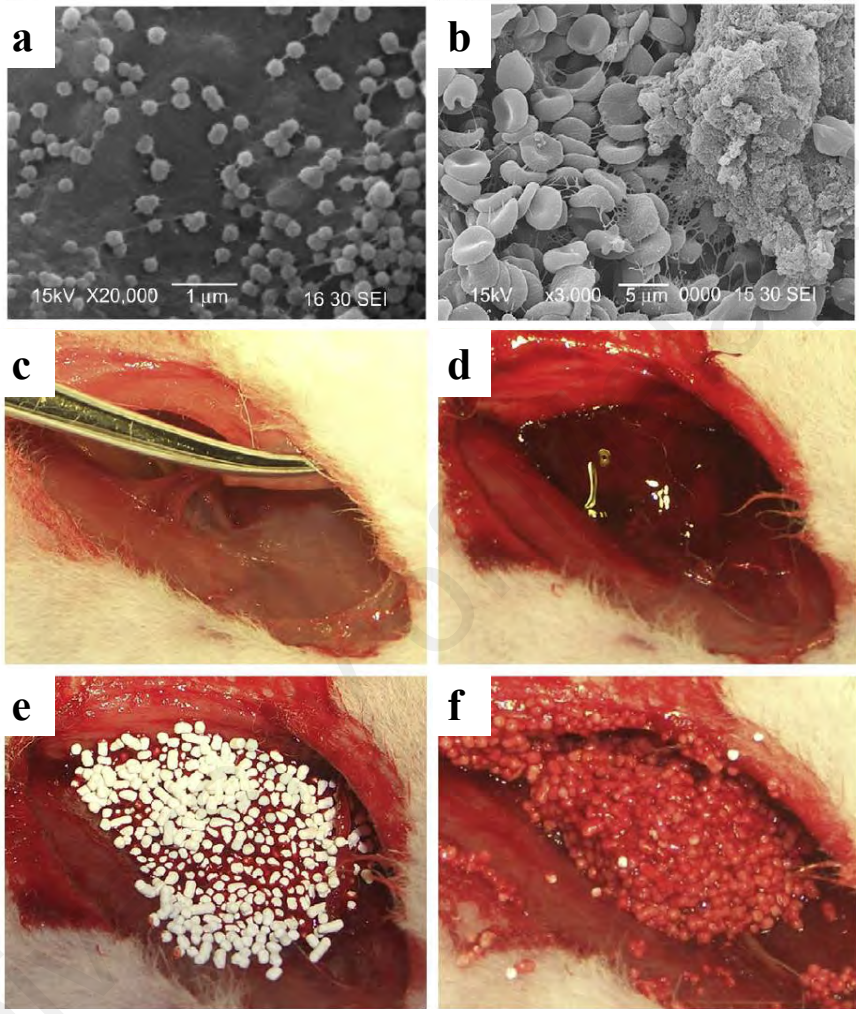

Figure 2.22: FESEM images of (a) platelet and (b) blood cells adhered to AgCaMSS. Hemostasis in rabbit femoral artery injury. (c) Opening overlying skin and muscle to cut femoral artery leading to blood loss. (d) Profuse bleeding instantly after cutting of artery. (e) Pouring AgCaMSS with granular form into the injury site. (f) hemostasis was achieved after manual compression over the wound [Reproduced with permission from (Dai *et al.*, 2009)].

Similar to the study performed by Dai *et al.*, Hu *et al.* demonstrated the superiority of the Ag-doped nanoporous bioactive glass (n-BGS) over the non-porous bioactive glass (BGS) in terms of pro-coagulant and antibacterial activity. Based on the APTT and PT results, a significant decrease in clotting time was observed in n-

BGS group compared with both BGS and control groups (without material). According to the authors, the higher specific surface area of n-BGS (467 m^2/g) compared with BGS (91 m^2/g) was responsible for its hemostatic ability (Hu *et al.*, 2012). This characteristic makes the n-BGS able to stimulate the blood clot formation through the absorption of a large quantity of water and subsequently lead to the concentration of blood components. These results translated *in vivo*, where application of the n-BGS to injured skin reduced time to hemostasis to 27 s compared to 86 and 193 s in BGS and control group respectively (Figure 2.23).

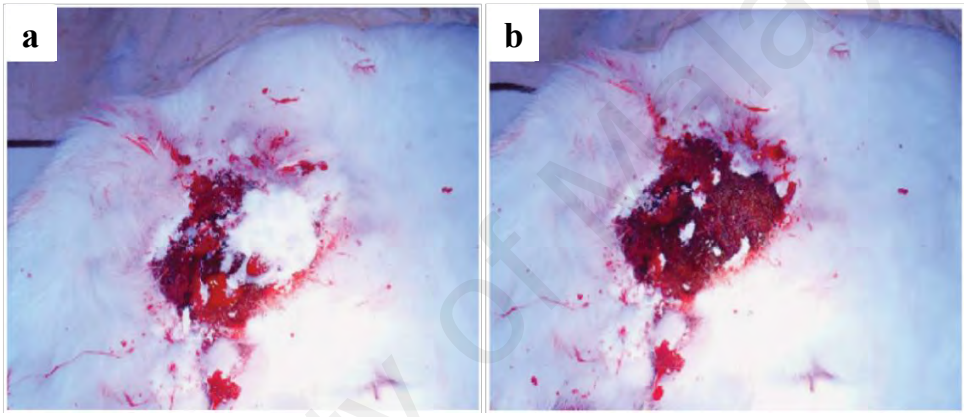

Figure 2.23: The skin injury of rabbit treated with a) n-BGS b) BGS [Reproduced with permission from (Hu *et al.*, 2012)].

In terms of antimicrobial activity, the n-BGS doped with 0.02 Ag was found to be most effective against *E. coli*, reaching antibacterial rate to 99% within 12 h.

2.10 Ga-doped BG and MBGs

Ga^{3+} is a chemotherapeutic ion whose biological function has already been approved by FDA (Malavasi *et al.*, 2013). Ga^{3+} exerts a broad spectrum of therapeutically useful biological activities which many of these activities appears to be owning to Ga^{3+}'s ability to act as an irreducible mimic of Fe^{3+} (Bernstein, 2013).

Due to the similarity between the Ga^{3+} and Fe^{3+} in electronegativity, ionic radius and ionization potentials, Ga^{3+} can be transported in the blood serum via the transferrin (Tf), a serum protein responsible for the transport of Fe^{3+} and therefore follow many of the uptake and transport pathways observed for Fe^{3+} (Bernstein, 1998). However, since Ga^{3+} is irreducible under physiological conditions, it cannot be involved in redox reactions, including the Fenton-type reactions that lead to free iron (mainly as Fe^{2+} in solution) to be highly toxic (Bernstein, 2013). Additionally, it is found that Ga^{3+} does not enter Fe^{2+}-bearing molecules like heme, and thus does not interfere with cytochrome-mediated reactions or transport of oxygen in blood which is undertaken by hemoglobin (Bernstein, 2013).

Ga^{3+} has shown to have various therapeutic activities including anti-inflammatory and immunomodulating activity as proved in animal models, anti-bone-resorptive, anti-hypercalcemic activity, as well as activity against pathological hyperproliferation, specifically against some aggressive cancers (Hall *et al.*, 1990; Verron *et al.*, 2010). It is also reported that Ga^{3+} can interfere with uptake and utilization of Fe^{3+} by cancer cells and so exert anticancer activities (Bernstein, 2013). As cancer cells need Fe^{3+} to synthesize DNA, they overexpress TF-receptor to take up sufficient Fe^{3+}. Therefore, due to similarity between Fe^{3+} and Ga^{3+}, cancer cells cannot discriminate between the ions and then Ga-TF will be taken into the cells which make them unable to synthesis DNA and lead to the cancer cells undergo apoptosis. It has been notably found that Ga^{3+} will not take up by healthy cells, even those that are quickly proliferating. Although the mechanism of action has not yet been fully elucidated, the efficient local iron recycling may be a possible reason the low Ga-avidity of other proliferating healthy cells (Bernstein, 2013).

Ga^{3+} was also found to be beneficial in treating localized infection (Kaneko *et al.*, 2007), inhibiting biofilm formation and imparting antibacterial activity against both

free living bacteria and biofilm cells (Kaneko *et al.*, 2007). As discussed earlier, Ga^{3+} as an analogue of Fe^{3+} can exhibit characteristics which enable it to interact with cellular processes and biologically important proteins, especially those involved in Fe^{3+} metabolism (Valappil *et al.*, 2008). Once the Ga^{3+} ions release into the physiological environment, it can disrupt the Fe^{3+} metabolism of many infecting bacteria so that they are unable to distinguish between Ga^{3+} and Fe^{3+} (Valappil *et al.*, 2009). In fact, the replacement of Fe^{3+}, a redox active species essential in electron transport and oxidative stress, with Ga^{3+}, redox inactive increase the vulnerability of these microorganisms (Malavasi *et al.*, 2013). Accordingly, in the recent years, there has been a growing interest in the development of certain Ga compounds as diagnostic and therapeutic agents especially used in the areas of bone resorption disorders, cancer, and infectious diseases (Rogosnitzky, 2014).

Ga-containing BGs with improved biological features have recently developed for specific clinical applications. Ga-containing phosphate glasses were synthesized by Valappin *et al*. and found to exert anti-bacterial activity against growth of *P. aeruginosa* due to Ga^{3+} delivery (Valappil *et al.*, 2009). Faranchini *et al*. prepared a series of bioactive phospho-silicate glasses containing up to 3.5 mol % of Ga_2O_3 and investigated the effect of Ga incorporation on hydroxyapatite (HA) formation (Franchini *et al.*, 2012). The results showed that all the glasses maintain the ability of HA formation, particularly with the glass containing up to 1.6% Ga_2O_3 content. The results of ion release also demonstrated that the maximum Ga^{3+} concentration measured for the glass with 3.5% Ga_2O_3 content is ~6 ppm which is about half of the toxic level (14 ppm).

In vitro bioactivity and controlled drug-release ability of Ga-substituted MBG have also been investigated by Maria Vallet-Regi's group (Salinas *et al.*, 2011; Shruti *et al.*, 2013). Their studies indicated that incorporation of Ga^{3+} into the

network of MBGs made them capable of exhibiting high bioactive response and facilitating drug loading and release while maintaining mesostructural order. Accordingly, it was proposed that Ga_2O_3-containing glasses can be suitable for bone tissue engineering applications and drug delivery.

2.11 Ga-containing hemostats

More recently, some Ga-containing compounds such as aqueous solution of gallium nitrate, $Ga(NO_3)_3$, have appeared to be efficient for the immediate treatment of wounds and for the enhancement of the early stage of hemostasis (coagulation, platelet activation, or clot formation) when directly applied to an open wound (Rogosnitzky, 2014). Although the exact mechanism of action for the ability of $Ga(NO_3)_3$ to facilitate hemostasis is not fully understood, the main principle behind this function may be dependent upon the presence of the Ga^{3+} in solution.

The hemostatic ability of 14% aqueous $Ga(NO_3)_3$ solution was assessed in human subjects who suffered from a 1-inch long gash to the index finger and 1-inch wide gash to the chin (Rogosnitzky, 2014). Immediate hemostasis was achieved after the finger was inserted into the solution and bleeding was stopped within a few seconds. A less concentrated $Ga(NO_3)_3$ solution (7%) was also applied in a human subject with 2-inch wide gash to the top of the forehead and the solution was also found to be capable of stopping bleeding (Rogosnitzky, 2014).

Goodley and Rogosnitzky studied the hemostatic activity of $Ga(NO_3)_3$ on ceasing blood flow from an open wound and concluded that the solution has the potential to considerably reduce clotting time in both a warfarin-treated (S_1) and non-warfarin-treated (S_2) subjects compared to the control that was not treated with $Ga(NO_3)_3$. It

was also found that the blood-stemming property of $Ga(NO_3)_3$ was not influenced by warfarin in S_1 (Table 2.7) (Goodley *et al.*, 2011).

Table 2.7: The effect of $Ga(NO_3)_3$ in reducing bleeding times from simple punctures (P_1 and P_2) in both warfarin and non-warfarin treated subjects [Reproduced with permission from (Goodley *et al.*, 2011)].

Subject	Time of bleeding to stop (s) P1 (control)	P2 (gallium nitrate)	Reduction in bleeding time (%)	Observation of P2
S1 (warfarin)	122	35	71%	Small pool of blood stayed about the incision site.
S2 (nonwarfarin)	238	45	81%	Visible clot started to form once had ceased

This behaviour of $Ga(NO_3)_3$ in individuals with an inhibited extrinsic pathway can lead to some support for the theory that Ga-containing compounds may achieve desirable hemostasis via another coagulation pathway including the intrinsic pathway or platelet activation (Rogosnitzky, 2014).

2.12 Critical discussion

In recent years, hemostatic agents based on inorganic species, such as QC, ACS^+, WS and QCG, among a number of novel products have been recognized as the most powerful agents for controlling haemorrhage in both combat and civilian trauma (B. S. Kheirabadi, Edens, *et al.*, 2009; B. S. Kheirabadi, Scherer, *et al.*, 2009). The chemical components of these hemostats (zeolite, smectite and kaolin) were found to be potent clot-inducing minerals when applied in the bleeding cites (B. S. Kheirabadi, Edens, *et al.*, 2009; B. S. Kheirabadi, Scherer, *et al.*, 2009). However, these hemostats are not without drawbacks. For instance, they may cause thermal

injuries, embolization to distal organs and high cytotoxicity toward human umbilical veins endothelial cells (Bijan S Kheirabadi *et al.*, 2010; Rhee *et al.*, 2008).

In order to address the problems associated with these previously developed hemostats, recently SMMs and MBGs with higher surface area and porosity than those of zeolites-based agents demonstrated to have ability to accelerate hemostasis in both *in vitro* and in *vivo*. However, these materials do not have any efficient antibacterial properties which is required to avoid infection of traumatic wounds.

Incorporation of small quantity of trace elements with antibacterial effect to glass matrix could be an effective solution to impart the antibacterial property to the materials. Although inclusion of Ag^{+} as an antibacterial element in the MBG framework improved both its antibacterial property and hemostatic efficiency (Dai *et al.*, 2009; Hu *et al.*, 2012), it has been found to be toxic toward fibroblast cells (Ong *et al.*, 2008). Therefore, to enhance both therapeutic action and hemostatic response of the MBGs while maintaining their cytocompatibility another therapeutic element could be replaced with Ag^{+} ions.

The Ga^{3+} ions have been found to exert potent antibacterial effects. Ga-based BGs and MBGs demonstrated great potential for various biomedical applications owning to the excellent therapeutic effect of Ga^{3+}. Additionally, it has been previously reported that Ga^{3+} in its pharmaceutical form, $Ga(No_3)$, to have the potential to accelerate early stage of hemostasis (Goodley *et al.*, 2011; Rogosnitzky, 2014).

Considering the inherent beneficial biological properties of Ga^{3+}, as well as its contributing role on hemostatic effect of ($Ga(NO_3)_3$), the present study aims to evaluate the effect of adding Ga_2O_3 to MBG which found to have hemostatic properties, and assess whether the presence of Ga^{3+} in MBG framework would lead to a more potent hemostat.

CHAPTER 3: METHODOLOGY

3.1 Introduction

This chapter details the synthesis of Ga-containing MBGs followed by a description of the techniques used to assess the physiochemical properties of the bioactive glasses and commercial hemostats, CX and ACS^+. The methods used to evaluate the hemostatic activity and biological features of the samples were also described in this chapter.

3.2 Materials and Methods

3.2.1 Materials

Tetraethyl orthosilicate (TEOS, 98%, Sigma-Aldrich), triethyl phosphate (TEP, ≥99.8 %, Sigma-Aldrich), calcium nitrate tetrahydrate [$Ca(NO_3)_2.4H_2O$, ≥99%, Sigma-Aldrich], gallium (III) nitrate hydrate [$Ga(NO_3)_3.\ xH_2O$, 99.9%, Sigma-Aldrich], Nonionic triblock copolymer $EO_{20}PO_{70}EO_{20}$ (P123, Sigma-Aldrich), ethyl alcohol (EtOH, Sigma-Aldrich) and nitric acid (HNO_3, Sigma-Aldrich) were reagent grade and used without further purification. CX (Medtrade Products Ltd. Crewe, United Kingdom) and ACS^+ (Z-Medica, Wallingford. Connecticut, USA), were also purchased from their commercial sources. Both FDA approved products are available for purchase without prescription. Notably, ACS^+ beads was removed from the porous bag that they were supplied in and were used in their bead form for all the tests.

3.2.2 Synthesis of MBGs

Ordered MBGs (80-x) %SiO_2–15%CaO–5%P_2O_5–xGa_2O_3, doped with different content of Ga_2O_3, were synthesized by using P123 as a SDA. The nominal chemical composition of the synthesized samples is reported in Table 3.1.

	Components (mol %)			
Glass code	SiO_2	CaO	P_2O_5	Ga_2O_3
MBG	80	15	5	0
1%Ga-MBG	79	15	5	1
2%Ga-MBG	78	15	5	2
3%Ga-MBG	77	15	5	3

Table 3.1. Nominal chemical composition of MBG and Ga-MBGs.

These concentrations of Ga_2O_3 were chosen according to the previous studies (Salinas *et al.*, 2011; Shruti *et al.*, 2013). It was found that the incorporation of Ga^{3+} into MBG frameworks by replacing parts of Si^{4+} influence the physiochemistry and biological property of MBG. It has been already reported that small and highly charged cations such as Al^{3+} which is similar in size to Si^{4+}, often substitute for Si^{4+} in tetrahedral cite and can be classified as ‘‘intermediate ions’’(Alhalawani *et al.*, 2013; White, 2013; Wren *et al.*, 2012; G.-d. Zhou, 1994). Ga^{3+} with a similar valence state to Al^{3+} , may perform a similar structural role and can act as either a network former or modifier (Wren *et al.*, 2012). Therefore, in the present work, while CaO and P_2O_5 content have been kept constant, SiO_2 content was reduced as Ga_2O_3 contents increased.

Typically, 4 g of P123 was dissolved in 60 g of EtOH, followed by the addition of TEOS, TEP, $Ca(NO_3)_2.4H_2O$, $Ga(NO_3)_3.xH_2O$ (the latter only in the case of Ga-MBGs) and 1.0 mL HNO_3 (0.5 M). The mixture was vigorously stirred overnight at room temperature, and then the as-derived clear sol was transferred into a petri dish to undergo the EISA process for 7 days. The dried gels were calcined at 600 ºC for 5

h to remove the redundant organic template and to obtain the final glass powder (Figure 3.1). The as-synthesized MBG and Ga-MBGs were then ground in two particle sizes ranging in the 32-75 and 250-300 µm intervals using mortar and pestle and stored in a desiccator at room temperature before usage.

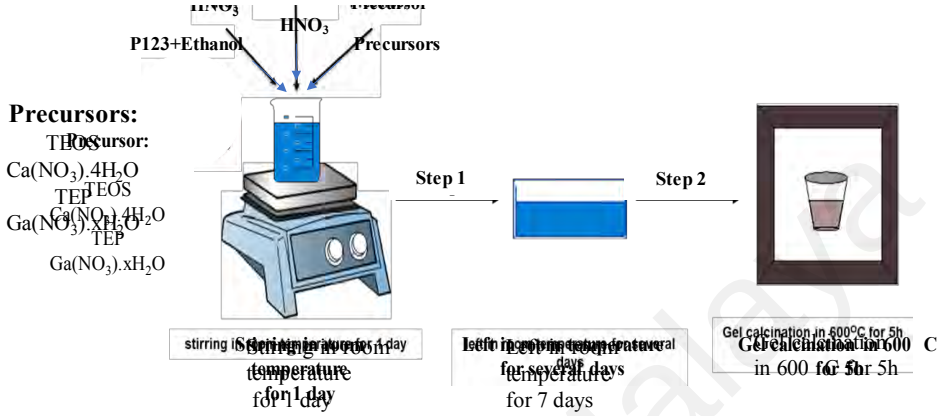

Figure 3.1: Schematic diagram showing the process of MBG synthesis.

3.3 Characterization

3.3.1 Nitrogen adsorption–desorption at 77K

The textural properties of the samples were assessed by Nitrogen (N_2) adsorption–desorption analysis at 77 K using a Micromeritics ASAP 2020 analyzer (Micromeritics, USA). The samples were degassed at 200 ºC for 5 h. Brunauer–Emmett–Teller (BET) and Barret–Joyner–Halenda (BJH) methods were used for the evaluation of specific surface area, pore size distribution and pore volume (Barrett *et al.*, 1951; Brunauer *et al.*, 1938).

3.3.2 Particle Size Analysis (PSA)

A particle size analyzer (Malvern Mastersizer 2000, Malvern Instruments Ltd.) was used to determine the particle size of Ga-MBG and CX ranging from 0.02 to 2000 mm. Laser diffraction (Malvern Mastersizer 3000, Malvern Instruments Ltd.)

was also employed for particle size distribution measurement of the ACS^+ granules dispersed in deionized water.

3.3.3 Small and wide-Angle X-Ray diffractions

Small and wide-angle X-ray diffraction (SAXRD and WAXRD, respectively) patterns were obtained using an Empyrean x-ray diffractometer (PANalytical, MA, USA) with Cu Kα (λ = 0.154 nm) radiation (40KV, 40 mA). The SAXRD patterns were collected in the 2θ range between 0.6° and 7° with a step size of 0.02° and counting time of 5 s per step. In addition, WAXRD patterns were collected in the 2θ range between 5° and 70° with a step size of 0.02° and counting time of 5 s per step.

3.3.4 High-resolution Transmission electron microscopy (HRTEM)

The inner microstructure of the samples was examined by high-resolution transmission electron microscope (TEM, JEOL JEM-2100F, Japan) operating at 200 kV. Prior to the observation, Ga-MBGs powders were dispersed in ethanol (1 mg/mL) by sonication for 15 min, followed by drop casting on carbon-coated copper grids.

3.3.5 Field emission scanning electron microscopy and energy-dispersive X-ray spectroscopic analysis (FESEM-EDS)

An energy-dispersive X-ray spectrometer (EDS: 20 mm X-Max, Oxford Instruments, Oxford, UK) and the INCA software connected to a Field emission scanning electron microscope (FESEM, Quanta^{TM} 250 FEG—FEI, USA) at 20 KV were used for the assessment of the surface morphology and composition of the glasses. The surface morphology of two commercial hemostats (CX and ACS^+) was also investigated by FESEM.

3.3.6 Fourier transform infrared spectroscopy (FT-IR)

FT-IR spectra of the samples were collected by a Fourier transform infrared spectrometer (ATR-FTIR400, Perkin Elmer instruments, USA) within the 400-1400 cm^{-1} wavelength range at room temperature. The resolution and scanning time were set at 4 cm^{-1} and 16 scans respectively.

3.3.7 Zeta potential measurement

Zeta potential determination was carried out in a Zetasizer Nanoseries (Malvern Instruments, UK) *via* suspending samples in phosphate buffered solution (PBS) at pH 7.4.

3.3.8 *In vitro* ion release measurements

Ion release measurements of MBG and Ga-MBGs were performed using microwave plasma–atomic emission spectrometer (MP–AES) Agilent 4100 (Agilent Technologies, Inc., Santa Clara, CA, USA) to investigate the concentration of silicate (SiO_4^{4-}), phosphate (PO_4^{3-}), Ca^{2+} and Ga^{3+} ions in the soaking solution. For this purpose, 20 mg of each dried sample was immersed in a polypropylene vial containing 10 mL of 0.05 M Tris (hydroxymethyl)aminomethane-HCl (Tris–HCl, Sigma-Aldrich) buffer solution (pH 7.4), and incubated up to 3 days at 37 °C with continuous shaking at 120 rpm (n = 3) (Wei *et al.*, 2015). At specified time points (0.5, 1, 2, 3, 6, 12, 24, 48 and, 72 h), the powders were collected by filtration, and the extract was used for ion release studies.

3.3.9 Degradation behaviour *in vitro*

The *in vitro* degradation behaviour of the samples was assessed by testing their weight loss ratio after immersing in 0.05 M Tris–HCl. For this purpose, 20 mg of each pre-dried sample was immersed in a polypropylene vial containing 10 mL Tris–HCl solution following incubation up to 14 days (Part 1) and 35 days (Part II) at 37 ºC with continuous shaking at 120 rpm (n = 3). At the selected time points, the samples were removed from the solution through filtration and carefully washed with distilled water. The samples were subsequently oven-dried to a constant weight at about 50 ºC. The weight loss ratio at different time points was calculated according to the following equation:

$$\text{Weight loss (\%)} = [(W_t - W_0)/ (W_0)] \times 100\% \qquad \textbf{3.1}$$

where W_0 is the initial dry weight and W_t is the weight of samples after immersion in the solution.

3.3.10 PBS absorption efficiency *in vitro*

The *in vitro* absorption efficiency of the samples was assessed in PBS (pH 7.4). The test was performed according to Dai's method as already described (Dai *et al.*, 2009). Before doing the test, the samples were dried at 50 ºC in vacuum overnight to completely eliminate the residual water. Briefly, the pre-weighed dried samples (20 mg, having mass W_{dry}) were placed at the center of a folded filter paper in a funnel so that fluid (PBS) can be uniformly absorbed by the samples. After that, the fluid was added dropwise at a rate of 10 mL/min until the absorption by the samples reached its saturation state (when the first drop of fluid trickled from the funnel). The mass of the wet sample was then recorded as W_{wet} after removing the filter paper.

The absorption ratio of samples with PBS was calculated by using the following equation:

$$\text{Absorption ratio (\%)} = [(W_{wet}-W_{dry})/W_{dry}] \times 100\% \quad \textbf{3.2}$$

where W_{dry} and W_{wet} are the weight of the samples before and after the PBS immersion, respectively. Each absorption assay was performed in triplicate.

3.3.11 *In vitro* blood plasma coagulation assay

To explore the effectiveness of the samples on blood plasma coagulation, the activated partial thromboplastin time (APTT) and prothrombin time (PT) were measured. Citrated Human blood samples (9:1 whole blood to 3.2 % sodium citrate) were freshly collected from healthy volunteers with approval from the Medical Ethics Committee of University of Malaya, Kuala Lumpur, Malaysia (UMMC reference number 967.10). The platelet poor plasma (PPP) was obtained *via* centrifugation of whole blood at 3500 rpm for 10 min at 25 °C. For each assay, the MBG and Ga-MBGs were placed into test tubes containing 100 µL PPP.

For APTT tests, 100 µL of pre-warmed plasma (37 °C) was incubated for 2 min with 100 µL APTT reagent and the samples at various concentrations (5 and 10 mg) followed by measurement of APTT after the addition of 100 µL of pre-warmed $CaCl_2$. For the PT assay, the pre-warmed plasma (100 µL) was incubated with the samples for 2 min at 37 °C. The PT was measured simultaneously after the addition of 100 µL of pre-warmed PT reagent. A negative control (no hemostatic material) was also included.

3.3.12 *In vitro* thrombus formation

The *in vitro* thrombogenic activity of the samples were evaluated with citrated human blood using a method adapted from Imai (Imai *et al.*, 1972). 30 mg (Part I) and 60 mg (Part II) of the samples were introduced into the wells of 24-well culture plates containing 1 mL of citrated human blood to start the thrombus formation followed by incubation at 37 ºC for two different time points (30 and 60 min). After each incubation period, the reaction was stopped by adding 10 mL of deionized water followed by soaking the materials in 37% formaldehyde solution for 10 min to fix the formed thrombus. The fixed samples were then placed in an oven overnight at 50 ºC until constant weight was obtained. the degree of thrombogenicity (DT) of the samples at a given time was determined by the equation:

$$\Delta = [(W_t - W_0)/W_0] \times 100\% \qquad \textbf{3.3}$$

where W_t and W_0 represent the weight of the materials before and after in contact with blood, respectively. The assay was done at least three times for each sample.

The thrombus formed on the materials' surfaces was photographed by a digital camera. The interaction of whole blood cells with the synthesized samples was also visualized by the FESEM. Prior to fixing as described above, the soaked samples were washed with PBS to remove the loosely adherent blood cells and then were fixed using 2.5% glutaraldehyde for 2 h, immediately after the rinsing step. Afterwards, the samples underwent a graded dehydration series of ethanol and then were dried in hexamethyldisilazane (HMDS) for 10 min. The materials were then left drying for 2 days in a fume hood at room temperature. The dried samples were

then sputtered with a thin layer of gold and the photomicrographs were collected with an accelerating voltage of 15 kV.

3.3.13 *In vitro* evaluation of platelet adhesion

A lactate dehydrogenase (LDH) assay was used to measure the number of adherent platelets as previously explained (Dai *et al.*, 2009). Human blood samples were freshly obtained from volunteers and anticoagulated with 3.2 % sodium citrate. The citrated human blood samples were centrifuged at 1500 rpm for 10 min to remove leukocytes and erythrocytes. Then the supernatant, platelet rich plasma (PRP), was again centrifuged at 3000 rpm for 10 min to yield a platelet pellet with platelet poor plasma as the supernatant. The platelet pellet was re-suspended in PBS to a concentration of 4×10^8 platelets/mL (first part) and 14×10^8 platelets/mL (second part). The samples in the concentration of 10 mg/0.3 mL were then exposed to the platelets and incubated at 37 °C for two different time intervals (30 and 60 min). At the end of each time interval, the samples were removed and dip rinsed ten times in PBS to remove the unattached platelets. The samples were then placed into PBS containing 1% Triton X-100 for 1 h at 37 °C to lyse the adherent platelets. The number of platelets adhered on the surface of the samples was quantified by the LDH assay kit (Sigma–Aldrich, USA). A platelet calibration curve was obtained using serial dilutions of a known number of platelets by measuring optical density (OD) at 450 nm by an Epoch microplate spectrophotometer (BioTek; Winooski, VT, USA). Each measurement was performed at least thrice. After platelet adhesion measurements, the interaction of platelets with the samples were observed by FESEM at 10-15 kV. In this regard, the samples were fixed in 2.5% glutaraldehyde followed by dehydration in an ascending series of ethanol up to 100%. The samples

were then dried in HMDS and coated with gold using a sputter coater for FESEM studies.

3.3.14 *In vitro* thrombin generation

To determine the thrombin-generating activity of the samples, a human thrombin ELISA (Enzyme-Linked Immunosorbent Assay) kit was used to measure thrombin–antithrombin complex (TAT) levels that is an indicator of how much thrombin was formed over a period of time. Fresh human blood anticoagulated with 3.2 % sodium citrate was freshly obtained from healthy volunteers. The PPP was immediately obtained by centrifuging the blood at 3000 rpm for 10 min. The samples in the concentration of 10 mg/0.3 mL were placed in a 24-well culture plates and incubated with PPP at 37 °C for 30 to 60 min to induce thrombin generation. After removal of the hemostatic materials at appropriate time intervals, 50 μL of PPP was taken from the each well and then was added to 96-well plates coated with human thrombin-specific antibody for the quantitative measurement of thrombin-antithrombin complex concentrations. A calibration curve was previously obtained in a series of known concentration of thrombin by measuring the optical density at 450 nm using a microplate reader. The levels of TAT over the materials was estimated using the calibration curve. There were three replicates for each sample at each time point.

3.3.15 Antibacterial efficacy

Killing time assays were used to evaluate antibacterial efficacy of the samples against *Echerichia coli* (*E. coli*) and *Staphylococcus aureus* (*S. aureus*) (Ip *et al.*, 2006; Ong *et al.*, 2008). Briefly, a suspension of *E. coli* or *S. aureus* was obtained from freshly grown colonies on tryptic soy agar after incubation at 37 ºC overnight. 10 μL of the bacteria suspension (4×10^8 CFU mL^{-1}) was added to each vial

containing 3 mL of tryptic soy broth. The samples that were previously sterilized under ultraviolet (UV) light for 12 h were then added in concentration of 2 mg/mL and incubated at a temperature of 37 °C for 0, 1, 3, 6 and 12 h. After that, aliquots were taken at specified time intervals and, subsequently, serial dilutions of each bacterial culture were plated on agar plates to count the number of living bacterial colonies. Each evaluation was carried out in triplicate. The antibacterial activity was quantitatively estimated by the following relationship: $R\ (\%) = [(B - C)/B] \times 100$, where R is the antibacterial activity (%), B is the mean number of survived bacteria on the control samples (CFU/mL), and C is the mean number of bacteria on the MBG and Ga-MBGs (CFU/mL). The MBG and pure LB broth culture were used as positive control and negative control, respectively. After 12 h incubation at 37 °C, digital images of the plates were captured.

3.3.16 *In vitro* biocompatibility assays

To assess Ga-MBGs biocompatibility, cell viability has been evaluated using human dermal fibroblast (HDF) after treatment with Ga-MBGs extracts. The effect of the Ga-MBG on cell viability was also assessed as compared with CX and ACS^{+} when these materials were in direct contact with the cells.

3.3.16.1 Biocompatibility assay using extracts

MBG and Ga-MBG samples, which were previously sterilized under UV light for 12 h, were soaked in Dulbecco's modified Eagle's medium (DMEM; Gibco-Invitrogen, USA) in the concentration of 2 mg/mL, and preheated to 37 °C. After 24 h under sterile conditions, DMEM was filtered to separate MBG and Ga-MBGs, and these extracts were used as culture medium. The HDF cells were seeded (1×10^4 cells/well) in a 24-well plate and allowed to attach overnight. Then the cells

were treated in the presence of different extracts obtained from MBG and Ga-MBGs. HDF cells without extract (treated with normal medium) were used as control. Each condition was set up in triplicate. Plates were assayed 1 and 3 days after the addition of extracts. The 3-(4,5-dimethylthiazol-2-yl)-2,5-diphenyl tetrazolium bromide (MTT) assay was used in this study to measure cell vitality and proliferation. The MTT agent (Biotium, Inc., Hayward, CA) reacts with its tetrazolium ring to produce blue formazan crystals in viable cells. At 1 and 3 days, the supernatant was removed from the wells, and the cells were rinsed three times with PBS to eliminate nonviable cells. 500 μL of fresh media was added to each well and then 50 μL of the MTT solution (5 mg/mL in PBS) was added in each well, and the cells were incubated at 37 °C for 4 h to allow the formation of formazan crystals. After incubation, the supernatant was removed, and 1 mL of dimethyl sulfoxide (DMSO) was then added to each well to dissolve the formazan crystals under continuous pipetting. The OD was measured at a wavelength of 570 nm using a microplate reader. The results from three individual experiments were averaged and normalized to the control.

3.3.16.2 Biocompatibility assessment by direct contact method

The *in vitro* cytotoxicity of Ga-MBG as compared with CX and ACS^+ was also assessed by MTT assays after the direct contact with HDF cells. Prior to performing the assays, the tested materials were sterilised under UV light for 12 h. The cells were seeded (1×10^4 cells per well) in a 24-wellplates and allowed to attach and grow. After 48 h of culture in growth medium (supplemented with normal growth medium containing L-DMEM supplemented with 5% fetal bovine serum (FBS; Gibco - Invitrogen, USA), 1% Penicillin/Streptomycin and 1% Glutamax-1), the cells were subjected to a serum reduction of 1% FBS to arrest cell cycle progression for 24 h; then 5 mg/mL of either 1%Ga-MBG, CX or ACS^+ was added directly to the cells.

The culture without sample was used as a negative control. Each condition was set up in triplicate. Cell viability was observed at 1 and 3 days using MTT assay according to the manufacturer's protocol.

The OD was measured spectrophotometrically at a wavelength of 570 nm using a microplate reader. The results from three individual experiments were averaged, normalised to control.

Fluorescence imaging was also used to qualitatively verify cell viability. A live/dead solution of 2 μM calcein AM/4 uM EthD-III (Biotium, USA) was prepared by adding 5 μL of 4 mM calcein AM and 20 μL of 2 mM EthD-III to 10 mL PBS. The tested materials were placed into a small cell-culture dish and covered with the live/dead solution, and the stains allowed to develop in the dark for 30 min. Images were obtained with a fluorescence microscope (CLSM; Leica TCS SP5 II, Leica Microsystems CMS GmbH, Mannheim, Germany) at excitation /emission, 495 nm/515 nm).

3.3.17 Statistical analysis

All data were expressed as mean ± standard deviations (SD) of a representative of three experiments carried out in triplicate. The data were analyzed using statistical software (IBM SPSS Statistics for Windows, Version 22). The non-parametric Mann–Whitney U-test was used to evaluate differences between two independent groups. In all the statistical evaluations, a value of $P < 0.05$ was considered statistically significant.

CHAPTER 4: RESULTS

4.1 Introduction

This chapter focuses on the presentation of the results which includes two parts: the first part describes research results on the effects of adding up to 3 mol % of Ga_2O_3 to MBG on hemostatic ability, physiochemical and biological properties of MBG; In the second part, the results of the comparative study of the 1%Ga-MBG with two commercial hemostats, CX and ACS^+, are presented.

4.2 Part I: Gallium-containing mesoporous bioactive glasses: physiochemistry, biological and hemostatic properties

4.2.1 Structural and morphological characterization of MBG and GaMBGs

MBGs with different concentrations of Ga_2O_3 were successfully synthesized *via* EISA. The N_2 adsorption–desorption isotherms at 77 K of the synthesized samples were measured and shown in Figure 4.1 together with the corresponding pore size distribution. The main textural parameters of the prepared samples are shown in Table 4.1.

Table 4.1: Textural parameters obtained by N_2 adsorption-desorption at 77 K for MBG and Ga-MBGs.

Sample code	Ga_2O_3 content (mol %)	Surface area (m^2/g)	Pore diameter (nm)	Pore volume (cm^3/g)
MBG	0	392 ± 21	5.14±0.69	0.6±0.07
1%Ga-MBG	1	472 ± 52	5.66±0.19	0.8±0.12
2%Ga-MBG	2	372 ± 20	5.31±0.92	0.59±0.10
3%Ga-MBG	3	324 ± 23	5.30±0.88	0.52±0.09

All the glasses revealed type IV isotherms along with H1 hysteresis loops, which are characteristic of a mesoporous structure and non-defective cylindrical pores, respectively (Figure 4.1a) (López-Noriega *et al.*, 2006). Figure 4.1b illustrates the pore size distribution curves as calculated from the desorption branches by the BJH model. Apparently, all the samples exhibited very narrow pore size distributions. As shown in table 4.1, 1%Ga-MBG showed a higher surface area and pore volume compared with MBG and higher substituted Ga-MBGs.

These results are in good agreement with those presented by Salinas *et. al* (Salinas *et al.*, 2011). The authors claimed that the inclusion of higher Ga_2O_3 content in the MBG framework result in a decrease of the textural properties (pore diameter, surface area and pore volume). In another study, it was also found that inclusion of 5 mol % Ga_2O_3 in 80%SiO_2-15%CaO system, resulted in less favourable structural features (Sanchez-Salcedo *et al.*).

The pore structure of the samples with different Ga_2O_3 contents was investigated by SAXRD (Figure 4.1c). All glasses exhibited two characteristic peaks at around $2\Theta = 1.1°$ and 1.8° that are associated with ordered p6mm hexagonal space group. The presence of these diffraction peaks indicated that the synthesized glasses have a high degree of hexagonal mesoscopic organization. However, 3%Ga-MBGs showed a weaker diffraction peak at around $2\Theta = 1.1º$ compared with MBG and 1%Ga-MBG. No evidence of residual crystallinity was observed in the WXRD pattern of the samples indicating each glass was completely amorphous (Figure 4.1d).

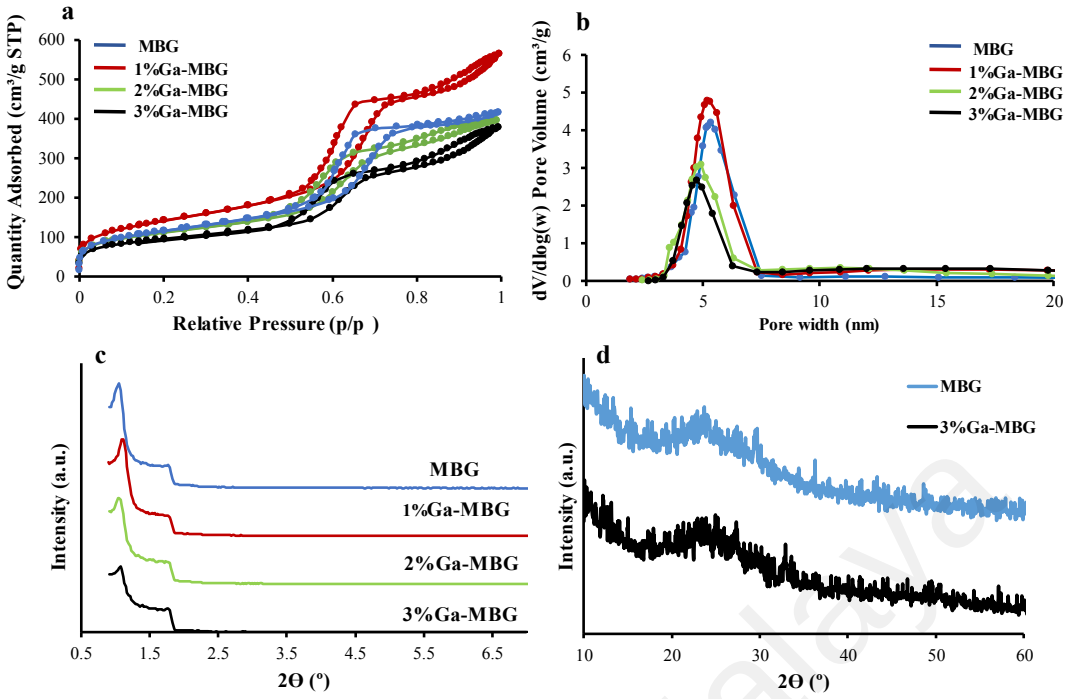

Figure 4.1: (a) N_2 adsorption–desorption isotherms and (b) corresponding pore size distributions of MBG and Ga-MBGs. (c) SAXRD of MBG and Ga-MBGs. (d) WXRD analysis of MBG and 3%Ga-MBG glasses.

The presence of ordered mesoporous channels in the prepared glasses was also confirmed by TEM images. All synthesized glasses showed a typical 2D-hexagonal ordered mesoporous arrangement. The TEM images of the samples are presented in Figure 4.2. Well-ordered pore arrays can be clearly observed in MBG (Figure 4.2a) and 1%Ga-MBG (Figure 4.2b) samples. However, the TEM images indicated a loss of order as the Ga_2O_3 content in the pores was increased (Figure 4.2c and d), confirming the results of SAXRD.

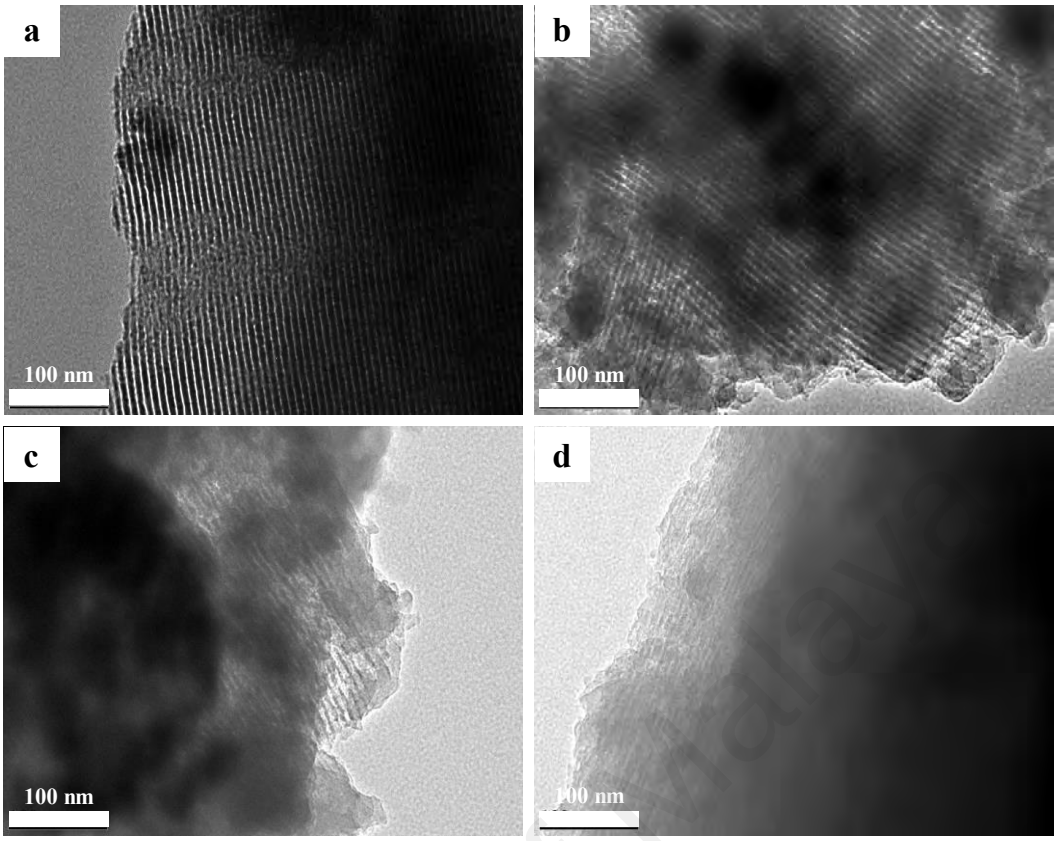

Figure 4.2: TEM images of the (a) MBG, (b) 1%Ga-MBG, (c) 2%Ga-MBG and (d) 3%Ga-MBG samples.

The EDS analysis of the synthesized samples confirmed the presence of Si, Ca, P, Ga and oxygen (O). The FESEM morphologies and EDS spectra of the samples are also shown in Figure 4.3.

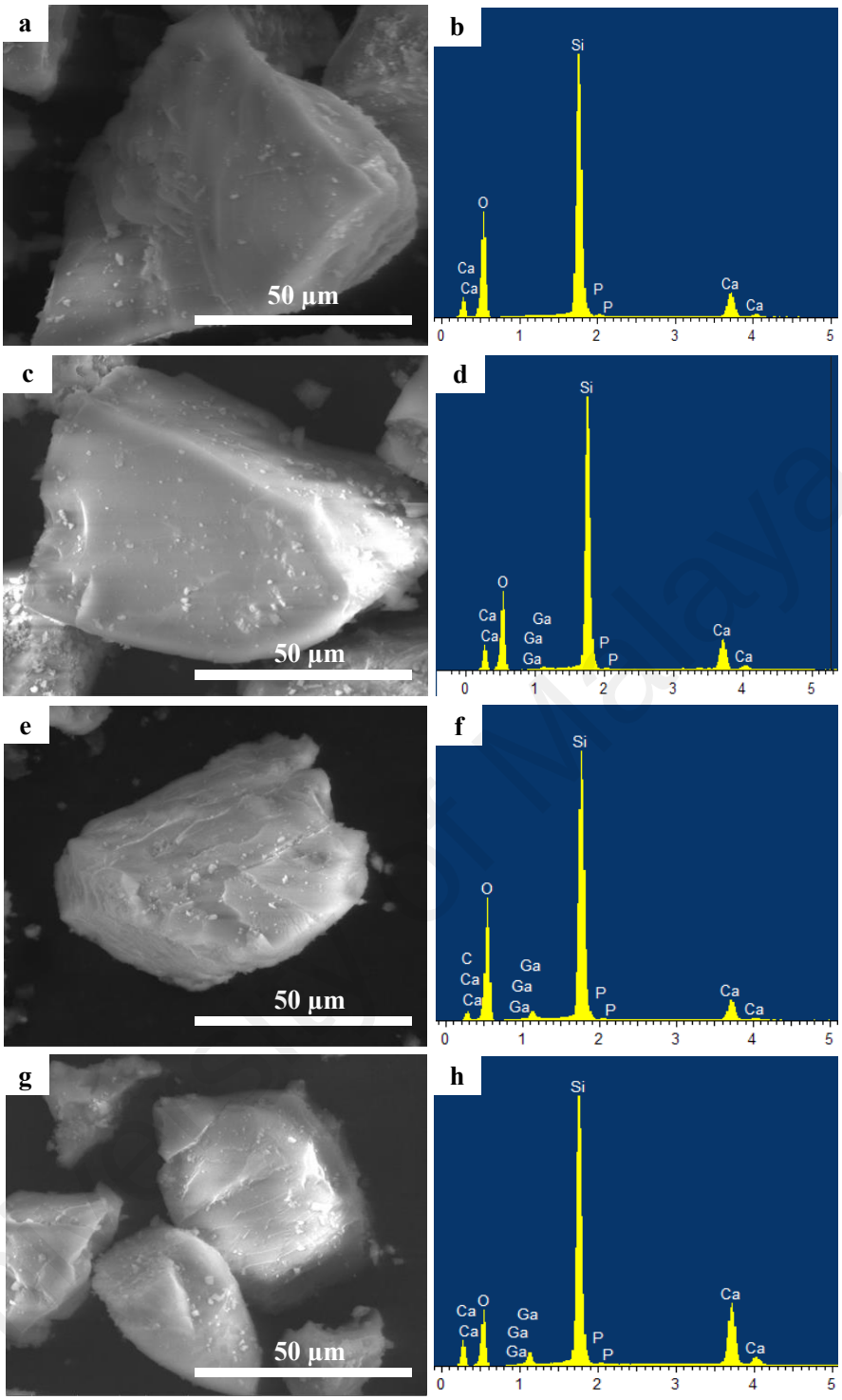

Figure 4.3: FESEM images and the EDS pattern of the (a and b) MBG, (c and d) 1%Ga-MBG, (e and f) 2%Ga-MBG and (g and h) 3%Ga-MBG.

Evidence for the local structural changes with addition of different concentrations of Ga_2O_3 can be obtained from the FT-IR spectroscopy. FT-IR spectra of the MBG and Ga-MBGs are given in Figure 4.4. All glasses represented two absorption peaks

centered around 1070 and 800 cm^{-1} corresponding to the Si–O–Si asymmetric stretching mode and symmetric Si–O–Si stretching or vibration modes of the silica ring structures, respectively (Arcos *et al.*, 2011; Vaid *et al.*, 2012). The peaks at around 460 cm^{-1} and 883 cm^{-1} are also assigned to the Si–O–Si bending mode and stretching vibration of Si–O–NBO (non-bridging oxygen) (Arcos *et al.*, 2011; Shah *et al.*, 2015). The peak at 1641 cm^{-1} and broad band around 3100-3750 cm^{-1} can be also ascribed to the bending and stretching vibrations of adsorbed water. As can be seen in Figure 4.4, the intensity of the 460, 800 and 1070 cm^{-1} bands decreased with increasing Ga_2O_3 content up to 3 mol % indicating the depolymerizing role of Ga^{3+} on the silicate network.

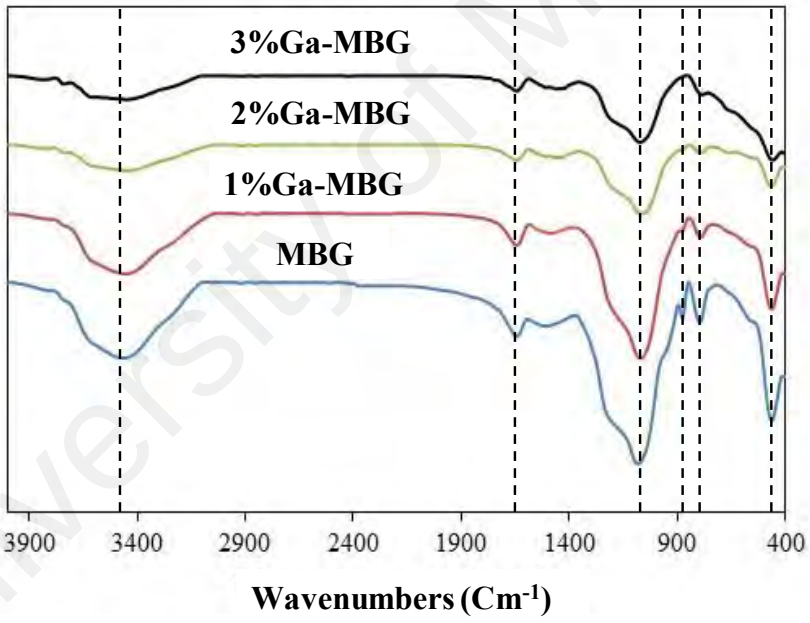

Figure 4.4: FT-IR spectra of the MBG; 1%Ga-MBG; 2%Ga-MBG; and 3%Ga-MBG.

The zeta potentials of MBG and Ga-MBGs in PBS solution were measured in order to characterize their surface properties (Table 4.2). The surface of MBG was highly negative; the zeta potential was -30.4 mV, as a result of negatively charged silanol groups. In contrast to MBG, Ga-MBGs negligibly increased the zeta potential which can be attributed to the incorporation of Ga^{3+}.

Table 4.2. Zeta potential measured for the MBG and Ga-MBGs.

Sample	Zeta potential (mV) in PBS at pH 7.4
MBG	-30.4
1%Ga-MBG	-27.3
2%Ga-MBG	-26.2
3%Ga-MBG	-25.5

4.2.2 Ion release and degradability of MBG and Ga-MBGs in Tris-HCl solution

Changes in SiO_4^{4-}, Ca^{2+}, PO_4^{3-} and Ga^{3+} concentrations in Tris–HCl buffer solution after various soaking times are presented in Figure 4.5. As can be observed in Figure 4.5a, the SiO_4^{4-} concentration drastically increased in all samples during the first 48 h and then reached a steady state ranging from 60-70 ppm. A sharp increase in the Ca^{2+} concentration was also detected during the first 72 h of the test for all samples (Figure 4.5 b). Nevertheless, the concentration of Ca^{2+} for the glasses with higher Ga_2O_3 content (2%Ga-MBG and 3%Ga-MBG) was lower than that of MBG and 1%Ga-MBG. PO_4^{3-} ion release profiles (Figure 4.5c) of all the glasses also followed the same trend and increased up to 72 h, reaching values close to 6–8 ppm. Surprisingly, the concentration of the PO_4^{3-} ions were higher for 1%Ga-MBG as compared with others.

These results suggested that higher Ga_2O_3 content, 2 and 3 mol %, are sufficient to significantly change the glass behaviour as the SiO_4^{4-}, Ca^{2+} and PO_4^{3-} leaching rates were slower for 2%Ga-MBG and 3%Ga-MBG with respect to 1%Ga-MBG. However, a different trend was found for Ga^{3+} ion release in Ga-substituted MBGs (Figure 4.5d). The 3%Ga-MBG sample with highest Ga content (3 mol %) presented a higher amount of Ga with respect to 1%Ga-MBG and 2%Ga-MBG. The Ga^{3+} concentration increased after 3 h in the three Ga-containing samples and then

experienced a steady state, reaching a value of 0.32 ppm in 3%Ga-MBG, that was approximately triple the amount found in 1%Ga-MBG. The reason why leaching of Ga^{3+} is low with respect to other ions is because of its high electric charge, which make it difficult to elute from the glass network into the solution (Franchini *et al.*, 2012). It is worth noting that the concentration of Ga^{3+} ions arrived to a steady state earlier than that of SiO_4^{4-}, Ca^{2+}, and PO_4^{3-} concentration in the glasses.

The *in vitro* degradation properties of the samples were also determined by testing the weight loss ratio of the samples after soaking in Tris-HCl solution for various times. As can be inferred from Figure 4.5e, the weight loss increased upon prolonged immersion up to 14 days for all the materials, and then negligibly increased or remained almost constant. However, the degradation rates of the MBGs with higher amount of Ga_2O_3 were found to be lower with respect to MBG and 1%Ga-MBG, probably due to their slow dissolution. The low dissolution of 3%Ga-MBG can be attributed to the acidic nature of its surface as a result of the presence of a high amount of Ga^{3+} (Aina *et al.*, 2011).

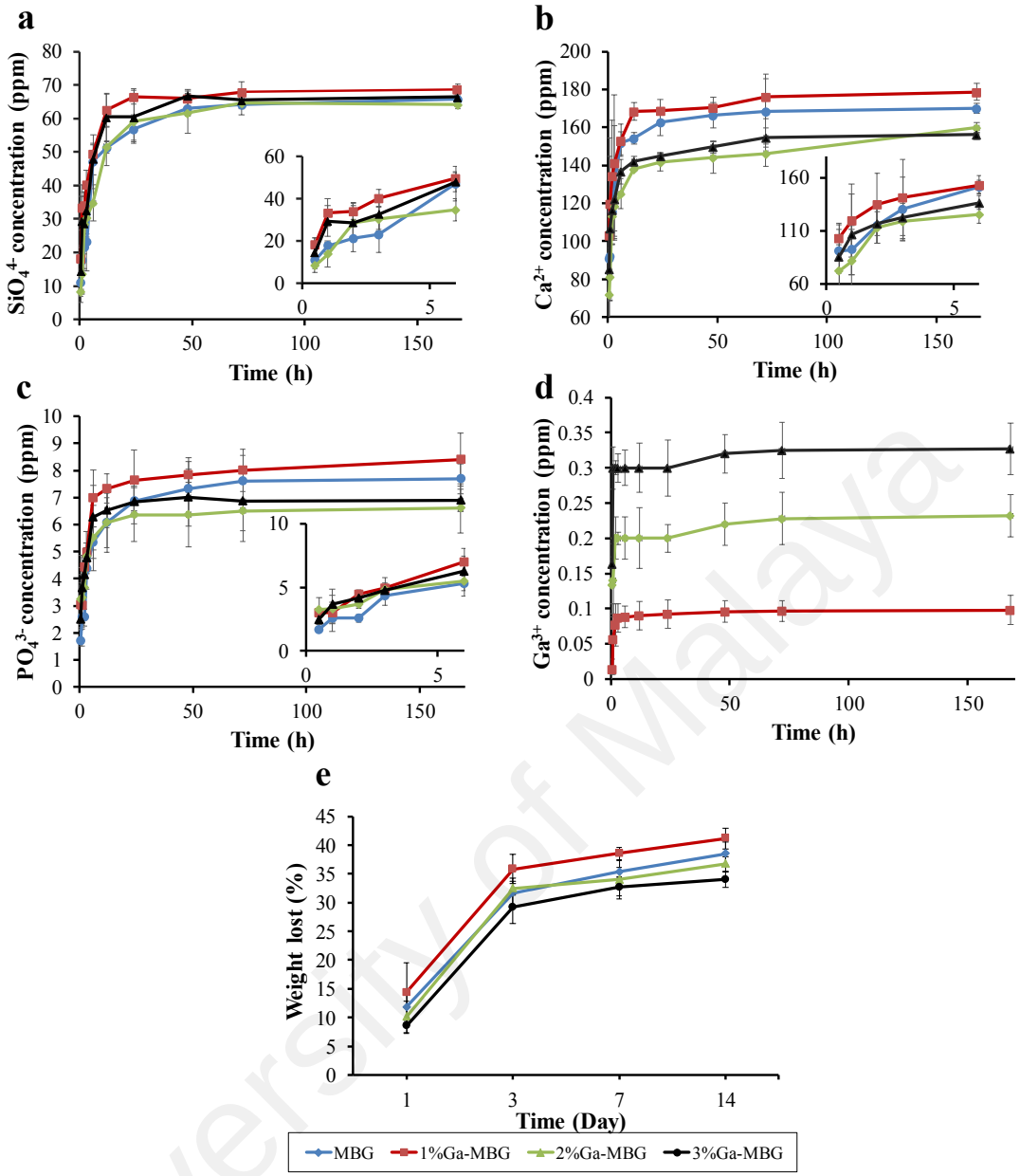

Figure 4.5: Concentration variation of (a) SiO_4^{4-}, (b) Ca^{2+}, (c) PO_4^{3-} and (d) Ga^{3+} with soaking time in Tris-HCl solution**.** Inset shows ion release profile of the ions during the first 6h**.** (e) Change of weight loss of MBG, 1%Ga-MBG, 2%Ga-MBG and 3%Ga-MBG samples in Tris-HCl solution.

4.2.3 PBS absorption study *in vitro*

The absorption capacity of the prepared samples was evaluated *in vitro* using PBS. The absorption ratios are presented in Figure 4.6. The results revealed that the absorption coefficient of MBG with lowest Ga_2O_3 content (1%Ga-MBG) increased

compared to other glasses, which may be due to its outstanding textural properties (high surface area and pore volume).

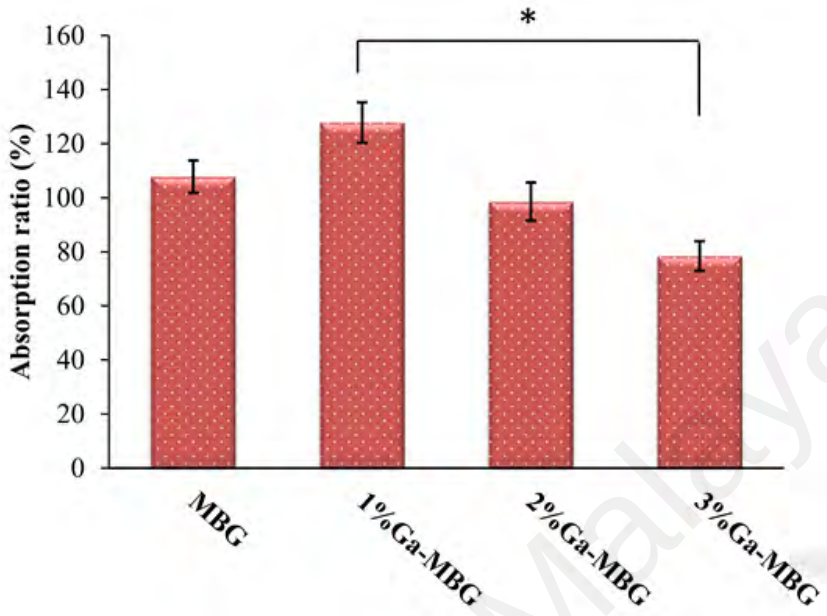

Figure 4.6: PBS absorption ratio of MBG and Ga-MBG samples. PBS absorption for 3%Ga-MBG indicated a tendency of lower absorption ratio. The difference between 1%Ga-MBG and 3%Ga-MBG was statistically significant. (*$p < 0.05$).

4.2.4 Blood coagulation experiments

To study the effect of the MBG and Ga-MBGs on the blood coagulation process, the PT and APTT of the glasses at two different amounts (5 and 10 mg per 0.3 mL) were measured. The APTT test is used to investigate the intrinsic pathway of blood coagulation and PT is a test performed to investigate extrinsic pathway of blood coagulation. The PT and APTT results are indicated in Figure 4.7. The APTT results (Figure 4.7a) revealed that all of the samples resulted in a significant activation of intrinsic pathways of coagulation cascade since the values obtained for APTT were significantly diminished with respect to the negative control (blood without sample). Notably, 1%Ga-MBG induced somewhat more pronounced effect on APTT value than that observed with other glasses. However, no significant dosage-dependent trends were observed in APTT values since increasing the amount of samples from 5

to 10 mg did not significantly decline the values of APTT (Figure 4.7a). Additionally, at 5 mg there was no significant difference in the PT values of the glasses (Figure 4.7b). All the glasses showed approximately the same effect on PT values of that of the negative control. However, in the case of the higher glass amount (10 mg), PT was prolonged.

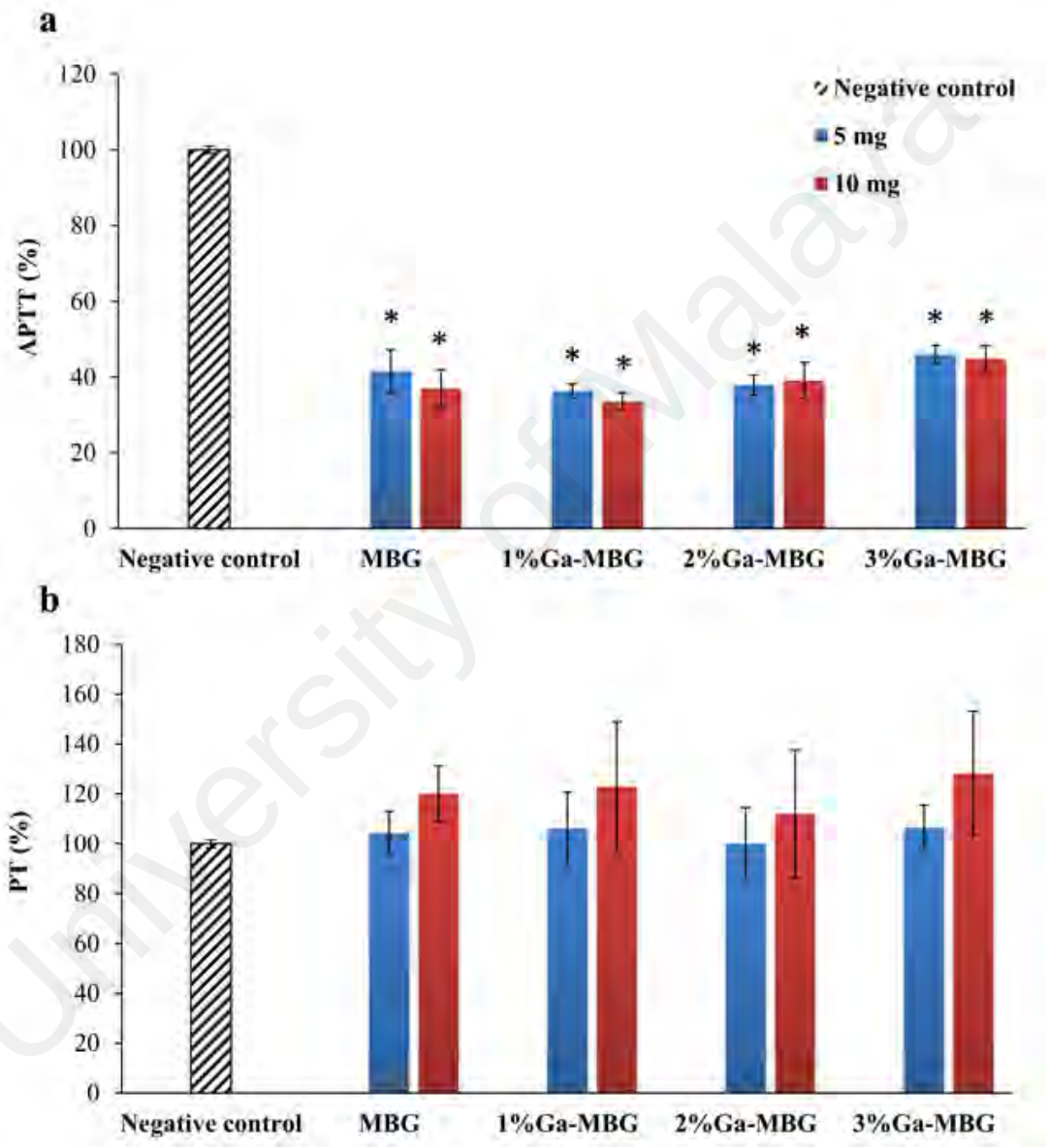

Figure 4.7: Influence of MBG and Ga-MBGs on (a) APTT and (b) PT of human plasma. * represented significant difference with respect to negative control at $P < 0.05$.

4.2.5 *In vitro* thrombus formation

The effect of Ga-substituted MBGs in comparison with MBG on thrombus formation is described in Figure 4.8a. In all cases, thrombus formation increased with incubation time. With increasing incubation periods up to 60 min, 1%Ga-MBG produced much more thrombus in contact with blood than MBG, indicating its higher thrombogenic activity, while 3%Ga-MBG exhibited lower thrombus formation. These results revealed the same trends as the blood coagulation experiments and PBS absorption studies. The digital image of MBG (Figure 4.8b) and 1%Ga-MBG (Figure 4.8c) also confirmed the results of thrombus formation. More red blood cells (RBCs) surrounded by a fibrin meshwork were aggregated on 1%Ga-MBG surface with respect to MBG. The interaction of whole blood with MBG and Ga-MBGs was also seen by FESEM; the images of which (Figure 4.8d-g) revealed that RBCs adhered onto their surface were dehydrated and aggregated, causing a change in cellular morphology.

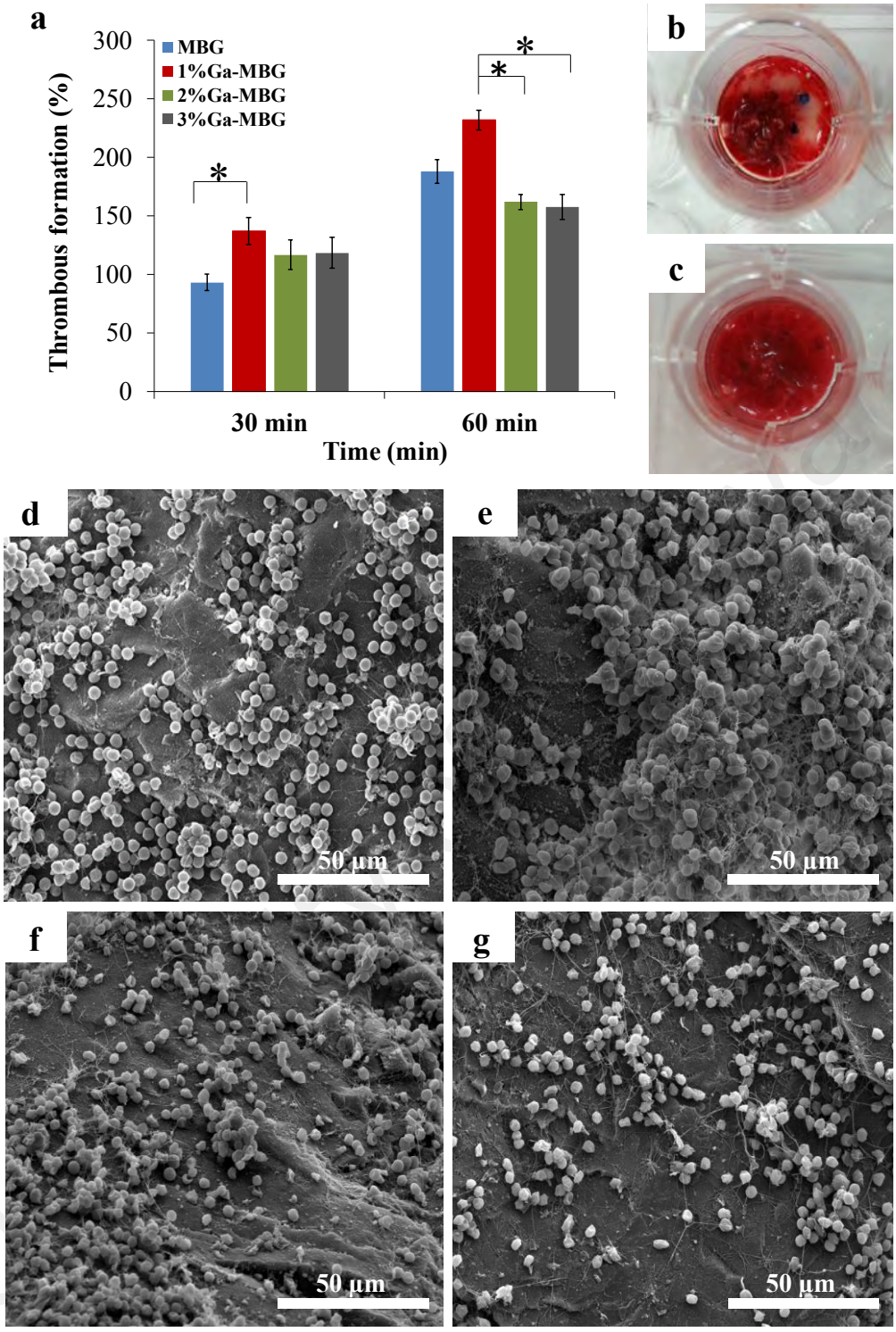

Figure 4.8: (a) Quantitative results of thrombus formation to the materials surface after different incubation time. The blood clot formed on (b) MBG and (c) 1%Ga-MBG surfaces captured by digital camera. FESEM images of the RBCs agglutination and adhesion on the surfaces of (d) MBG, (e) 1%Ga-MBG, (f) 2%Ga-MBG and (g) 3%Ga-MBG after 30 min of incubation. Many RBCs are trapped in a mesh of fibrin fibers and coalesced into thrombus on the 1%Ga-MBG surface. * indicated a significant difference, $p < 0.05$.

More specifically, the RBCs on 1%Ga-MBG surface (Figure 4.8e) seemed to form larger aggregates and coalesced into an erythrocyte plug trapped in the more extensive fibrin protein mesh with respect to MBG (Figure 4.8 d), for which much fewer aggregates were observed on its surface. The images were in agreement with the results of thrombus formation measurements.

4.2.6 Platelet adhesion

To assess the ability of Ga-substituted MBGs in enhancing platelet adhesion and aggregation *in vitro,* the synthesized materials were mixed with platelet suspensions for two time intervals (30 and 60 min), and platelet adhesion was quantitatively measured using an LDH. assay kit. Figure 4.9 illustrates the qualitative and quantitative results of platelet adhesion on MBG and Ga-MBGs. It can be deduced from the results (Figure 4.9a) that all the synthesized materials were able to significantly increase the number of adherent platelets at different time intervals. As compared with non-Ga-containing MBG, 2%Ga-MBG and 3%Ga-MBG, numerous platelets adhered on the surface of 1%Ga-MBG after 30 and 60 min incubation with PRP. However, the results showed an almost negligible increment in the number of platelets adhered onto the surface of other glasses with increasing incubation time. The FESEM also confirmed the significant ability of the 1%Ga-MBG to initiate platelet aggregation (Figure 4.9c) after 30 min of incubation with PRP. The images show that 1%Ga-MBG surface was covered with more platelets alongside silky fibrin than other samples and also many pseudopodia were observed on the surface of 1%Ga-MBG, implying higher activation and aggregation of platelets. By contrast, less platelet adhesion and fibrin formation occurred on the surface of MBG, 2%Ga-MBG and 3%Ga-MBG.

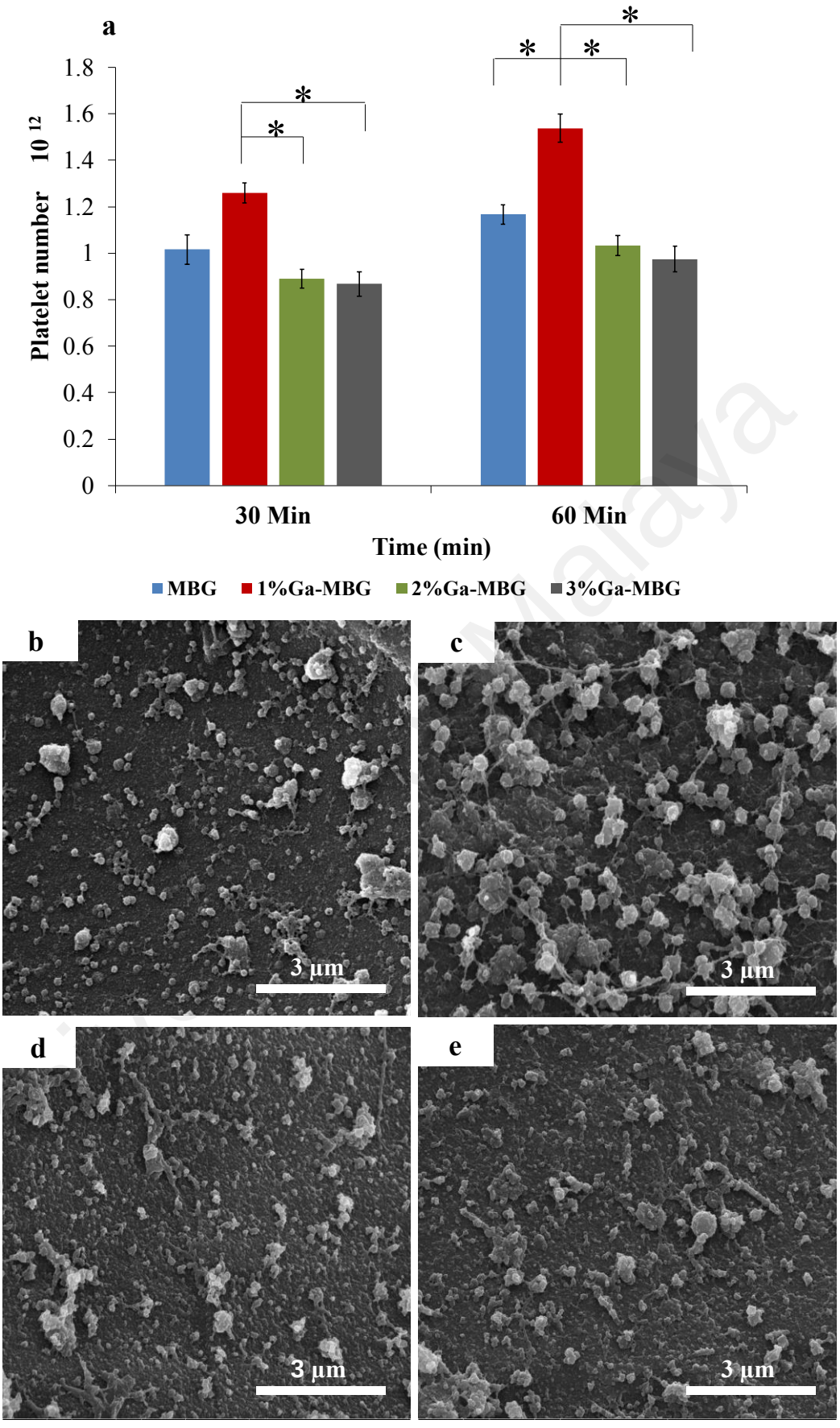

Figure 4.9: (a) Quantification of platelet adhesion on the MBG and Ga-MBGs. FESEM images of platelets adhered on the glasses: (b) MBG, (c) 1%Ga-MBG, (d) 2%Ga-MBG, (e) 3%Ga-MBG. * represented a significant difference, $p < 0.05$.

4.2.7 Antibacterial activity

The antibacterial activity of Ga-MBGs was compared with that of non-Ga-containing MBG against both *E. coli* and *S. aureus* over 12 h as shown in Figure 4.10a and b. Ga-MBGs demonstrated a potent antibacterial effect against both pathogens which can be attributed to the presence of Ga^{3+}, since MBG did not impart a significant antibacterial effect. Of note, the antibacterial efficacy of Ga-MBGs against both *E. coli* and *S. aureus* increased with Ga_2O_3 content over time. Figure 4.10a indicated that 3%Ga-MBG exerted higher antibacterial activity against *E. coli* compared to MBGs with lower Ga_2O_3 content (1%Ga-MBG and 2%Ga-MBG) and achieved significant reduction in the number of viable cells within 12 h (Figure 4.10a). However, differences between the antibacterial effect of 1%Ga-MBG and 2%Ga-MBG were not significant. In the case of *S. aureus* (Figure 4.10b), 3%Ga-MBG had slightly more inhibitory effect compared to 1%Ga-MBG and 2%Ga-MBG, reaching its antibacterial rate of 99 % at 12 h. Figure 4.10 also presents images of colonies of *E. coli* (c-k) and *S. aureus* (d-l) incubated on agar plates obtained from cultured suspensions with MBG and Ga-MBGs. Obvious reduction was detected in the population of the *E. coli* colonies after exposure to the 3%Ga-MBG for 12 h (Figure 4.10k) compared with negative control (Figure 4.10c). A more pronounced reduction in *S. aureus* colonies was also seen upon exposure to 3%Ga-MBG (Figure 4.10l) with respect to the negative control (Figure 4.10d). It should be noted that Ga-MBGs displayed a more significant antibacterial impact against *S. aureus* than against *E. coli*.

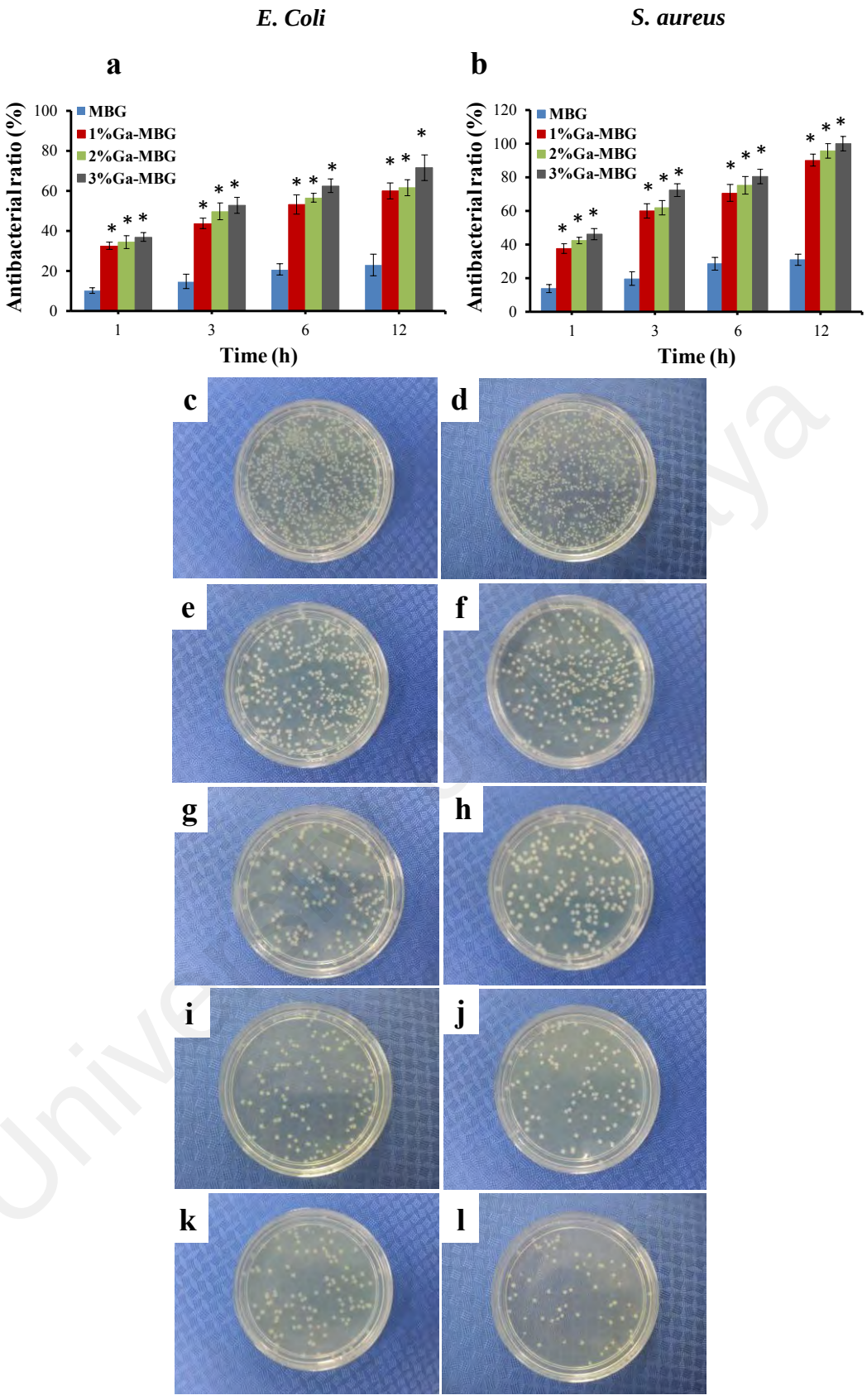

Figure 4.10: Bacteriostatic efficacies of Ga-MBGs against (a) *E. coli* and (b) *S. aureus*. Digital images representing the bacterial culture plates of *E. coli* upon the exposure to (c) the negative control and (e-k) Ga-MBGs and the bacterial culture plates of *S. aureus* treated with (d) the negative control and (f-l) Ga-MBG. * represented a significant difference, $p < 0.05$.

4.2.8 Cytotoxicity effects

To study the biocompatibility of the MBG and Ga-MBGs, cell viability of HDF cells was evaluated after they were treated with extracts of the bioactive glasses for 1 and 3 days. The MTT assay (Figure 4.11) indicated that the cell viability of HDF cells in the presence of the MBG and Ga-MBG extracts increases with culture time, suggesting that all glasses were non-cytotoxic to HDF cells. A slightly higher cell viability was noted for all MBG materials at day 1. However, a significant increase in cell numbers for all the materials were observed after 3 days. Interestingly, the increment in the cell viability was more pronounced in the presence of 1% Ga-MBG.

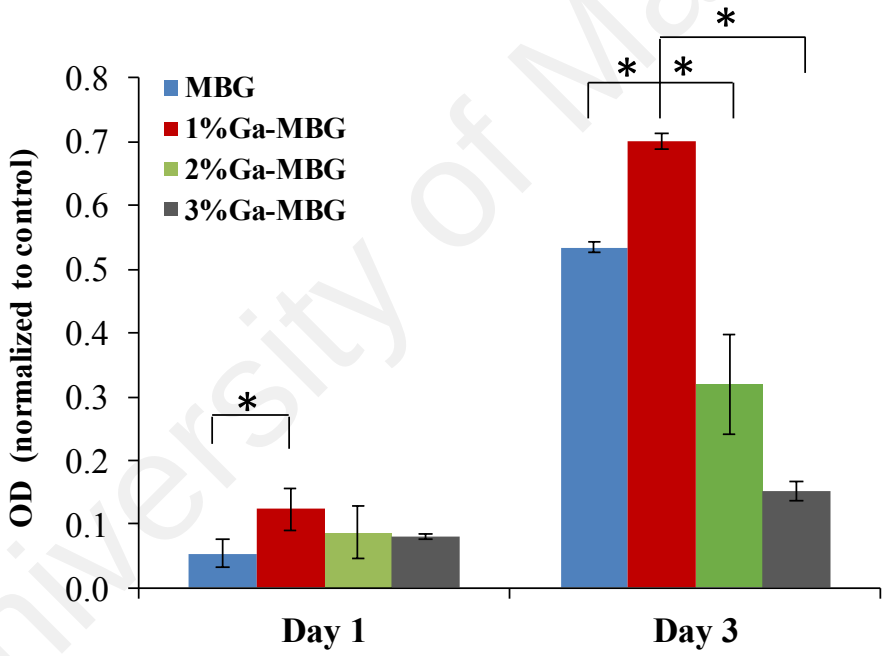

Figure 4.11: Viability of HDF cells after 1 and 3 days exposure to the extracts obtained from MBG and Ga-MBGs. Data were obtained using MTT assay. * represented a significant difference, $p < 0.05$.

4.3 Part II: Comparison of hemostatic efficacy of 1%Ga-MBG with CX and ACS$^+$

4.3.1 Physicochemical characterisation of the hemostats

The N_2 adsorption–desorption isotherm at 77 K of 1%Ga-MBG, which was found to be type IV with an H1 hysteresis loop (Figure 4.12a), further confirmed the presence of a mesoporous structure with hexagonally packed cylindrical channels. The pore size distribution of the sample also indicates a monomodal distribution centred in the mesoporous range (Figure 4.12c). As compared to 1%Ga-MBG, the isotherm of ACS$^+$ exhibits an intermediate behaviour between type I and IV isotherm (Figure 4.12b), suggesting the presence of both microporosity and mesoporosity (Schneider, 1995). The obtained pore size distribution also displays the bimodal micro- and mesoporous nature of ACS$^+$ (Figure 4.12d). However, CX showed the lowest surface area and pore volume.

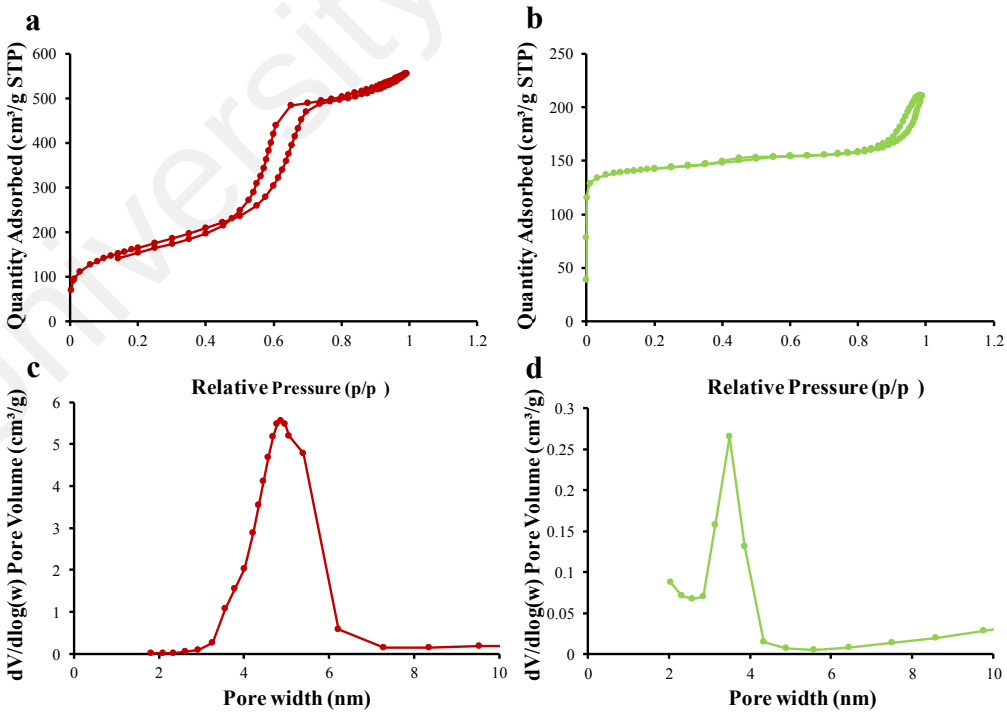

Figure 4.12: (a and b) N_2 adsorption-desorption isotherms and (c and d) corresponding pore size distributions of 1%Ga-MBG and ACS$^+$.

Table 4.3 presents the main textural parameters including specific surface area, pore diameter and pore volume of the various samples measured by the N_2 adsorption porosimetry at 77 K. The textural studies revealed that 1%Ga-MBG possesses better textural properties compared to those of CX and ACS^+. Although ACS^+ has comparable surface area to that of 1%Ga-MBG, its pore volume is significantly smaller. Table 4.3 also shows the mean particle size for the samples. ACS^+ was found to have the highest mean particle diameter of 2240 µm.

Table 4.3. Textural properties of 1%GaMBG, CX and ACS^+.

Samples	Surface area (m^2/g)	Pore diameter (nm)	Pore volume (cm^3/g)	Particle size (µm)
1%Ga-MBG	565 ± 45.09	4.98 ± 0.03	0.84 ± 0.04	283 ± 32
CX	1.41 ± 0.58	6.49 ± 2.91	0.001 ± 0.001	318 ± 36
ACS^+	535 ± 36.73	9.13 ± 1.63	0.130 ± 0.01	2240 ± 83

The ordered mesoporous structures of the 1%Ga-MBG were also confirmed by SAXRD. The SAXRD patterns of the 1%Ga-MBG (Figure 4.13a) displayed two diffraction peaks in the small-angle regime, at around $2\Theta = 1.09^o$ and 1.7^o demonstrating the presence of a high degree of mesoscopic organisation and local hexagonal symmetry thus confirming the results obtained by TEM. However, the SAXRD of ACS^+ (Figure 4.13b) exhibited two poorly resolved peaks in 2Θ range 1-1.5°.

WXRD patterns were also collected to determine the amorphous or crystalline states of 1%Ga-MBG, CX and ACS^+. In contrast to WAXRD patterns of 1%Ga-MBG (Figure 4.13c) and CX (Figure 4.13d), which show only one broad diffraction peak at $2\Theta = 15–35°$ revealing their amorphous states, the WAXRD pattern of ACS^+ (Figure 4.13e) shows several crystal diffraction peaks associated with the zeolite

Linde type 5A (LTA-5A) confirming the highly crystalline state of ACS^+ (Ahuja *et al.*, 2006).

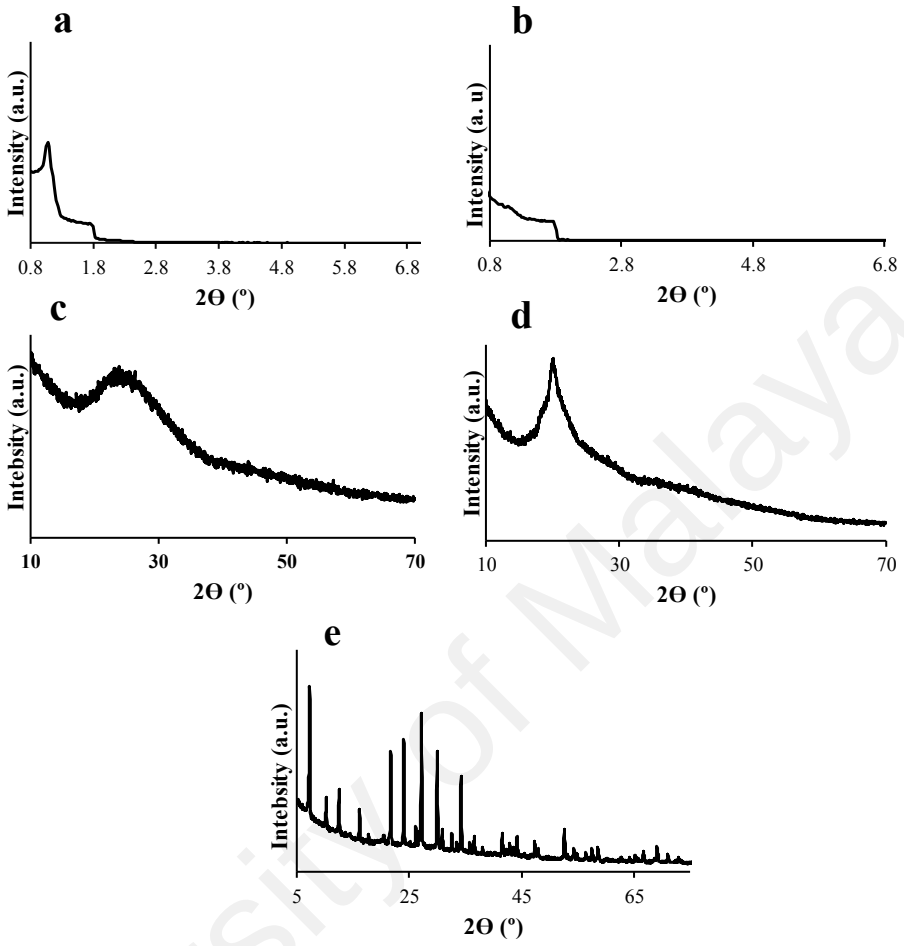

Figure 4.13: SAXRD of (a) 1%Ga-MBG and (b) ACS^+. WXRD analysis of (c) 1%Ga-MBG, (d) CX and (e) ACS^+.

To identify the internal morphology of 1%Ga-MBG and ACS^+, HRTEM was used. Indeed, the HRTEM image of 1%Ga-MBG (Figure 4.14a) revealed a highly ordered two-dimensional (2D) hexagonal mesostructure with uniform cylindrical pore channels, whereas the image of ACS^+ (Figure 4.14b), which is a primarily microporous material, barely evidences a secondary mesoporous structure.

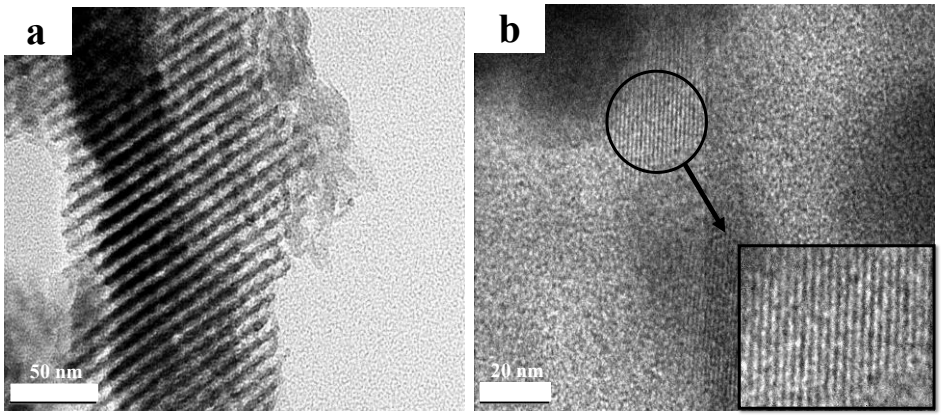

Figure 4.14: HRTEM images of (a) 1%Ga-MBG and (b) ACS^+ respectively. The mesoporosity in the ACS^+ was marked by black arrows.

The surface morphologies and microstructures of 1%Ga-MBG and both commercial hemostats (CX and ACS^+), examined using FESEM, are depicted in Figure 4.15. 1%Ga-MBG consisted of irregularly shaped particles, (Figure 4.15a and b) exhibiting less roughness than the ACS^+ (Figure 4.15e, and f) which exhibit a spherical particle shape. The FESEM micrographs of CX (Figure 4.15c and d) also show a rough and folded surface morphology.

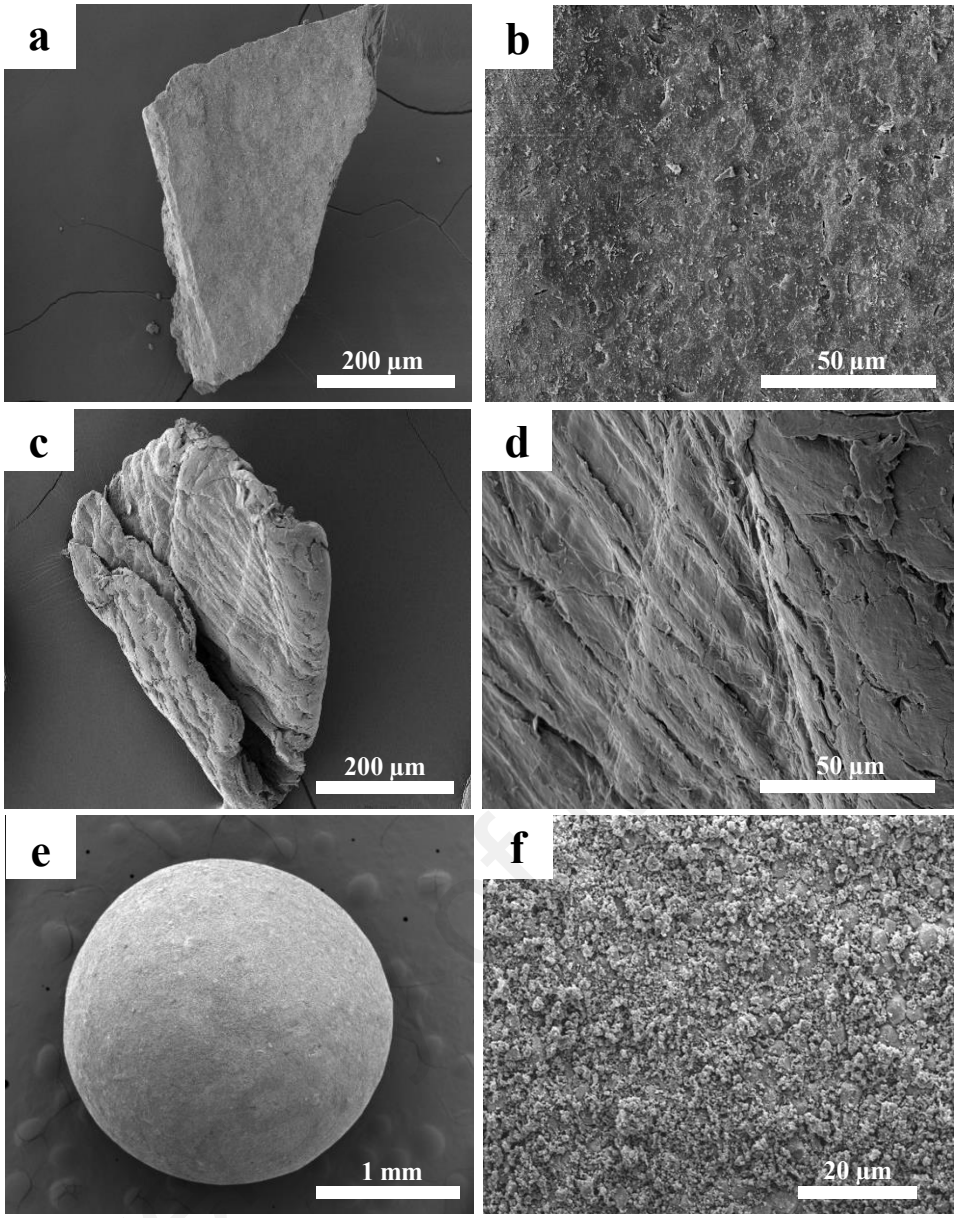

Figure 4.15: Low and high magnification FESEM images of (a,b) 1%Ga-MBG, (c,d) CX and (e,f) ACS^{+}. The high magnification FESEM image reveals a rough surface texture of all materials.

4.3.2 Degradation behaviour *in vitro*

The *in vitro* degradation behaviours of the materials have been investigated in Tris–HCl solution at 37 °C. As can be seen in Figure 4.16, the degradation rate of all samples increased with prolonged immersion time particularly during the first three days. However, a notable difference between the groups was observed in their degradation at either of the 7-time points. 1%Ga-MBG demonstrated a higher weight

loss than that of CX and ACS^+ over 35 days which can be attributed to its larger specific surface area, higher pore volume and smaller particle size, making the 1%Ga-MBG dissolve faster over time. Of note, ACS^+ showed the lowest weight loss, indicating its poor degradability.

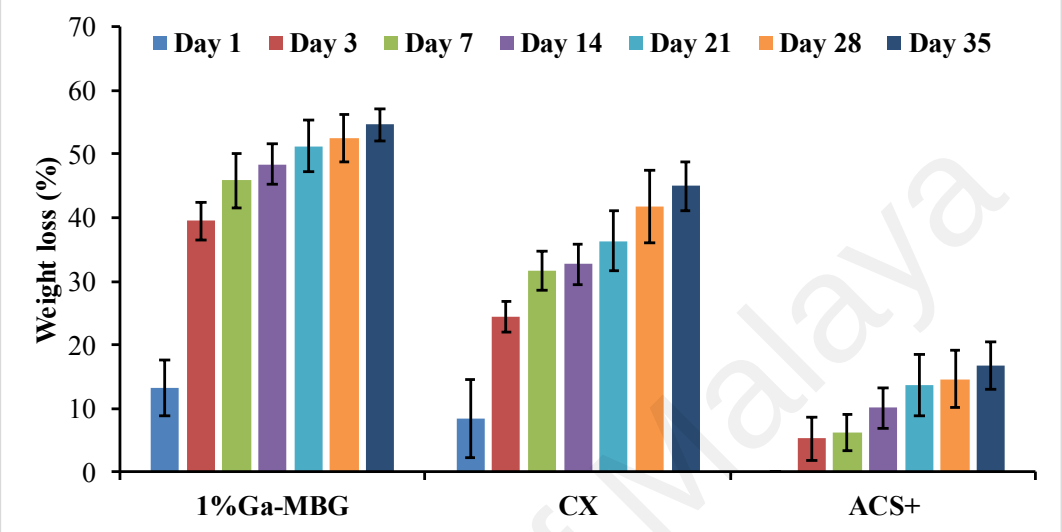

Figure 4.16: Weight loss against immersion time for the 1%Ga-MBG, CX and ACS^+.

4.3.3 PBS absorption *in vitro*

Figure 4.17 shows the absorption ratio of the samples in PBS. CX had greater absorption than those of 1%Ga-MBG and ACS^+. As compared with ACS^+, 1%Ga-MBG also exhibited a higher absorption ratio which may be due to its higher surface area and pore volume.

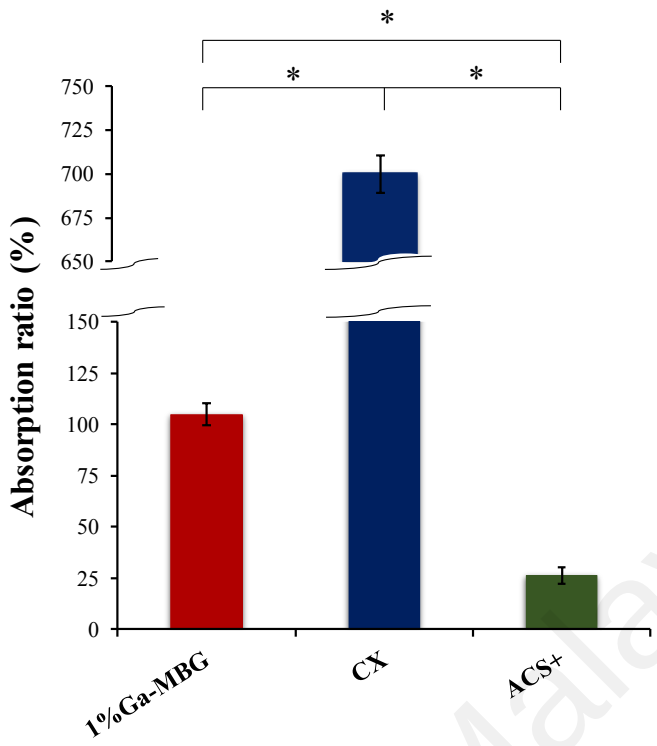

Figure 4.17: Water absorption of 1%Ga-MBG, CX and ACS^{+}. * indicates a significant difference, $p < 0.05$.

4.3.4 APTT and PT assay

To assess the *in vitro* pro-coagulant activity of hemostatic materials (1%Ga-MBG, CX and ACS^{+}), two commonly used parameters, APTT and PT were measured on two different amounts (5 and 10 mg). APTT and PT tests are used to investigate the intrinsic and extrinsic pathway, respectively. Both methods are used to investigate the common coagulation pathways. Figure 4.18 presents the APTT and PT results of the materials. It was found that the administration of the hemostatic materials to the blood serum remarkably affected the values of APTT in a dosage-dependent way. As can be seen in Figure 4.18a, at the lowest dosage examined (5 mg), a shortened APTT was observed for the blood plasma treated with 1%Ga-MBG and ACS^{+} in comparison to the negative control, whereas, conversely, APTT was found to be substantially prolonged in the presence of CX. Most notably, unlike CX that led to formation of a mechanically unstable gel layer at higher amount (10 mg)

interfering with the clotting mechanism, the time to initiate the intrinsic pathway (APTT) was significantly decreased with 1%Ga-MBG (19.55 s) in comparison to the ACS^+ (26.81 s) and negative control (44.26 s). It is also worth noting that stable and strong hemostatic clots were formed by trapping 1%Ga-MBG and ACS^+ particles in a fibrin meshwork, whereas CX caused the clot to rupture. On the other hand, PT of the investigated materials remained unchanged at the given amounts (5 and 10 mg), suggesting that the hemostatic materials had no remarkable effect on PT (Figure 4.18b). However, in the case of the higher CX amount (10 mg), PT was markedly prolonged similar to that of APTT.

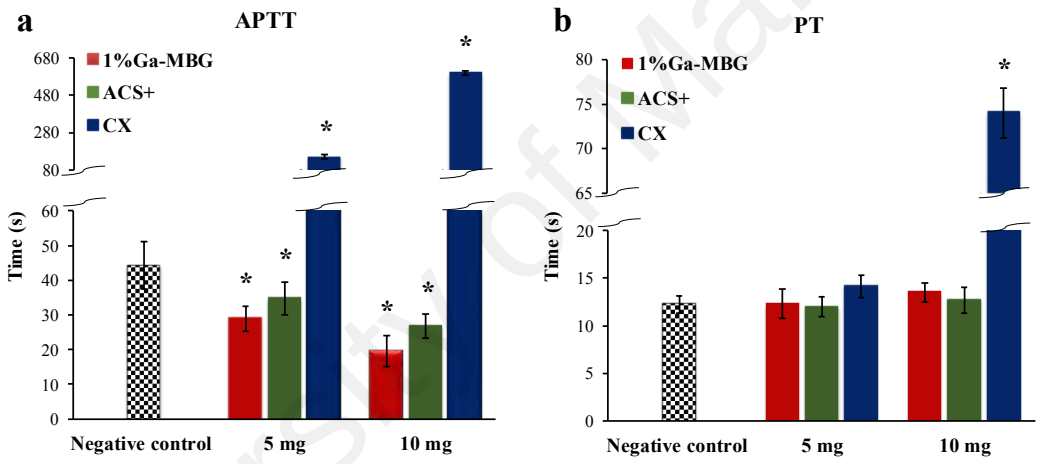

Figure 4.18: APTT and PT measurements of 1%Ga-MBG, CX and ACS^+. Influence of the materials on (a) APTT and (b) PT of human plasma. * represents a significant difference with respect to negative control at $p < 0.05$.

4.3.5 *In vitro* blood clot formation

The induced thrombotic effects of 1%Ga-MBG were compared with those of CX and ACS^+ and the results are depicted in Figure 4.19a. As compared to the lower thrombus formation ability of CX and ACS^+, 1%Ga-MBG resulted in the highest thrombus formation over the 60 min incubation period, confirming its thrombogenic nature. These results exhibited the same trend as the blood coagulation experiments (APTT and PT), where 1%Ga-MBG was found to be superior to other samples. The

results of the thrombus formation test were further confirmed by digital photographs and FESEM (Figure 4.19b-m). As can be seen from the digital images, unlike CX (Figure 4.19c and f) and ACS^+ (Figure 4.19d and g), which resulted in the formation of small and unstable hemostatic clots, more RBCs were coalesced into an erythrocyte clot on the 1%Ga-MBG (Figure 4.19b and c) surface forming a physically more stable clot surrounded by a dense meshwork of fibres. It is also worth noting that the clots formed on the surface of the 1%Ga-MBG were darker in colour with respect to CX and ACS^+. FESEM images also demonstrated the interaction of blood components with 1%Ga-MBG, CX and ACS^+ to form a clot. Although adhesion of RBCs was observed on all investigated materials, more RBCs seemed to clump in a fibrin protein mesh, forming a larger agglomerate on the 1%Ga-MBG surface (Figure 4.19h and k) compared with CX (Figure 4.19i and l) and ACS^+ (Figure 4.19j and m), where fewer erythrocyte plugs were noted on their surface. The FESEM images presented in Figure 4.18 also confirmed that the 1%Ga-MBG (Figure 4.19h and k) surface was more favorable for the agglutination and adhesion of RBCs compared with that of CX (Figure 4.19i and l) and ACS^+ (Figure 4.19j and m). Meanwhile, it should be noted that RBCs formed more aggregates on the CX surface compared to ACS^+, while more fibrin was observed on ACS^+. These results were in line with the previous observation in clot formation tests.

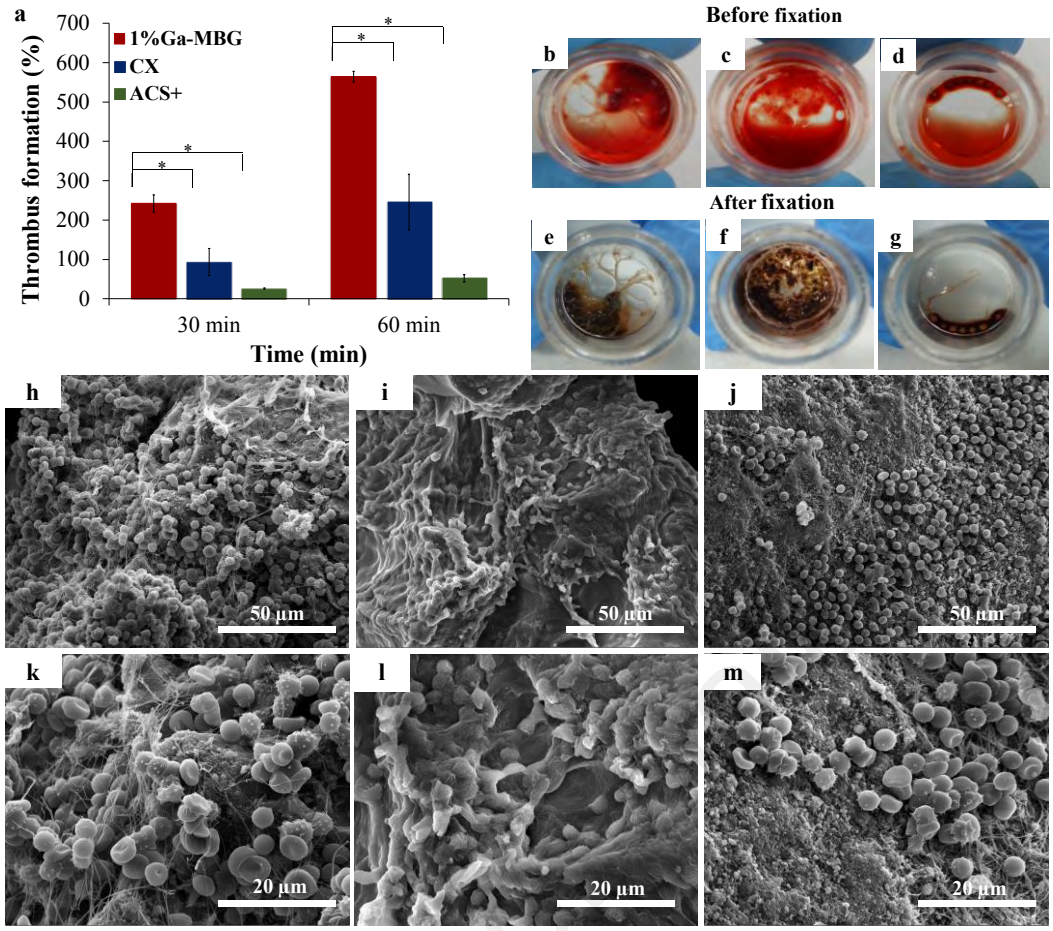

Figure 4.19: The *in vitro* thrombogenic activity of the samples. (a) Quantitative analysis of thrombus formation on the hemostatic materials surface upon incubation over a 60 min period. Digital photographs of the thrombus formed on (b, e) 1%Ga-MBG, (c, f) CX and (d, g) ACS^+ before and after fixation by glutaraldehyde. FESEM observations at low and high magnification of agglutinated RBCs on the surface of (h, k) 1%Ga-MBG, (i, l) CX and (j, m) ACS^+. More RBCs clumped in fibrin threads to form a thrombus on 1%Ga-MBG surface compared with CX and ACS^+. * represents a significant difference, $p < 0.05$.

4.3.6 Platelet adhesion and activation

The *in vitro* capability of 1%Ga-MBG to aggregate and activate platelets were compared to CX and ACS^+. In this regard, the number of platelets adhered on the surface of the hemostats was quantified by the activity of LDH and the morphology of the adherent platelets was visualised using FESEM (Figure 4.20). The quantitative result (Figure 4.20a) demonstrated that the number of adherent platelets to the surface of these three hemostatic materials increased with increasing incubation time

up to 60 min. However, while the number of adherent platelets to the surface of 1% Ga-MBG and CX increased significantly after 60 min incubation with PRP, a negligible increase occurred in the number of platelets adhered on the surface of ACS^+. These results were further confirmed by FESEM micrographs, as shown in Figure 4.20b-g. Much more platelet aggregates and spread platelets were observed on the surface of 1%Ga-MBG (Figure 4.20b and c) and CX (Figure 4.20d and e) in comparison with ACS^+ (Figure 4.20f and g), for which only few aggregates were observed. However, although no significant difference was found in the number of adhering platelets among the 1%Ga-MBG and CX groups, the platelets adhered to the 1%Ga-MBG were remarkably more activated than those on the CX, as platelets extended long pseudopodia.

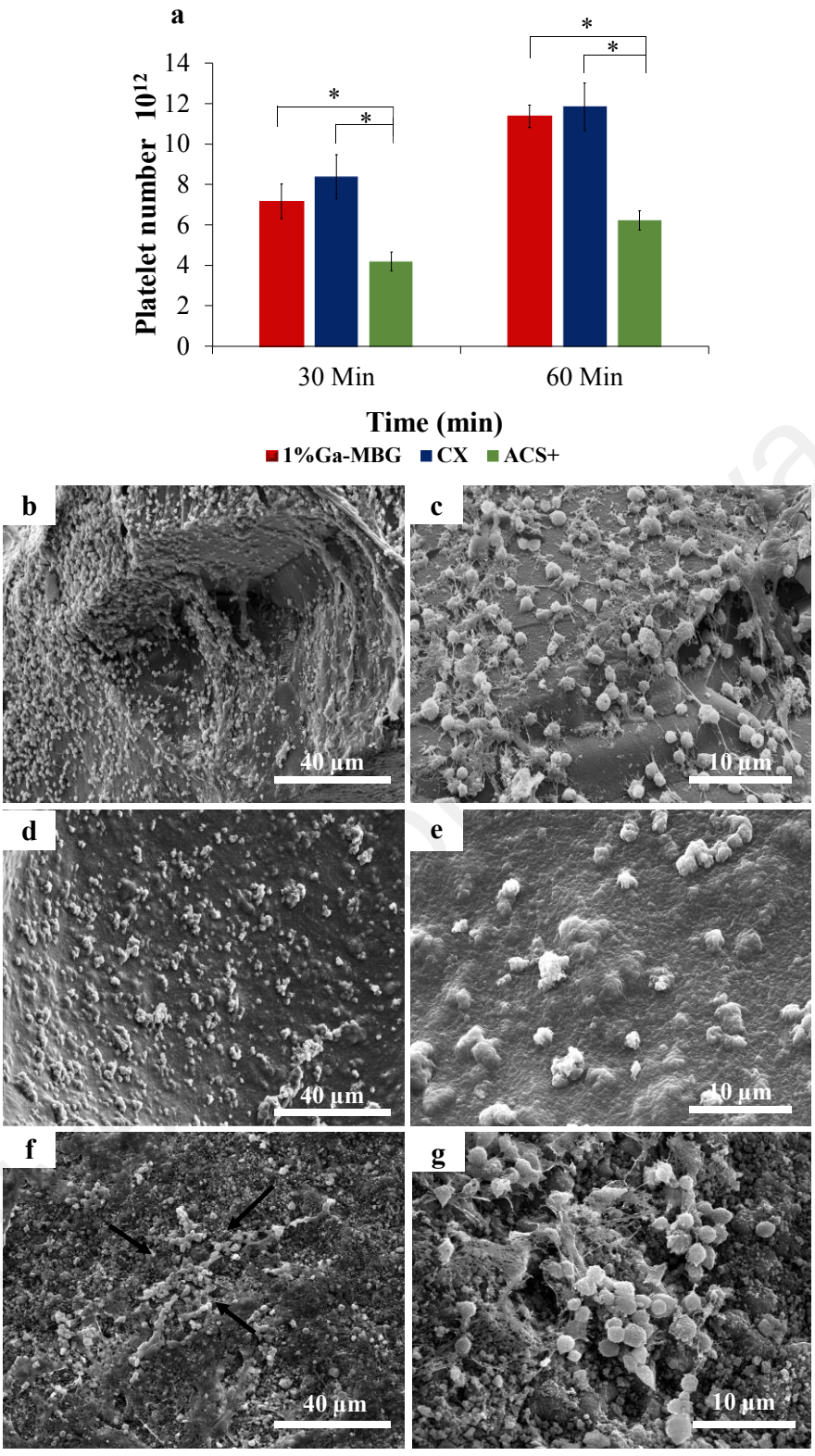

Figure 4.20: Qualitative and quantitative results of platelet adhesion on the hemostats. (a) Quantification of platelet adhesion on the hemostatic materials after different incubation times in PRP. FESEM micrographs at low and high magnification of platelets adhered to the surface of (b, c) 1%Ga-MBG, (d, e) CX and (f, g) ACS^{+} after 30 min of incubation in PRP. The black arrows represent the platelet aggregation on the surface of ACS^{+}. * indicates a significant difference, $p < 0.05$.

4.3.7 Thrombin generation assay

To evaluate the thrombin-generating activity of the tested materials, the TAT of the materials was measured in PPP. The results (Figure 4.21) revealed that the TAT levels were elevated over 60 min in PPP contacted with all the samples and it was found to be higher in 1%Ga-MBG as compared with CX and ACS$^+$ (Figure 4.21).

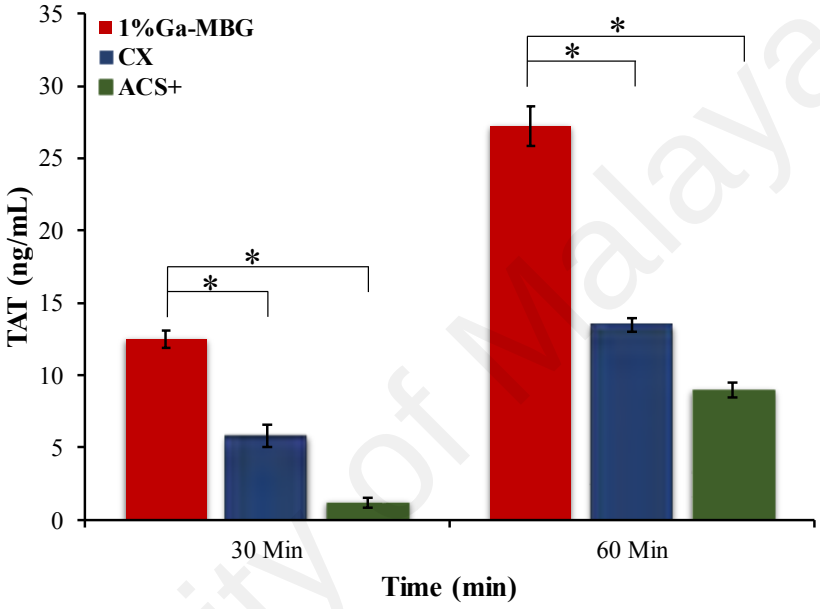

Figure 4.21: Representative thrombin generation in PPP treated with 1%Ga-MBG, CX and ACS$^+$. Effect of the different hemostatic materials on thrombin generation over time, as measured by the levels of TAT complex. * represents a significant difference, $p < 0.05$.

4.3.8 Cytotoxicity effects

To use a biomaterial as a hemostatic agent for stopping bleeding, its cellular toxicity needs to be evaluated. Figure 4.22a illustrates potential effects of 1%Ga-MBG, CX and ACS$^+$ on HDF viability as assessed by MTT assays. The results revealed that all these samples were non-toxic to HDF cells and potentially suitable for hemostatic applications. As can be seen from 4.22a, direct exposure of the tested samples to HDF cells increased slightly the HDF cell viability after day 1. However,

the viability of 1%Ga-MBG, CX and ACS^{+}-treated cells considerably increased at the further time point (3 days), especially in the presence of 1%Ga-MBG, confirming the high biocompatibility of the tested materials. The result was also confirmed by a Live/Dead assay using confocal microscopy. The fluorescence images (Figure 4.22b-d) showed that, by extending the culture period to 3 days, a high number of cells exposed to the investigated materials appeared green, indicating a significant increase in viability of HDF cells. While 1%Ga-MBG showed a relatively higher proportion of living cells, the ACS^{+} group exhibited the greatest number of dead cells.

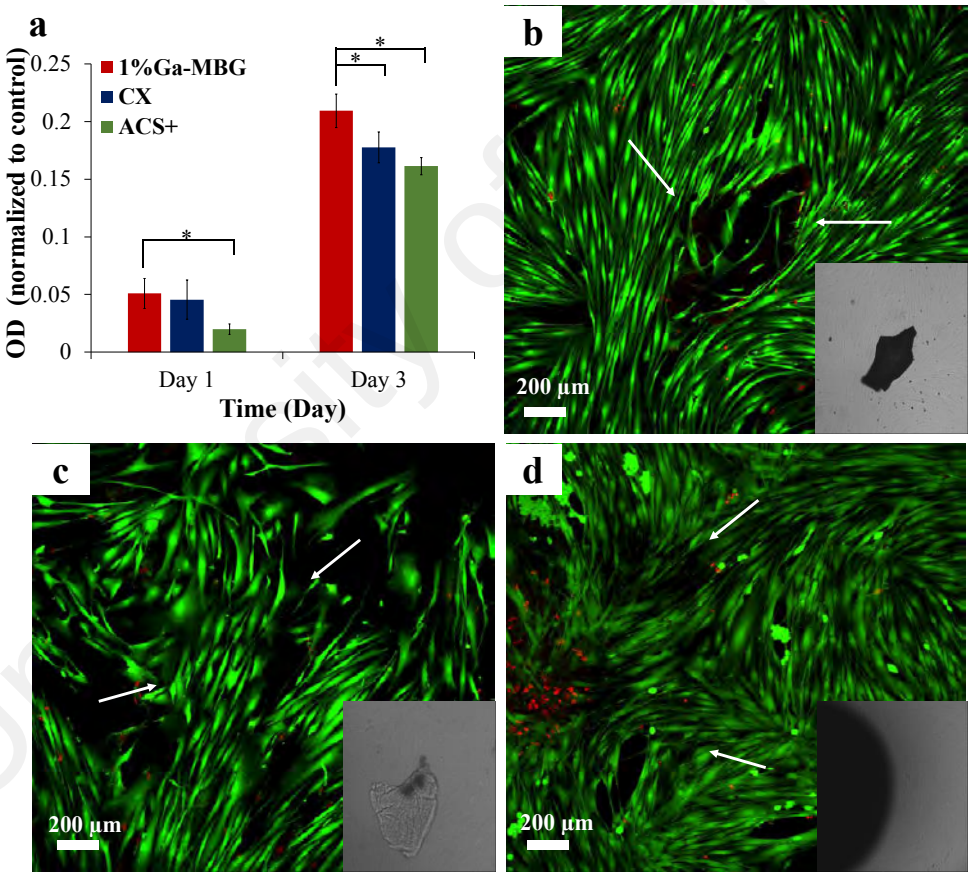

Figure 4.22: Cytotoxicity effects and Confocal microscopy images of 1%Ga-MBG, CX and ACS^{+}. (a) Quantitative analysis by MTT assay of HDF cells viability after 1 and 3 days exposure to 1%Ga-MBG, CX and ACS^{+}. Fluorescent microscopy images of HDF cells cultured in the presence of (b) 1%Ga-MBG, (c) CX and (d) ACS^{+} for 3 days. Live and dead cells were appeared as green and red fluorescence respectively. White arrows show the particles surrounded by HDFs cells. Inset picture shows phase contrast micrographs of 1%Ga-MBG, CX and ACS^{+}. * indicates a significant difference, $p < 0.05$.

CHAPTER 5: DISCUSSION

5.1 Introduction

This chapter is divided into 2 parts. Part I discusses the crucial parameters affecting the hemostatic activity and cellular response of Ga-MBGs. Part II discusses on the factors that make the Ga-MBG superior to the commercial hemostats.

5.2 Part I: Gallium-containing mesoporous bioactive glasses: physiochemistry, biological and hemostatic properties

Much attention has focused on the fabrication of inorganic mesoporous materials as a new generation of inorganic hemostats that may be able to overcome any shortcoming associated with the commercial inorganic hemostats such as QC and QCG. Whilst some reports highlight the hemostatic performance and antibacterial property of MBGs (Dai *et al.*, 2010; Dai *et al.*, 2009; Ip *et al.*, 2006), more studies are needed to clarify the hemostatic properties and antibacterial activity of these materials. Chemical modification of MBGs through incorporation of therapeutic elements into their frameworks may be one way to improve their hemostatic capacity and antibacterial activity. It has been found that $Ga(NO_3)_3$ has the ability to induce the earliest stages of hemostasis (Goodley *et al.*, 2011). Considering this, in the first part of the present study, Ga-MBGs with different Ga contents (1, 2 & 3 mol%) were prepared and the effect of incorporation of Ga^{3+} on physiochemistry property, blood clotting response, antibacterial activity and biocompatibility of MBG was assessed.

Hemostasis is a complex physiological process that prevents blood loss and proceeds *via* the synchronized action of three mechanisms including

vasoconstriction, formation of a platelet plug and blood coagulation (di Lena, 2014). So, the hemostatic agents that perform their task by accelerating one or more of the processes above can achieve hemostasis efficiently.

The results of this study demonstrated that hemostatic performance of Ga-MBGs independently of particle size which was in the same range (250-300 μm) for all the glasses, was mainly affected by the physicochemical parameters such as mesoporous structure, textural properties, zeta potential and chemical composition. It was found that all the mentioned parameters were significantly influenced by incorporation of different concentration of Ga_2O_3.

There are multiple mechanisms underlying MBG and Ga-MBGs' hemostatic properties. Based on the obtained results in the coagulation assays, it was observed that, unlike the extrinsic pathway that was insignificantly affected by the bioactive glasses, the intrinsic coagulation pathway was considerably accelerated in the presence of the synthesized materials with respect to the negative control (Figure 4.7).

The accelerated coagulation response induced by the synthesized samples can depend on multiple factors. In details, both MBG and Ga-MBGs, due to possessing mesoporous interconnected structures with large specific surface areas, can act as factor concentrators and share a mechanism of action similar to QC. Such materials capture and store large volumes of water within their pores resulting from the electrostatic interaction with Ca^{2+} ions residing in their pores. These interactions lead to the hyperconcentration of coagulation factors and other protein and cellular components of the plasma that in turn would accelerate the coagulation cascade and the subsequent fibrin clot formation. However, a prolonged APTT was observed with increasing Ga_2O_3 content in the MBG network (*i.e.* for 3%Ga-MBG) in comparison with MBG (Figure 4.7). It may be speculated that this prolonged effect of MBG with

higher Ga_2O_3 content on APTT values can be related to deterioration of the hexagonal ordered structures of the MBG, which decreases its textural properties (specific surface area and pore volume) and subsequently reduces its water absorption coefficient. In contrast to 3%Ga-MBG and other prepared bioactive glasses, a shortening of the APTT was occurred as a result of adding MBG with lowest Ga_2O_3 content (1%Ga-MBG), which can be attributed to its outstanding textural properties. The 1%Ga-MBG, due to its larger specific surface area and pore volume, serve plenty of spaces resulting in greater permeability of the water molecules to their pores and subsequent blood clot formation. Accordingly, the mesoporous structure of the MBG materials plays a pronounced role in the activation of the intrinsic pathway. These results were consistent with the PBS absorption results: indeed, the 1%Ga-MBG samples were superior to all other synthesized glasses in water absorption ability (Figure 4.6).

Another favorable factor that contributes to the hemostatic function of the glasses can be related to their potent procoagulant activity resulting from their negative surface charge. The presence of the negative charge on the surface of all synthesized materials were confirmed by zeta potential measurements (Table 4.2). The synthesized materials exhibited significant negative zeta potential in PBS at pH 7.4. The accepted explanation is that, when the bioactive glasses come in contact with body fluids, a unique surface reaction occurs including rapid ion exchange reactions between the glass network modifiers with H^+ (or H_3O^+) ions from the solution (Grover *et al.*, 2013; Rahaman *et al.*, 2011). This reaction leads to hydrolysis of the silica groups, subsequent formation of silanol (Si−OH) groups on the glass surface and, eventually, the production of a negatively charged surface with functional groups ($Si–O^-$).

As previously proved, negatively charged materials such as kaolin can accelerate the hemostasis of the blood *via* activation of a coagulation cascade (Alam *et al.*, 2004; Dai *et al.*, 2009) (Ostomel, Shi, & Stucky, 2006; Walsh, 1972). Due to this, such materials are expected to have a hemostatic mode of action similar to that of QCG, which is a kaolin-based hemostat (Carraway *et al.*, 2008; B. S. Kheirabadi, Edens, *et al.*, 2009).

When the MBG and Ga-MBGs are exposed to blood, their negative surface charge triggers the intrinsic blood coagulation cascade. The basic principle of such phenomena relies on the fact that coagulation factor XII (Hageman factor) binds to negatively charged surfaces through positively charged amino acids in its heavy chain (Colman *et al.*, 1997; Sperling *et al.*, 2009). The binding facilitates subtle conformational changes in FXII, leading to formation of active FXIIa through auto-activation. It is evident that this activated factor directly contributes to fibrin formation (Renné *et al.*, 2012). Therefore, negatively charged surfaces of Ga-MBGs are considered as a key contributor to the activation of the intrinsic pathway of blood coagulation. However, the zeta potential became less negative when a higher amount of Ga_2O_3 was incorporated in the MBG framework as compared with Ga-free MBG (Table 4.2). The less negative charge imparted on the surface of highest substituted Ga-MBG can be correlated with the presence of a high amount of acidic Ga^{3+} species at the surface of the glass as previously demonstrated by Aina *et al* (Aina *et al.*, 2011). The authors demonstrated that the presence of abundant surface Ga^{3+}-species acting as strong Lewis acid sites is responsible for the enhanced surface acidity of the Ga-modified glasses compared with Ga-free glasses. Therefore, this could be another acceptable reason for the prolongation of the APTT in the presence of 3%Ga-MBG.

Another possible component that dominates the pro-coagulant trend of the investigated samples is ascribed to their polar framework resulting from the silanol

groups resident on their surface, which have very strong polar interactivity. Previous reports have suggested that blood coagulates faster on polar glass surfaces than nonpolar plastic surfaces; this phenomenon is referred to as the "glass effect" (Ahuja *et al.*, 2006; Ostomel *et al.*, 2007). The underlying principle for this observation is that polar surfaces are involved in the autocatalytic activation of clotting Factors XII and XI along with prekallikrein and high-molecular-weight-kininogen (HMWK), and in the subsequent activation of the multiple mechanisms responsible for the association of the thrombin enzyme and, eventually, of fibrin production (Holden *et al.*, 2010; Sperling *et al.*, 2009). The polar framework of the MBG materials that is generated by the presence of surface silanol groups can thus act as a desirable surface for the contact activation of the intrinsic pathway.

More specifically, FTIR spectra of the MBG and Ga-MBGs confirmed the presence of the NBOs in the glass network, which in turn facilitates the formation of Si–OH functional groups on the surface of glasses. It is assumed that increasing the Ga_2O_3 content in MBG framework shifts its role from network former to network modifier, since a significant decrease in the intensity of 460, 800 and 1070 cm^{-1} bands were observed in higher substituted Ga-MBG. These results prove the discussion presented by Franchini *et al*. who investigated the structural role of different concentrations of Ga^{3+} on bioactive phospho-silicate glasses (Franchini *et al.*, 2012). The authors explained that the structural behavior of this ion relies on its amount in the glass network so that the increasing Ga_2O_3 content changes its role from that of network former to network modifier. However, in this study, it was found that the role of surface area can be more noticeable in the formation of nucleation sites (Si–OH) rather than the presence of network modifier. Indeed, 1%Ga-MBG with high surface area released ions quickly, inducing a large number of OH^- groups to deposit on its surface, and further activation of intrinsic pathway.

Similarly to zeolite-based hemostats, the presence of Ca^{2+} in the glass network also plays an important role in its procoagulant action. The synthesized materials have ability to present Ca^{2+} to blood, which speeds up the intrinsic pathway of blood coagulation. Ca^{2+} (known as clotting factor IV) is a cofactor that plays a ubiquitous role in the coagulation cascade. It is involved in the immobilization and orientation of clotting enzymes on cellular surfaces, serving as the ionic bridge between two negatively charged residues (such as cellular surface and clotting factors) (Hoffman, 2003). It also serves as a required co-factor for several enzymatic reactions, including conversion of prothrombin to thrombin, the enzyme that aids in the generation of insoluble fibrin from the soluble fibrinogen. Ca^{2+} ions are also consumed during splitting fibrinogen into fibrin monomer and polymerization of monomers to fibrin strand and, eventually, lead to crosslinking and formation of ticker fibrin strands (Greenberg *et al.*, 2006; Mikaelsson, 1991). Indeed, they act as an adhesive to hold the fibrin monomers to each other to form the polymeric fibrin fibers.

Hence, Ca^{2+} availability in the MBG framework is another factor favorable to the activation of intrinsic pathway and subsequent shortened APTT. Interestingly, comparing the results from ion release study and coagulation assay indicated a very close correlation between shortened APTT and Ca^{2+} release profile so that 1%Ga-MBG, having a higher capability to release Ca^{+2} than other glass formulations, led to the further reduction of APTT.

Contrary to what occurs in conventional glasses (melt and sol-gel bioactive glasses), where a higher amount of network modifier leads to lower network connectivity, a rapid ion exchange and a subsequent rapid ion release, the MBGs do not apparently exhibit the same trend.

Here, we observed that an increase in the Ga_2O_3 content provoked a decrease in the release rate of the ions, which is evidenced by MP-AES results. Such results may support the idea that the incorporation of a higher amount of Ga^{+3} into MBG disrupts the order of the mesostructure, resulting in a decrement of the textural properties, which are essential parameters to produce a unique ion release profile in the MBGs. Therefore, the lower Ca^{2+} release rate of 3%Ga-MBG system was considered to be another leading cause of APTT prolongation. On the contrary, in the case of 1%Ga-MBG, with the lowest Ga_2O_3 content and outstanding textural properties, Ca^{2+} release profile evidenced that, just after 0.5h immersion in Tris-HCl solutions, a substantial amount of Ca^{2+} (~103 ppm) was released. These results could be explained as owing to the synergy of both the low Ga_2O_3 content (1 mol%) and high specific surface area, which provoked a larger Ca^{2+} release, necessary for the activation of intrinsic pathway.

It is reported that polyvalent cations such as trivalent ions can also promote the blood clotting cascade (Keene *et al.*, 2001; Patterson, 2003). The Fe^{3+} is an example of the ions that can generate the most biologically reactive hydroxyl radicals (HRs) through reaction with hydroxyl groups of water (Keene *et al.*, 2001; Lipinski & Pretorius, 2012; Lipinski, Pretorius, *et al.*, 2012; Pretorius *et al.*, 2013). These radicals, in turn, lead to polymerization of fibrinogen into strong fibrin clots and subsequently stimulate blood coagulation cascade (Lipinski *et al.*, 2013). It is interesting to note that Ga^{3+} not only is a polyvalent cation, but also has an ionic radius similar to that of Fe^{3+}. There is some speculation that Ga^{3+} may share with Fe^{3+} a similar mechanism of action to accelerate coagulation and blood clotting. Therefore, another reason why 1%Ga-MBG despite lower Ga_2O_3 content is a stronger activator of coagulation cascade compared to the other samples can be

attributed to the synergy of both its excellent intrinsic textural and structural features alongside the presence of Ga^{3+}.

Besides the role of the glasses in activation of the intrinsic pathway, they were also found to be effective in thrombus formation and platelet aggregation. From the results of thrombus formation assay in Figure 4.8, distinct amounts of thrombus were noted on four MBGs, in particular on the 1% Ga-MBG surface. It is encouraging that, unlike typical clotting which is composed of platelet plug and a mesh of cross-linked fibrin protein, the unique blood clot formed by MBG materials also consisted of a homogenous layer of RBCs that are stuck in the fibrin mesh to form a clot. It is expected that two main factors, including silanol-rich surface of MBGs that bind with the phosphatidyl choline-rich RBC membrane (Zhao *et al.*, 2011) and the large surface area and pore volume of the glasses that provide more lattice to trap cellular and blood plasma components, are involved in this process. Hence, a possible explanation for the higher thrombogenic potential of 1%Ga-MBG is attributed to its higher surface area that increases the accessibility of silanol groups to the RBCs, leading to production of a stable hemostatic clot.

These results were consistent with those of the platelet adhesion assay (Figure 4.9). 1%Ga-MBG dramatically enhanced the platelet adhesion and activation compared to other glasses, since a large number of platelets were detected on its surface with spread morphology and protruding pseudopodia. The larger surface area in 1%Ga-MBG can be served as a favourable surface for interaction with platelets and fibrinogen, causing clumping and activation of platelets. Likewise, the Ca^{2+} ions that are released from the synthesized materials can contribute to platelet activation, since they accelerate the production of the proteolytic enzyme thrombin. Thrombin is a serine protease that stimulates platelet activation and aggregation through

activation of protease-activated receptors on the platelet cell membrane (Coughlin, 2000).

The major concern with inorganic hemostats such as QC and WS is related to their non-biodegradability, which can lead to thrombosis in distal organs such as brain and lungs (B. S. Kheirabadi, Edens, *et al.*, 2009). For this reason, the degradability properties of hemostatic agents should be evaluated. It has been already reported that the mesoporous silica-based can biodegrade within the body over time (Hudson *et al.*, 2008) and the degradation products can enter the bloodstream or lymph, and then can be excreted via urine (Kortesuo *et al.*, 2000; Radin *et al.*, 2005). Here, the degradation ability of MBG and Ga-MBGs have been assessed after immersion in Tris–HCl solution over time (Figure 4.5e). 1%Ga-MBG showed higher degradation over 14 days compared with other glasses and lost about 41% of its initial weight after soaking for 14 days.

It has been previously reported that the substitution of lower valence ions (*i.e.* Ga^{3+}) for Si can inhibit the hydroxycarbonate apatite formation on BG containing 3.5 mol % Ga_2O_3 through increasing the surface acidity, which could be a reason for its late *in vitro* response (Shruti *et al.*, 2012). Additionally, in a study by Aina *et al*. the enhanced surface acidity of Ga_2O_3 containing BG, compared to the Ga_2O_3-free BG, has been proposed to be responsible for the delayed formation of an apatite-like layer on the glass surface as well as the slower glass dissolution in SBF (Aina *et al.*, 2011). These behaviour could be due to the incorporation of different Ga^{3+} content into glass framework which can affect on/or change the glass composition and hence significantly affect degradation ratio of the glass. This study found that the incorporation of Ga_2O_3 with different amount (1, 2 and 3 mol %) did change the degradation ratio. Si is the main component (80 mol %) in MBG and Ca^{2+} is a network modifier, therefor their release can significantly influence the degradation

process (C. Wu *et al.*, 2011). Considering the linear relationships between ion release and degradation property, inclusion of 1 mol % Ga_2O_3 in MBG framework led to faster dissolution and degradation of MBG, while MBG with higher Ga_2O_3 contents (2 and 3 mol %) demonstrated lower rate of SiO_4^{4-} and Ca^{2+} ions (important contributing factors to material degradation) and hence lower rate of degradation. These results are consistent with previous study demonstrating an increase in Ga_2O_3 content reduced the ion release in SBF (Franchini *et al.*, 2012).

Additionally, higher textural properties are expected to have a beneficial effect on degradation, since they can facilitate the dissolution process. Thus, the higher surface area and pore volume of 1%Ga-MBG compared to the other glasses may be thought of as another possible factor responsible for its higher ability to release the ions and faster degradation.

In addition to assessing the hemostatic functions of the prepared bioactive glasses, their antibacterial properties and biocompatibility were investigated, since infection and cellular toxicity at the site of bleeding are other challenges facing hemostatic agents. Based on the results of the antibacterial activity (Figure 4.10), incorporation of Ga^{3+} into MBG framework implied a faster and more potent bacteriostatic action than non-Ga-containing MBG against both pathogens that were tested. As compared to both pure LB broth culture and MBG, 3%Ga-MBG had a significant inhibitory effect on the growth of both *E. coli* and *S. aureus* in time-kill assays, in particular at 12h. Moreover, 1%Ga-MBG and 2%Ga-MBG samples exhibited more bacteriostatic activity with respect to either pure LB broth culture or MBG.

These results were in good agreement with the Ga^{3+} release profile from the glass network (Figure 4.5d). Although Ga^{3+} had a slower release rate than other ions, it was good enough to achieve a significant antibacterial effect. Based on the results, MBG demonstrated slight antibacterial activity against the two bacterial strains

considered in this work. It is well documented that the glass dissolution can result in a pH increase owing to immediate ion exchange between glass modifiers (*i.e.* Ca^{2+}) and H^+ (Leppäranta *et al.*, 2008; Wei *et al.*, 2015). Therefore, pH increment as a result of the glass dissolution can be considered a possible antibacterial mechanism of MBG. Although pH values of Tris-HCl buffer also increased in Ga-MBGs samples due to the leaching of ions, the glasses exerted significantly higher antibacterial activity against both *E. coli* and *S. aureus* than MBGs. Therefore, the antibacterial property of Ga-MBGs was not attributed to pH, but resulting from Ga^{3+} ions release, as it increased with increasing Ga^{3+} content in MBG framework.

The maximum concentration range of Ga^{3+} ions measured in Tris-HCl for Ga-MBGs was 0.1-0.3 ppm which was sufficient to exert an antimicrobial activity. Kaneko *et al*. (Kaneko *et al.*, 2007) reported that the Ga^{3+} ions in a concentration range as low as 0.007–1.4 ppm can disrupt Pseudomonas aeruginosa Fe^{3+} metabolism and impart antimicrobial activity. In this study, it was also found that the amount of Ga^{3+} released from the glasses is good enough to exert antibacterial effect against both *E. coli* and *S. aureus*.

One possible explanation of the antibacterial effect of Ga^{3+} may be that, differently from another well-known antibacterial ion such as Ag^+ (Gargiulo *et al.*, 2013), this ion has an ionic radius nearly identical to that of Fe^{+3}, which is critical in the pathogenesis of infections (Valappil *et al.*, 2008). It is believed that Ga^{3+} may compete with the Fe^{3+} ions in various biochemical reactions and function as a Trojan horse since many biological systems are unable to distinguish it from Fe^{3+} (C. Chitambar *et al.*, 1991). Notably, supplementation of Ga^{3+} can result in disruption or inhibition of those biomedical reactions requiring Fe^{3+}. However, unlike Fe^{3+}, Ga^{3+} cannot be reduced under the same conditions and can lead to inhibition of a number of essential biological reactions such as those responsible for DNA and protein

synthesis (C. R. Chitambar, 2010; Valappil *et al.*, 2008). Accordingly, Ga^{3+} has the potential to serve as a Fe^{3+} analog and is an effective antibacterial. However, compared with *S. aureus* that was found to be the most susceptible organism to Ga^{3+}, *E. coli* developed resistance to Ga^{3+}, which might can be ascribed to structural differences in the cell walls of these two pathogens. *S. aureus* is surrounded by a peptidoglycan layer with a loosely-packed network structure, which allows Ga^{3+} to pass through the cell wall into the interior without much difficulty, while *E. coli* have a thicker peptidoglycan cell wall, which protects the cell from penetrating Ga^{3+} (Silhavy *et al.*, 2010). For these reasons, Ga-MBG samples exerted better antibacterial effect against *S. aureus* than *E. coli*. Furthermore, the MTT assay illustrated that HDF cells maintained high levels of viability in the presence of extract of both non-Ga-containing MBG and Ga-MBGs, indicating that the synthesized materials have good cytocompatibility. The higher OD values in MBG and Ga-MBGs showing more live cells, demonstrated an enhanced HDF cells' proliferation in the presence of extracts obtained from the glasses in a short culture time period such as 1 day. For a longer culture time, such as 3 days, we found that cells can grow in the presence of 1%Ga-MBG extract dramatically better than those of other glass samples.

A fibroblast is a type of cell responsible for the production of collagen and other connective tissue substances, and plays a critical role in wound healing (Kendall *et al.*, 2014; Tracy *et al.*, 2016). Previous studies showed that BGs can stimulate the secretion of basic fibroblast growth factor (bFGF) and vascular endothelial growth factor (VEGF) (angiogenic growth factors) from human fibroblast cell (Day, 2005; Gerwins *et al.*, 2000; Keshaw *et al.*, 2005; Mao *et al.*, 2015; Shamosi *et al.*, 2015). Additionally, it has been documented that bFGF can stimulates the proliferation of HDFs (Gerwins *et al.*, 2000; Makino *et al.*, 2010). It was reported that the increased

level of Si^{4+} and Ca^{2+} released from the BGs can stimulate the synthesis of VEGF and bFGF (Mao *et al.*, 2015). Therefore, high viability of HDF cells in the presence of the extracts may be due to the fact that the prepared glasses is able to stimulate a significant increase in the secretion of bFGF from fibroblasts by releasing the ions, hence increasing the HDF cells proliferation. The mentioned factors may therefore be possible reasons of higher cell viability of HDF cells in the presence of 1%Ga-MBG extract. It is interesting to find that Ga^{3+} does not appear cytotoxic to HDF cells as its release was maintained well below the toxicity level (14 ppm) (Franchini *et al.*, 2012). It has been also reported that inclusion of higher Ga^{3+} content (5 mol %) into MBG framework cannot result in toxicity, since the maximum concentration released in DMEM was 2.5 ppm, below the toxicity limit of Ga^{3+} ions in blood plasma (14 ppm) (Sanchez-Salcedo *et al.*).

In short, the synergistic effect of all the factors presented above, including chemical activation and physical absorption, promote the blood coagulation cascade and render Ga-MBG materials very suitable hemostatic materials. Taking into account the particles in a same size ranges, the results suggested that incorporation of Ga_2O_3 with concentration variation from 1 to 3 mol % had great influence on the physiological properties of Ga-MBGs. when comparing among the Ga-MBGs in the same dose, it was found that the hemostatic performance and biocompatibility were improved when the concentration of Ga_2O_3 in MBG framework was 1 % mol, but decreased when increasing the Ga_2O_3 concentration to 3 mol %. In order to accurately evaluate the feasibility of any new developed hemostatic agent, the ability of the materials to promote hemostasis need to be compared with some of the commercial products which have already received FDA approval. Accordingly, in the second part of the present study, we selected two products including CX and ACS^{+}. The reason why we choose these products is that both of them were in granule

forms and therefore were comparable with 1%Ga-MBG. On the other hands, CX and ACS^+ are chitosan and zeolite based-hemostatic agents respectively which have already showed promising results in cession of bleeding. Therefore, comparison of 1%Ga-MBG with these products can be a good choice to evaluate its hemostatic advantage.

5.3 Part II: Comparison of hemostatic efficacy of 1%Ga-MBG with CX and ACS^+

We assessed the influence of 1%Ga-MBG properties on the promotion of the very early stages of hemostasis (coagulation, thrombin generation, platelet activation and thrombus formation) as compared with CX and ACS^+.

Evaluation of the APTT and PT assays (Figure 4.18) indicated that, while the extrinsic pathway appears to be unaffected by the tested samples, the intrinsic pathway was significantly accelerated by 1%Ga-MBG and ACS^+ with respect to CX and the negative control. There are several factors which cumulatively contribute to the ability of 1%Ga-MBG and ACS^+ to do this. We believe that both 1%Ga-MBG and ACS^+ share a similar mechanism of action and act as factor concentrators and/or pro-coagulants. Due to possessing a porous structure and a high specific surface area, both inorganic materials are thought to rapidly absorb and sequester fluid phase components from the blood matrix and to concentrate cells, platelets and coagulation factors in the hemorrhaging blood, thus promoting hemostasis (that is the effect promoted by factor concentrators). However, the shortening of APTT was more pronounced in the presence of 1%Ga-MBG than in the presence of ACS^+. While 1%Ga-MBG with unique mesoporous interconnected structure provided higher specific surface area and larger pore volume, being crucial to the fastest rate of

contact-activated coagulation, ACS^+ possess a microporous structure that is too small for plasma proteins to enter.

These results were in good agreement with the PBS absorption results, where the 1%Ga-MBG sample presented greater capacity for water absorption compared with ACS^+ (Figure 4.17). In comparison to both 1%Ga-MBG and ACS^+, CX showed no effect on the activation of the intrinsic pathway, indicating an inverse relationship between water absorption and APTT results of the same material. So, despite its higher absorption rate, CX significantly prolonged the APTT. This result demonstrates that the action mechanism of CX is independent of the classical coagulation cascade as proved previously (B. Kheirabadi, 2011; Rao *et al.*, 1997).

The presence of Ca^{2+} in 1%Ga-MBG and ACS^+'s frameworks is another factor favourable for the activation of the intrinsic blood coagulation cascade. These materials speed up the intrinsic pathway by supplying Ca^{2+} that reside in their open porous internal space, thus accelerating the generation of required thrombin for fibrin polymerisation and clot stabilisation (that is the effect promoted by pro-coagulants). With respect to the degradation and ion release rate which are generally linear, it is reasonable to assume that 1%Ga-MBG possessing quicker degradation, higher surface area and mesoporous structure, have higher capability to release sufficient amounts of Ca^{+2} than ACS^+, inducing an accelerated coagulation response.

The effect of the materials analysed on the induction of the earliest stages of hemostasis (*i.e.* thrombus formation, platelet aggregation and thrombin generation) was also investigated. A different trend was found in the case of thrombus formation (Figure 4.19), platelet aggregation (Figure 4.20) and thrombin generation (Figure 4.21) in 1%Ga-MBG, CX and ACS^+. 1%Ga-MBG was found to be superior over CX and ACS^+ at thrombin generation and thrombus formation. The increased thrombin generation and resultant fibrin formation in 1%Ga-MBG with respect to CX and

ACS^+ can be attributed to the synergy of both its higher Ca^{2+} release rate and negative surface charge alongside the structural features. As previously discussed, 1%Ga-MBG, due to possessing higher specific surface area and pore volume compared with ACS^+, may have more capability to present Ca^{2+} to blood, which not only is a required cofactor in the activation of the intrinsic pathway, but would also accelerate the production of sufficient amounts of thrombin, a pivotal enzyme of the coagulation cascade, to support early fibrin generation. Thrombin acts as a serine protease that converts circulating soluble fibrinogen into insoluble strands of fibrin, leading to formation of a stable thrombus (Coughlin, 2000).

The negative surface charge of 1%Ga-MBG also is another critical parameter contributing to its significant ability to enhance thrombin and thrombus formation better than CX and ACS^+. Negatively-charged surfaces are found to initiate the intrinsic pathway, a network of feedback-dependent reactions that, when activated, leads to a stable thrombus (Sperling *et al.*, 2009). It is known that the adsorption of coagulation factor FXII on negatively charged surfaces leads to subtle conformational changes in the enzyme, which in turn provoke auto-activation (Sperling *et al.*, 2009). As previously described,, the negative surface charge density influences the intensity of FXII activation by positively charged amino acids in its heavy chain, triggering its activation and leading to a strong amplification of contact activation proteins and subsequent activation of the intrinsic pathway (Colman *et al.*, 1997; Sperling *et al.*, 2009). This activation has been shown to play a significant role in thrombin formation and subsequent fibrin clot formation. The results support the hypothesis that 1%Ga-MBG with negative surface charge and strong contact activation causes substantially higher thrombin and thrombus formation than CX and ACS^+.

As noted earlier, the textural properties of 1%Ga-MBG are involved in its increased thrombotic effect with respect to CX and ACS^+, allowing the material to rapidly absorb high amounts of water from the blood, and to concentrate cellular and blood plasma components, thus promoting thrombus formation. However, while ACS^+ was also expected to induce a more pronounced effect on early stages of hemostasis compared with CX due to carrying a negative charge, it produced much less thrombin and thrombus. This observation can be attributed to the smaller pore volume of the zeolite in ACS^+ (0.13 cm^3g^{-1}) compared to 1%Ga-MBG (0.84 cm^3g^{-1}), which decreases the accessibility of the interior zeolite surface area for contact activation and is not beneficial to accommodate coagulation proteins such as FXII (Baker *et al.*, 2008).

It is therefore likely to be an underlying cause for thrombin and thrombus formation on the surface of CX. It is known that most plasma proteins such as fibrinogen are negatively charged in blood, so that the negatively charged surfaces can inhibit their adsorption (He *et al.*, 2013). Thus, it is expected that stronger fibrinogen adsorption can occur on positively charged-surfaces, which in turn could be correlated with maximum platelet adhesion (Sperling *et al.*, 2009). It is also evident that platelets play a major role in thrombin generation, leading to fibrin clot formation (Monroe *et al.*, 2002). Therefore, higher thrombin formation in the presence of CX compared to ACS^+ can be ascribed to a supporting effect of platelet adhesion on thrombin formation. The higher thrombus formation of CX with respect to ACS^+ can also be related to the positive charge of CX that cross-links with negatively charged RBCs and subsequently undergo chemical and mechanical linkages to form a sticky pseudo clot, blocking blood flow (that is the effect promoted by mucoadhesive hemostatic materials).

In the case of platelet adhesion, although 1%Ga-MBG and CX revealed similar trends and were found to be superior over ACS^{+}, the platelets on 1%Ga-MBG exhibited typical signs of activation such as spread morphology and protruding filipodia, whereas a lower spreading rate of platelets was observed on CX. Contrary to what happens with CX, where only its positive charge may lead to fibrinogen adsorption *via* electrostatic attraction subsequently promoting the adhesion and activation of platelets, the synergy of both the excellent intrinsic textural properties (high specific surface area) and high release rate of Ca^{2+} can greatly affect the platelet adhesion and activation on the surface of 1%Ga-MBG. These crucial parameters make 1%Ga-MBG an ideal surface for contact activation of the intrinsic pathway, causing a submicron scale interaction with platelets and fibrinogen as well as a higher production of the proteolytic enzyme thrombin, causing clumping and activation of platelets on the surface itself. These results were consistent with those of the blood coagulation, thrombus and thrombin formation assays, where 1%Ga-MBG was found to be more effective compared with CX and ACS^{+}.

Another important factor which can affect the hemostatic activity of 1%Ga-MBG and make it superior to the commercial hemostats could be attributed to the presence of Ga^{3+} ions in its framework that released from material into blood. As it discussed in the first part of the study, the Ga^{3+} ions similar to that of Fe^{3+} ions as trivalent ions may lead to accelerate blood clotting cascade. The ions may play a critical role in polymerisation of fibrinogen into strong fibrin clots through generation of most biologically reactive HRs resulting from its reaction with hydroxyl groups of water. So, this can be another possible explanation for the higher hemostatic efficacy of 1%Ga-MBG which resulted in formation of more stable and robust clots compared to CX and ACS^{+}.

As to particle size, ACS^{+} consisting of zeolite granules, showed to have larger particle size around 2240 μm compared with those of 1%Ga-MBG (283 μm) and CX (318 μm). The effect of particle size of MSN on blood clot initiation has been already assessed and it was found that hemostatic parameters including, the R value, α angle, MA, PT, APTT and FXII adsorption were not significantly affected by variation of the particle sizes (60, 100, 150, 220 nm) (Z. Chen *et al.*, 2016). Here, in this study, it is supposed that hemostatic efficacy could be mainly influenced by physiochemical properties (surface area, pore volume, surface charge and chemical composition), not particle size. Considering with the results of APTT, although there was no significant difference between the particle size of 1%Ga-MBG (283 μm) and CX (318 μm), 1%Ga-MBG significantly shortened APTT value compared with CX that prolonged APTT. Additionally, the result of thrombin generation assay revealed that while there was not significant difference between the size of 1%Ga-MBG and CX, 1%Ga-MBG could significantly stimulate thrombin generation compared to CX. Therefore, it can be assumed that hemostatic response of the samples depends on their physiochemical properties than particle size.

Based on the above analysis, a combination hemostatic mechanism model of 1%Ga-MBG has been proposed in Figure 5.1.

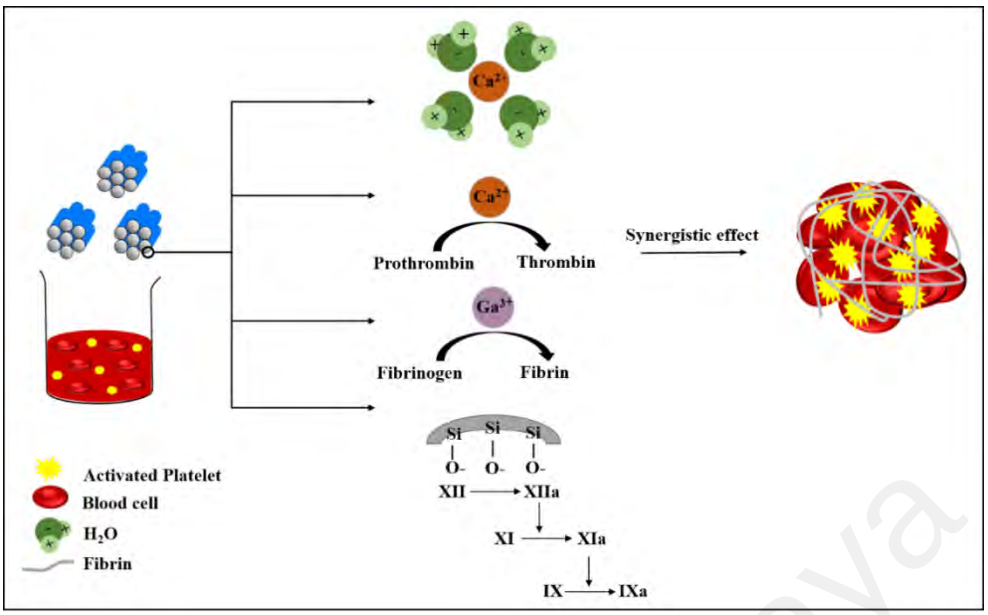

Figure 5.1: Schematic illustration of blood clotting formation by 1%Ga-MBG through multiple modes of action.

As previously described, the direct contact of the inorganic-based hemostats such as WS with the cells present in wounds can lead to cytotoxicity (Bowman *et al.*, 2011); Therefore, to evaluate the biocompatibility of the new developed inorganic hemostasis seems necessary when the materials are in direct contact with the cells. Here, it was observed that the viability of HDF cells was increased in the direct presence of the hemostatic materials without signs of cytotoxicity. To be noted, as shown in Figure 4.22a, the MTT assay demonstrated that, after 3 days of culture time, higher viability was observed for HDF cells in the presence of 1%Ga-MBG than CX and ACS^{+}, as confirmed by fluorescence imaging (Figure 4.22 b-d). However, as shown in figure 4.22d, ACS^{+} could induce noticeable cell death. Regardless of the amounts of materials used for biocompatibility assessment which was constant, differences in the chemical composition and particle sizes of the samples may affect their biocompatibility. As discussed earlier, the BGs can stimulate fibroblasts to secrete a multitude of growth factors such as bFGF and VEGF that are critical for wound healing (Yu *et al.*, 2015). Therefore, it is

hypothesized that 1%Ga-MBG with high specific surface and porosity can lead to high Si^{4+} and Ca^{2+} leaching, which seems to play a positive role in HDF cell proliferation. Although, the cytocompatibility of chitosan as main component of CX and ACS^{+} in powder from (1-2 μm) has been previously reported (Bowman *et al.*, 2011; Kim *et al.*, 2004), their larger particles sizes may have negative effect on the HDF cells viability.

Degradation is considered as an important property for a hemostatic material. It is well documented that non-biodegradable hemostats that remains in the body may stimulate an inflammatory reaction and impair mucosal regeneration (F. Chen *et al.*, 2015). In contrast to CX and ACS^{+}, the weight loss of 1%Ga-MBG was greater in Tris–HCl solution over 35 days. Apart from the high textural properties of 1%Ga-MBG which resulted in higher dissolution and degradation, its smaller particle size could be also a reason for its higher degradability compared with CX and ACS^{+}. It has been reported that the hemostatic particles with smaller size will be broken down more rapidly by the body's own enzymes (Peng, 2010).

In summary, this study evaluated *in vitro* hemostatic efficiency of developed Ga_2O_3-contaning MBGs with different Ga_2O_3 contents as compared with Ga-free MBG. All of the above-mentioned experiments demonstrate the potential of the 1%Ga-MBG in achieving hemostasis. Among the glasses, 1%Ga-MBG was found to possess most of required parameters for achieving an efficient hemostasis. It was also more effective in activation of blood clotting cascade, thrombus formation, platelet activation and thrombin generation than any ACS^{+} or CX. These results evidence that the larger surface area per unit material mass, pore volume and the prothrombotic potential per unit surface area are more favourable for interaction with platelets and fibrinogen for enhancement of hemostasis (Dai *et al.*, 2009; Flemming *et al.*, 1999; Yim *et al.*, 2005). In addition, other chemical and physical parameters

including surface silanol groups and mesoporous structure, negative surface charges and content of Ca^{2+}, all have been involved in the improved hemostatic efficacy of 1%Ga-MBG.

Although all tested materials demonstrated non-cytotoxicity towards HDF cells, the 1%Ga-MBG was also found to be more biocompatible than other samples as the cells showed a higher proliferation rate with increasing time of incubation up to 3 days.

However, this study was not sufficiently powered to determine the suitability of the Ga-MBGs to use in clinical applications as their capability of accelerating hemostasis are only proved *in vitro*. Therefore, one of the major limitation in this study has been the lack of animal models which are certainly required to judge the validity of the in *vitro* data. Additionally, the current study investigated only the hemostatic effect of the materials on blood collected from healthy volunteers while many patients requiring hemostatic agents are coagulopathic or taking anticoagulant drugs (*i.e*. warfarin or heparin), who their coagulation functions are impaired. Moreover, the safety tests applied to the materials may be inadequate in evaluating their biocompatibility, since *in vitro* cytotoxicity test using HDF cells culture was only evaluated. The powder form of Ga-MBGs also make their applications challenging, as the materials can be flushed away by severely bleeding wounds before they can coagulate blood.

CHAPTER 6: CONCLUSION AND FUTURE DIRECTIONS

6.1 Introduction

This chapter presents a summary of the key findings of the research, followed by some suggestions of topics for future areas of research.

6.2 Summary and conclusion

In the present study, MBGs including up to 3 mol % Ga_2O_3 have been successfully fabricated using EISA process (objective 1).

The results demonstrated that the proportion of Ga_2O_3 in MBG framework not only influenced its the physiochemistry and biological property (*i.e.* antibacterial properties and biocompatibility) but also was a critical parameter affecting hemostatic events. While incorporation of lowest amount of Ga_2O_3 (1 mol %) into MBG network has favored the formation of more well-ordered cylindrical mesopores and increased the specific surface area from 392 m^2/g in MBG to 472 m^2/g, the incorporation of higher Ga_2O_3 content (3 mol %) resulted in the reduction of surface area (324 m^2/g) and significant loss of ordering. Considering that the presence of Ga_2O_3 has altered the mesostructure of MBG, effect of textural properties on the ion release and degradation properties appeared significant. MBG with lowest Ga_2O_3 concentration exhibited faster SiO_4^{4-}, Ca^{2+} and PO_4^{3-} release profiles, and thus significantly improved degradation compared to the other glasses (objective 2).

The higher porosity of 1%Ga-MBG compared to other samples also play a crucial role in its higher hemostatic efficiency by improving its absorption ability. The prepared 1%Ga-MBG could not only activate the intrinsic pathway of coagulation

cascade but also resulted in higher absorption and aggregation of platelets and RBCs compared to the MBG. FESEM images confirmed that more clot and platelet aggregated on the surface of MBG with 1%Ga_2O_3 compared with other glasses. These results further proved that the benefits of Ga_2O_3 were negated at higher concentrations (3 mol %). The *in vitro* antibacterial studies also illustrated that antibacterial activity of MBG increased with increasing Ga^{3+} ion release against both *E. coli* and *S. aureus* with respect to Ga-free MBG. Although the Ga^{3+} concentration was lower in 1%Ga-MBG than 3%Ga-MBG, it was sufficient to exert antiracial activity. Moreover, *in vitro* biocompatibility studies revealed that extract of 1%Ga-MBG could enhance proliferation of HDF cells more than other samples. These results suggested that the ionic dissolution products released from the glasses can be crucial parameters affecting HDFs proliferation rate (objective 3).

To fully elucidate the applicability of the 1%Ga-MBG for hemostatic application, the effectiveness of the glass on the promotion of hemostasis was evaluated as compared with two commercially-available hemostatic products, CX and ACS^+. Noticeably, 1%Ga-MBG appeared to be the most efficacious product, in the tests performed than CX and ACS^+. In comparison to CX that did not affect the clotting activity of the blood, 1%Ga-MBG resulted in greatest contact activation compared to negative control and ACS^+ as it significantly shortened APTT values from 44.26 s and 26.81 s in negative control and ACS^+ respectively to 19.55 s. The glass also led to greater clot formation and platelet activation on its surface with respect to CX and ACS^+. Additionally, 1%Ga-MBG induced significantly faster thrombin generation than those of CX and ACS^+ as much more TAT complex was generated in contact of 1%Ga-MBG. It was found that neither platelet adhesion on CX surfaces without concurrent contact activation, nor contact activation on ACS^+ with lower number of the activated platelets leads to strong thrombus formation. Such results may support

the idea that both contact activation and platelet adhesion are regarded as essential factors for biomaterials related coagulation activation, so that each single mechanism is not adequate to promote substantial thrombin formation. In addition, the cytotoxicity evaluation results demonstrated that HDF cells could significantly proliferate in direct presence of 1%Ga-MBG than CX and ACS^+ with no signs of cell damage. The larger particle sizes of ACS^+ may to be a reason for the lower proliferation of HDF cells in contact with ACS^+ (Objective 4).

Overall, the above results provide evidence that the prepared Ga-MBGs with optimized composition (1%Ga-MBG) have potential for use as hemostatic agent since it achieved a desirable hemostasis *in vitro* through the interplay of the mentioned activation processes.

6.3 Recommendations for future work

Although MBGs containing Ga_2O_3 show great promise of effectiveness, future tests need to be progressively conducted to more precisely delineate the principle behind the hemostatic efficacy of Ga-MBGs and further validate of their safety.

The effectiveness of the glasses to accelerate of hemostasis need to be assessed in the large animal models of severe hemorrhage as compared with commercial products (*i.e.* femoral artery or liver injuries models) to further verify the *in vitro* findings. Animal survival, time to hemostasis, and blood loss are crucial parameters that need to be examined to measure hemostatic efficacy of the Ga-MBGs. Additionally, since some patients and combat casualties requiring blood transfusion are coagulopathic, an enhanced hemostatic agent is therefore needed to be efficacious in trauma-induced coagulopathic patients to stop bleeding independently

of host coagulation status. Therefore, a future focus should be to evaluate the efficacy of the glasses under coagulopathic conditions.

Although the MTT assay in this study demonstrated the good biocompatibility of Ga-MBGs, more cell culture studies are needed to further investigate the cytocompatibility of the glasses. Considering that hemostats can contact with endothelial cells and macrophages in the injured blood vessels, the biocompatibility of the materials should be also evaluated towards these cells. Additionally, as previously mentioned, non-degradable inorganic hemostats such as microscopic WS and kaolin can cause thrombotic complications. Therefore, to evaluate the long-term effect of the glasses on the wound, large animal survival studies need to be designed in which critical blood vessels will be injured. The animals need to be monitored and computed tomography (CT) scanned for evidence of thrombosis and infarction. The histopathologic effects (*i.e.* inflammation, formation of granulation tissue and tissue necrosis) of the glasses also need to be investigated and compared with the previously developed inorganic-based hemostats. Moreover, there is a growing need to fabricate composite scaffolds composed of Ga-MBGs and polymers with inherently hemostatic efficacy to overcome some challenges presented by powder hemostatic materials that might be rapidly washed away by hemorrhaging blood before reaching the site of injury.

REFERENCES

Acheson, E. M., Kheirabadi, B. S., Deguzman, R., Dick Jr, E. J., & Holcomb, J. B. (2005). Comparison of hemorrhage control agents applied to lethal extremity arterial hemorrhages in swine. *J. Trauma Acute Care Surg., 59*(4), 865-875.

Achneck, H. E., Sileshi, B., Jamiolkowski, R. M., Albala, D. M., Shapiro, M. L., & Lawson, J. H. (2010). A comprehensive review of topical hemostatic agents: efficacy and recommendations for use. *Ann. Surg., 251*(2), 217-228.

Ahuja, N., Ostomel, T. A., Rhee, P., Stucky, G. D., Conran, R., Chen, Z., . . . Alam, H. B. (2006). Testing of modified zeolite hemostatic dressings in a large animal model of lethal groin injury. *Journal of Trauma and Acute Care Surgery, 61*(6), 1312-1320.

Aina, V., Morterra, C., Lusvardi, G., Malavasi, G., Menabue, L., Shruti, S., . . . Bolis, V. (2011). Ga-modified (Si–Ca–P) Sol–Gel glasses: possible relationships between surface chemical properties and bioactivity. *The Journal of Physical Chemistry C, 115*(45), 22461-22474.

Alam, H. B., Burris, D., DaCorta, J. A., & Rhee, P. (2005). Hemorrhage control in the battlefield: role of new hemostatic agents. *Military Medicine, 170*(1), 63-69.

Alam, H. B., Chen, Z., Jaskille, A., Querol, R. I. L. C., Koustova, E., Inocencio, R., . . . Toruno, K. (2004). Application of a zeolite hemostatic agent achieves 100% survival in a lethal model of complex groin injury in swine. *Journal of Trauma and Acute Care Surgery, 56*(5), 974-983.

Alam, H. B., Uy, G. B., Miller, D., Koustova, E., Hancock, T., Inocencio, R., . . . Rhee, P. (2003). Comparative analysis of hemostatic agents in a swine model of lethal groin injury. *Journal of Trauma and Acute Care Surgery, 54*(6), 1077-1082.

Alcaide, M., Portoles, P., López-Noriega, A., Arcos, D., Vallet-Regí, M., & Portoles, M. (2010). Interaction of an ordered mesoporous bioactive glass with osteoblasts, fibroblasts and lymphocytes, demonstrating its biocompatibility as a potential bone graft material. *Acta Biomater., 6*(3), 892-899.

Alhalawani, A. M., Curran, D. J., Pingguan-Murphy, B., Boyd, D., & Towler, M. R. (2013). A novel glass polyalkenoate cement for fixation and stabilisation of the ribcage, post sternotomy surgery: an ex-vivo study. *Journal of functional biomaterials, 4*(4), 329-357.

Arcos, D., Vila, M., López-Noriega, A., Rossignol, F., Champion, E., Oliveira, F., & Vallet-Regí, M. (2011). Mesoporous bioactive glasses: Mechanical reinforcement by means of a biomimetic process. *Acta Biomater., 7*(7), 2952-2959.

Arnaud, F., Teranishi, K., Okada, T., Parreño-Sacdalan, D., Hupalo, D., McNamee, G., . . . McCarron, R. (2011). Comparison of Combat Gauze and TraumaStat in two severe groin injury models. *Journal of Surgical Research, 169*(1), 92-98.

Arnaud, F., Teranishi, K., Tomori, T., Carr, W., & McCarron, R. (2009). Comparison of 10 hemostatic dressings in a groin puncture model in swine. *Journal of Vascular Surgery, 50*(3), 632-639. .

Arnaud, F., Tomori, T., Carr, W., McKeague, A., Teranishi, K., Prusaczyk, K., & McCarron, R. (2008). Exothermic reaction in zeolite hemostatic dressings: QuikClot ACS and ACS+®. *Annals of Biomedical Engineering, 36*(10), 1708-1713.

Arnaud, F., Tomori, T., Saito, R., McKeague, A., Prusaczyk, W. K., & McCarron, R. M. (2007). Comparative efficacy of granular and bagged formulations of the hemostatic agent QuikClot. *Journal of Trauma and Acute Care Surgery, 63*(4), 775-782.

Aronson, N. E., Sanders, J. W., & Moran, K. A. (2006). In harm's way: infections in deployed American military forces. *Clinical Infectious Diseases, 43*(8), 1045-1051.

Ayadi, A. J., Soro, J., Kamoun, A., & Baklouti, S. (2013). Study of clay's mineralogy effect on rheological behavior of ceramic suspensions using an experimental design. *International Journal of Research and Reviews in Applied Sciences, 14*(2), 374–384.

Baeza, A., Colilla, M., & Vallet-Regí, M. (2015). Advances in mesoporous silica nanoparticles for targeted stimuli-responsive drug delivery. *Expert opinion on drug delivery, 12*(2), 319-337.

Baker, S. E., Sawvel, A. M., Fan, J., Shi, Q., Strandwitz, N., & Stucky, G. D. (2008). Blood clot initiation by mesocellular foams: dependence on nanopore size and enzyme immobilization. *Langmuir, 24*(24), 14254-14260.

Balamurugan, A., Balossier, G., Laurent-Maquin, D., Pina, S., Rebelo, A., Faure, J., & Ferreira, J. (2008). An in vitro biological and anti-bacterial study on a sol–gel derived silver-incorporated bioglass system. *dental materials, 24*(10), 1343-1351.

Barrett, E. P., Joyner, L. G., & Halenda, P. P. (1951). The determination of pore volume and area distributions in porous substances. I. Computations from nitrogen isotherms. *Journal of the American Chemical Society, 73*(1), 373-380.

Beck, J., Vartuli, J., Roth, W., Leonowicz, M., Kresge, C., Schmitt, K., . . . Sheppard, E. (1992). A new family of mesoporous molecular sieves prepared with liquid crystal templates. *Journal of the American Chemical Society, 114*(27), 10834-10843.

Behrens, A. M., Sikorski, M. J., & Kofinas, P. (2014). Hemostatic strategies for traumatic and surgical bleeding. *J. Biomed. Mater. Res., Part A, 102*(11), 4182-4194.

Behrens, A. M., Sikorski, M. J., Li, T., Wu, Z. J., Griffith, B. P., & Kofinas, P. (2014). Blood-aggregating hydrogel particles for use as a hemostatic agent. *Acta Biomaterialia, 10*(2), 701-708.

Bellantone, M., Coleman, N. J., & Hench, L. L. (2000). Bacteriostatic action of a novel four-component bioactive glass. *Journal of Biomedical Materials Research Part A, 51*(3), 484-490.

Bellantone, M., Williams, H. D., & Hench, L. L. (2002). Broad-spectrum bactericidal activity of Ag2O-doped bioactive glass. *Antimicrobial agents and chemotherapy, 46*(6), 1940-1945.

Belly, R., & Kydd, G. (1982). Silver resistance in microorganisms. *Developments in industrial microbiology, 23*, 567-578.

Bennett, B. L., & Littlejohn, L. (2014). Review of New Topical Hemostatic Dressings for Combat Casualty Care. *Military Medicine, 179*(5), 497-514.

Bennett, B. L., Littlejohn, L. F., Kheirabadi, B. S., Butler, F. K., Kotwal, R. S., Dubick, M. A., & Bailey, J. A. (2014). Management of External Hemorrhage in Tactical Combat Casualty Care: Chitosan-Based Hemostatic Gauze Dressings - TCCC Guidelines Change 13-05. *J. Spec. Oper. Med., 14*, 40-57.

Bermudez, P., Beushausen, M., & Horan, M. P. (2016). Management of Inherited, Acquired, and Iatrogenically Induced Coagulopathies in Oral Surgery. *A Textbook of Advanced Oral and Maxillofacial Surgery Volume 3*.

Bernstein, L. R. (1998). Mechanisms of therapeutic activity for gallium. *Pharmacological Reviews, 50*(4), 665-682.

Bernstein, L. R. (2013). Gallium, therapeutic effects. *Encyclopedia of Metalloproteins* (pp. 823-835): Springer.

Blaker, J., Nazhat, S., & Boccaccini, A. (2004). Development and characterisation of silver-doped bioactive glass-coated sutures for tissue engineering and wound healing applications. *Biomaterials, 25*(7), 1319-1329.

Boateng, J. S., Matthews, K. H., Stevens, H. N., & Eccleston, G. M. (2008). Wound healing dressings and drug delivery systems: a review. *Journal of Pharmaceutical Sciences, 97*(8), 2892-2923.

Bowlin, G. L., Carr, M. E., Diegelmann, R. F., & Ward, K. R. (2012). Mineral Technologies (MT) for Acute Hemostasis and for the Treatment of Acute Wounds and Chronic Ulcers. . *U.S. Patent No. US 20120219612 A1. Washington, DC: U.S. Patent and Trademark Office.*

Bowman, P. D., Wang, X., Meledeo, M. A., Dubick, M. A., & Kheirabadi, B. S. (2011). Toxicity of aluminum silicates used in hemostatic dressings toward human umbilical veins endothelial cells, HeLa cells, and RAW267. 4 mouse macrophages. *Journal of Trauma and Acute Care Surgery, 71*(3), 727-732.

Brinker, C. J., Lu, Y., Sellinger, A., & Fan, H. (1999). Evaporation-induced self-assembly: nanostructures made easy. *Advanced Materials, 11*(7), 579-585.

Broos, K., Feys, H. B., De Meyer, S. F., Vanhoorelbeke, K., & Deckmyn, H. (2011). Platelets at work in primary hemostasis. *Blood Rev., 25*(4), 155-167.

Brunauer, S., Emmett, P. H., & Teller, E. (1938). Adsorption of gases in multimolecular layers. *Journal of the American Chemical Society, 60*(2), 309-319.

Buderi, R. (2013). *Naval Innovation for the 21st Century: The Office of Naval Research Since the End of the Cold War*: Naval Institute Press.

Butenas, S., & Mann, K. (2002). Blood coagulation. *Biochemistry (Moscow), 67*(1), 3-12.

Carraway, J. W., Kent, D., Young, K., Cole, A., Friedman, R., & Ward, K. R. (2008). Comparison of a new mineral based hemostatic agent to a commercially available granular zeolite agent for hemostasis in a swine model of lethal extremity arterial hemorrhage. *Resuscitation, 78*(2), 230-235.

Casey, G. (2003). Haemostasis, anticoagulants and fibrinolysis. *Nursing standard, 18*(7), 45-51.

Castle, R. R., & Sedory, E. J. (2016). Tourniquets and Hemostatic Agents to Manage Mass Hemorrhage. *Athletic Training and Sports Health Care, 8*(6), 245-255.

Causey, M. W., McVay, D. P., Miller, S., Beekley, A., & Martin, M. (2012). The efficacy of Combat Gauze in extreme physiologic conditions. *Journal of Surgical Research, 177*(2), 301-305.

Champion, H. R., Bellamy, R. F., Roberts, C. P., & Leppaniemi, A. (2003). A profile of combat injury. *Journal of Trauma and Acute Care Surgery, 54*(5), S13-S19.

Chávez-Delgado, M. E., Kishi-Sutto, C. V., de la-Riva, X. N. A., Rosales-Cortes, M., & Gamboa-Sánchez, P. (2014). Topic usage of kaolin-impregnated gauze as a hemostatic in tonsillectomy. *Journal of Surgical Research, 192*(2), 678-685.

Chen, F., Cao, X., Chen, X., Wei, J., & Liu, C. (2015). Calcium-modified microporous starch with potent hemostatic efficiency and excellent degradability for hemorrhage control. *Journal of Materials Chemistry B, 3*(19), 4017-4026.

Chen, Z., Li, F., Liu, C., Guan, J., Hu, X., Du, G., . . . Tian, F. (2016). Blood clot initiation by mesoporous silica nanoparticles: dependence on pore size or particle size? *Journal of Materials Chemistry B, 4*(44), 7146-7154.

Chitambar, C., & Narasimhan, J. (1991). Targeting iron-dependent DNA synthesis with gallium and transferrin-gallium. *Pathobiology, 59*(1), 3-10.

Chitambar, C. R. (2010). Medical applications and toxicities of gallium compounds. *International Journal of Environmental Research and Public Health, 7*(5), 2337-2361.

Çinar, Ç., Odabas, M. E., Akca, G., & Isik, B. (2012). Antibacterial effect of a new haemostatic agent on oral microorganisms. *Journal of Clinical and Experimental Dentistry, 4*(3), 151-155.

Clay, J. G., Grayson, J. K., & Zierold, D. (2010). Comparative testing of new hemostatic agents in a swine model of extremity arterial and venous hemorrhage. *Military Medicine, 175*(4), 280-284.

Colman, R. W., & Schmaier, A. H. (1997). Contact system: a vascular biology modulator with anticoagulant, profibrinolytic, antiadhesive, and proinflammatory attributes. *Blood, 90*(10), 3819-3843.

Cosgriff, N., Moore, E. E., Sauaia, A., Kenny-Moynihan, M., Burch, J. M., & Galloway, B. (1997). Predicting life-threatening coagulopathy in the massively transfused trauma patient: hypothermia and acidoses revisited. *Journal of Trauma and Acute Care Surgery, 42*(5), 857-862.

Coughlin, S. R. (2000). Thrombin signalling and protease-activated receptors. *Nature, 407*(6801), 258-264.

Cox, E. D., Schreiber, M. A., McManus, J., Wade, C. E., & Holcomb, J. B. (2009). New hemostatic agents in the combat setting. *Transfusion, 49*(s5), 248S-255S.

Dai, C., Liu, C., Wei, J., Hong, H., & Zhao, Q. (2010). Molecular imprinted macroporous chitosan coated mesoporous silica xerogels for hemorrhage control. *Biomaterials, 31*(30), 7620-7630.

Dai, C., Yuan, Y., Liu, C., Wei, J., Hong, H., Li, X., & Pan, X. (2009). Degradable, antibacterial silver exchanged mesoporous silica spheres for hemorrhage control. *Biomaterials, 30*(29), 5364-5375.

Day, R. M. (2005). Bioactive glass stimulates the secretion of angiogenic growth factors and angiogenesis in vitro. *Tissue Engineering, 11*(5-6), 768-777.

di Lena, F. (2014). Hemostatic polymers: The concept, state of the art and perspectives. *Journal of Materials Chemistry B, 2*(23), 3567-3577.

Dubick, M. A., & Kheirabadi, B. (2010). New technologies for treating severe bleeding in far-forward combat areas (Vol. 21).

Eryilmaz, M., Ozer, T., Mentes, O., Torer, N., Durusu, M., Gunal, A., & Uzar, A. İ. (2009). Is the zeolite hemostatic agent beneficial in reducing blood loss during arterial injury? *Turkish Journal of Trauma & Emergency Surgery, 15*(1), 7-11.

Esmon, C. T. (1993). Cell mediated events that control blood coagulation and vascular injury. *Annual Review of Cell Biology, 9*(1), 1-26.

Evans, J. A., van Wessem, K. J., McDougall, D., Lee, K. A., Lyons, T., & Balogh, Z. J. (2010). Epidemiology of traumatic deaths: comprehensive population-based assessment. *World journal of surgery, 34*(1), 158-163.

Fedor, P. J. (2012). Novel use of a hemostatic dressing in the management of a bleeding leech bite: a case report and review of the literature. *Wilderness & Environmental Medicine, 23*(1), 44-48.

Ferraris, V. A., Boral, L. I., Cohen, A. J., Smyth, S. S., & White, G. C. (2015). Consensus review of the treatment of cardiovascular disease in people with hemophilia A and B. *Cardiology in Review, 23*(2), 53.

Flemming, R., Murphy, C., Abrams, G., Goodman, S., & Nealey, P. (1999). Effects of synthetic micro-and nano-structured surfaces on cell behavior. *Biomaterials, 20*(6), 573-588.

Floyd, C. T., Rothwell, S. W., Risdahl, J., Martin, R., Olson, C., & Rose, N. (2012). Salmon thrombin-fibrinogen dressing allows greater survival and preserves distal blood flow compared to standard kaolin gauze in coagulopathic swine with a standardized lethal femoral artery injury. *Journal of Special Operations Medicine, 12*(2), 16-26.

Franchini, M., Lusvardi, G., Malavasi, G., & Menabue, L. (2012). Gallium-containing phospho-silicate glasses: Synthesis and in vitro bioactivity. *Materials Science and Engineering: C, 32*(6), 1401-1406.

Gargiulo, N., Cusano, A. M., Causa, F., Caputo, D., & Netti, P. A. (2013). Silver-containing mesoporous bioactive glass with improved antibacterial properties. *Journal of Materials Science: Materials in Medicine, 24*(9), 2129-2135.

Gegel, B., Burgert, J., Gasko, J., Campbell, C., Martens, M., Keck, J., . . . Johnson, D. (2012). The effects of QuikClot Combat Gauze and movement on hemorrhage control in a porcine model. *Military Medicine, 177*(12), 1543-1547.

Gerlach, T., Grayson, J. K., Pichakron, K. O., Sena, M. J., DeMartini, S. D., Clark, B. Z., . . . Zierold, D. (2010). Preliminary study of the effects of smectite granules (WoundStat) on vascular repair and wound healing in a swine survival model. *Journal of Trauma and Acute Care Surgery, 69*(5), 1203-1209.

Gerwins, P., Sköldenberg, E., & Claesson-Welsh, L. (2000). Function of fibroblast growth factors and vascular endothelial growth factors and their receptors in angiogenesis. *Critical Reviews in Oncology/Hematology, 34*(3), 185-194.

Glick, J. B., Kaur, R. R., & Siegel, D. (2013). Achieving hemostasis in dermatology-Part II: Topical hemostatic agents. *Indian dermatology online journal, 4*(3), 172.

Gonzalez, G., Sagarzazu, A., & Zoltan, T. (2013). Infuence of Microstructure in Drug Release Behavior of Silica Nanocapsules. *Journal of drug delivery, 2013*, 803585.

Goodley, P. H., & Rogosnitzky, M. (2011). The effect of gallium nitrate on arresting blood flow from a wound. *Case Reports in Medicine, 2011*, 1-3.

Gorbet, M. B., & Sefton, M. V. (2004). Biomaterial-associated thrombosis: roles of coagulation factors, complement, platelets and leukocytes. *Biomaterials, 25*(26), 5681-5703.

Gordy, S. D., Rhee, P., & Schreiber, M. A. (2011). Military applications of novel hemostatic devices. *Expert Review of Medical Devices, 8*(1), 41-47.

Granville-Chapman, J., Jacobs, N., & Midwinter, M. (2011). Pre-hospital haemostatic dressings: a systematic review. *Injury, 42*(5), 447-459.

Greenberg, C., Sane, D., & Lai, T. (2006). Hemostasis and Thrombosis. *The American Society of Hematology*, 317-334.

Griffin, J. H. (1978). Role of surface in surface-dependent activation of Hageman factor (blood coagulation factor XII). *Proceedings of the National Academy of Sciences, 75*(4), 1998-2002.

Grover, V., Kapoor, A., Malhotra, R., & Uppal, R. S. (2013). Evaluation of the efficacy of a bioactive synthetic graft material in the treatment of intrabony periodontal defects. *Journal of Indian Society of Periodontology, 17*(1), 104.

Gustafson, S. B., Fulkerson, P., Bildfell, R., Aguilera, L., & Hazzard, T. M. (2007). Chitosan dressing provides hemostasis in swine femoral arterial injury model. *Prehospital Emergency Care, 11*(2), 172-178.

Halkier, T. (1991). *Mechanisms in blood coagulation, fibrinolysis and the complement system*: Cambridge University Press.

Hall, T. J., & Chambers, T. J. (1990). Gallium inhibits bone resorption by a direct effect on osteoclasts. *Bone and Mineral, 8*(3), 211-216.

He, Q., Gong, K., Ao, Q., Ma, T., Yan, Y., Gong, Y., & Zhang, X. (2013). Positive charge of chitosan retards blood coagulation on chitosan films. *Journal of biomaterials applications, 27*(8), 1032-1045.

Hench, L. L. (1998). Bioceramics. *Journal of the American Ceramic Society, 81*(7), 1705-1728.

Hoffman, M. (2003). Remodeling the blood coagulation cascade. *Journal of Thrombosis and Thrombolysis, 16*(1), 17-20.

Holcomb, J. B. (2005). Use of recombinant activated factor VII to treat the acquired coagulopathy of trauma. *Journal of Trauma and Acute Care Surgery, 58*(6), 1298-1303.

Holden, P. A., Ostomel, T. A., Shi, Q., Stoimenov, P. K., & Stucky, G. D. (2010). Inorganic materials for hemostatic modulation and therapeutic wound healing. *U.S. Patent No. US 7858123 B2. Washington, DC: U.S. Patent and Trademark Office.*

Hu, G., Xiao, L., Tong, P., Bi, D., Wang, H., Ma, H., . . . Liu, H. (2012). Antibacterial hemostatic dressings with nanoporous bioglass containing silver. *International Journal of Nanomedicine, 7*, 2613.

Huang, X., Young, N. P., & Townley, H. E. (2014). Characterisation and comparison of mesoporous silica particles for optimised drug delivery. *Nanomater Nanotechnol, 4*, 2.

Hudson, S. P., Padera, R. F., Langer, R., & Kohane, D. S. (2008). The biocompatibility of mesoporous silicates. *Biomaterials, 29*(30), 4045-4055.

Huirache-Acuña, R., Nava, R., Peza-Ledesma, C. L., Lara-Romero, J., Alonso-Núez, G., Pawelec, B., & Rivera-Muñoz, E. M. (2013). SBA-15 mesoporous silica as catalytic support for hydrodesulfurization catalysts—review. *Materials, 6*(9), 4139-4167.

Imai, Y., & Nose, Y. (1972). A new method for evalution of antithrombogenicity of materials. *J. Biomed. Mater. Res., 6*(3), 165-172.

Inaba, K., Branco, B. C., Rhee, P., Putty, B., Okoye, O., Barmparas, G., . . . Demetriades, D. (2013). Long-term preclinical evaluation of the intracorporeal use of advanced local hemostatics in a damage-control swine model of grade IV liver injury. *Journal of Trauma and Acute Care Surgery, 74*(2), 538-545.

Inaba, K., Rhee, P., Teixeira, P. G., Barmparas, G., Putty, B., Branco, B. C., . . . Demetriades, D. (2011). Intracorporeal use of advanced local hemostatics in a damage control swine model of grade IV liver injury. *Journal of Trauma and Acute Care Surgery, 71*(5), 1312-1318.

Insel, T., Cuthbert, B., & Garvey, M. (2016). Murray CJL, Lopez AD. Alternative projections of mortality and disability by cause 1990-2020: the global burden of disease study. Lancet. 1997; 349: 1498–1504. US Department of Health and Human Services. National Strategy for Suicide Prevention: Goals and Objectives for Action. Rockville. *The Yale Textbook of Public Psychiatry, 349*, 111.

Ip, M., Lui, S. L., Poon, V. K., Lung, I., & Burd, A. (2006). Antimicrobial activities of silver dressings: an in vitro comparison. *Journal of Medical Microbiology, 55*(1), 59-63.

Izquierdo-Barba, I., Colilla, M., & Vallet-Regí, M. (2008). Nanostructured mesoporous silicas for bone tissue regeneration. *Journal of Nanomaterials, 2008*, 60.

Izquierdo-Barba, I., & Vallet-Regí, M. (2015). Mesoporous bioactive glasses: Relevance of their porous structure compared to that of classical bioglasses. *Biomedical glasses, 1*(1), 140-150.

Izquierdo-Barba, I., Salinas, A. J., & Vallet-Regí, M. (2013). Bioactive glasses: from macro to nano. *International Journal of Applied Glass Science, 4*(2), 149-161.

Jiang, P., Qu, F., Lin, H., Wu, X., Xing, R., & Zhang, J. (2012a). Macroporous/mesoporous bioglasses doped with Ag/TiO_2 for dual drug action property and bone repair. *IET nanobiotechnology, 6*(3), 93-101.

Jiang, P., Qu, F., Lin, H., Wu, X., Xing, R., & Zhang, J. (2012b). Macroporous/mesoporous bioglasses doped with Ag/TiO 2 for dual drug action property and bone repair. *IET nanobiotechnology, 6*(3), 93-101.

Johnson, D., Bates, S., Nukalo, S., Staub, A., Hines, A., Leishman, T., . . . Burgert, J. (2014). The effects of QuikClot Combat Gauze on hemorrhage control in the presence of hemodilution and hypothermia. *Annals of Medicine and Surgery, 3*(2), 21-25.

Johnson, D., Gegel, B., Burgert, J., Gasko, J., Cromwell, C., Jaskowska, M., . . . Taylor, A. (2012). The effects of QuikClot Combat Gauze, fluid resuscitation, and movement on hemorrhage control in a porcine model. *ISRN Emergency Medicine, 2012*, 6.

Kaneko, Y., Thoendel, M., Olakanmi, O., Britigan, B. E., & Singh, P. K. (2007). The transition metal gallium disrupts Pseudomonas aeruginosa iron metabolism and has antimicrobial and antibiofilm activity. *The Journal of clinical investigation, 117*(4), 877.

Katic, M., Bosnjak, B., Gall-Troselj, K., Dikic, I., & Pavelic, K. (2006). A clinoptilolite effect on cell media and the consequent effects on tumor cells in vitro. *Frontiers in Bioscience, 11*(1), 1722-1732.

Katzenell, U., Ash, N., Tapia, A. L., Campino, G. A., & Glassberg, E. (2012). Analysis of the causes of death of casualties in field military setting. *Military Medicine, 177*(9), 1065-1068.

Kauvar, D. S., Lefering, R., & Wade, C. E. (2006). Impact of hemorrhage on trauma outcome: an overview of epidemiology, clinical presentations, and therapeutic considerations. *Journal of Trauma and Acute Care Surgery, 60*(6), S3-S11.

Keene, T. K., Patterson, J. A., Reding, J. W., & Thompson, J. A. (2001). Hemostatic agent, method and carrier for applying a blood clotting agent. *U.S. Patent No. WO 2001082896 A1. Washington, DC: U.S. Patent and Trademark Office.*

Kelly, J. F., Ritenour, A. E., McLaughlin, D. F., Bagg, K. A., Apodaca, A. N., Mallak, C. T., . . . Wade, C. E. (2008). Injury severity and causes of death from Operation Iraqi Freedom and Operation Enduring Freedom: 2003–2004 versus 2006. *Journal of Trauma and Acute Care Surgery, 64*(2), S21-S27.

Kendall, R. T., & Feghali-Bostwick, C. A. (2014). Fibroblasts in fibrosis: novel roles and mediators. *Frontiers in Pharmacology, 5*.

Keshaw, H., Forbes, A., & Day, R. M. (2005). Release of angiogenic growth factors from cells encapsulated in alginate beads with bioactive glass. *Biomaterials, 26*(19), 4171-4179.

Kheirabadi, B. (2011). Evaluation of topical hemostatic agents for combat wound treatment. *US Army Med. Dep. J., 2*(1), 25-37.

Kheirabadi, B. S., Edens, J. W., Terrazas, I. B., Estep, J. S., Klemcke, H. G., Dubick, M. A., & Holcomb, J. B. (2009). Comparison of new hemostatic granules/powders with currently deployed hemostatic products in a lethal model of extremity arterial hemorrhage in swine. *Journal of Trauma and Acute Care Surgery, 66*(2), 316-328.

Kheirabadi, B. S., Mace, J. E., Terrazas, I. B., Fedyk, C. G., Estep, J. S., Dubick, M. A., & Blackbourne, L. H. (2010). Safety evaluation of new hemostatic agents, smectite granules, and kaolin-coated gauze in a vascular injury wound model in swine. *Journal of Trauma and Acute Care Surgery, 68*(2), 269-278.

Kheirabadi, B. S., Mace, J. E., Terrazas, I. B., Fedyk, C. G., Valdez, K. K., MacPhee, M. J., . . . Blackbourne, L. H. (2010). Clot-inducing minerals versus plasma protein dressing for topical treatment of external bleeding in the presence of coagulopathy. *Journal of Trauma and Acute Care Surgery, 69*(5), 1062-1073.

Kheirabadi, B. S., Scherer, M. R., Estep, J. S., Dubick, M. A., & Holcomb, J. B. (2009). Determination of efficacy of new hemostatic dressings in a model of extremity arterial hemorrhage in swine. *Journal of Trauma and Acute Care Surgery, 67*(3), 450-460.

Kim, C. H., Park, H.-S., Gin, Y. J., Son, Y., Lim, S.-H., Choi, Y. J., . . . Park, C. W. (2004). Improvement of the biocompatibility of chitosan dermal scaffold by rigorous dry heat treatment. *Macromolecular research, 12*(4), 367-373.

Kortesuo, P., Ahola, M., Karlsson, S., Kangasniemi, I., Yli-Urpo, A., & Kiesvaara, J. (2000). Silica xerogel as an implantable carrier for controlled drug delivery—evaluation of drug distribution and tissue effects after implantation. *Biomaterials, 21*(2), 193-198.

Kozen, B. G., Kircher, S. J., Henao, J., Godinez, F. S., & Johnson, A. S. (2008). An alternative hemostatic dressing: comparison of CELOX, HemCon, and QuikClot. *Academic Emergency Medicine, 15*(1), 74-81.

Kresge, C., Leonowicz, M., Roth, W., Vartuli, J., & Beck, J. (1992). Ordered mesoporous molecular sieves synthesized by a liquid-crystal template mechanism. *Nature, 359*(6397), 710-712.

Leebeek, F. W., & Eikenboom, J. C. (2016). Von Willebrand's Disease. *New England Journal of Medicine, 375*(21), 2067-2080.

Leppäranta, O., Vaahtio, M., Peltola, T., Zhang, D., Hupa, L., Hupa, M., . . . Eerola, E. (2008). Antibacterial effect of bioactive glasses on clinically important anaerobic bacteria in vitro. *Journal of Materials Science: Materials in Medicine, 19*(2), 547-551.

Li, J., Cao, W., Lv, X.-x., Jiang, L., Li, Y.-j., Li, W.-z., . . . Li, X.-y. (2013). Zeolite-based hemostat QuikClot releases calcium into blood and promotes blood coagulation in vitro. *Acta Pharmacologica Sinica, 34*(3), 367-372.

Li, X., Zhang, L., Dong, X., Liang, J., & Shi, J. (2007). Preparation of mesoporous calcium doped silica spheres with narrow size dispersion and their drug loading and degradation behavior. *Microporous and Mesoporous Materials, 102*(1), 151-158.

Li, Y., Li, H., Xiao, L., Zhou, L., Shentu, J., Zhang, X., & Fan, J. (2012). Hemostatic efficiency and wound healing properties of natural zeolite granules in a lethal rabbit model of complex groin injury. *Materials, 5*(12), 2586-2596.

Li, Y., Liu, Y.-Z., Long, T., Yu, X.-B., Tang, T. T., Dai, K.-R., . . . Zhu, Z.-A. (2013). Mesoporous bioactive glass as a drug delivery system: fabrication, bactericidal properties and biocompatibility. *Journal of Materials Science: Materials in Medicine, 24*(8), 1951-1961.

Liau, S., Read, D., Pugh, W., Furr, J., & Russell, A. (1997). Interaction of silver nitrate with readily identifiable groups: relationship to the antibacterialaction of silver ions. *Letters in applied microbiology, 25*(4), 279-283.

Linares, N., Silvestre-Albero, A. M., Serrano, E., Silvestre-Albero, J., & García-Martínez, J. (2014). Mesoporous materials for clean energy technologies. *Chemical Society Reviews, 43*, 7681-7717.

Lipinski, B., & Pretorius, E. (2012). Novel pathway of ironinduced blood coagulation: implications for diabetes mellitus and its complications. *Polskie Archiwum Medycyny Wewnetrznej, 122*(3), 115-122.

Lipinski, B., & Pretorius, E. (2013). The role of iron-induced fibrin in the pathogenesis of Alzheimer's disease and the protective role of magnesium. *Frontiers in Human Neuroscience, 7*, 735.

Lipinski, B., Pretorius, E., Oberholzer, H. M., & Van Der Spuy, W. J. (2012). Iron enhances generation of fibrin fibers in human blood: implications for pathogenesis of stroke. *Microscopy Research and Technique, 75*(9), 1185-1190.

Littlejohn, L. F., Devlin, J. J., Kircher, S. S., Lueken, R., Melia, M. R., & Johnson, A. S. (2011). Comparison of Celox-A, ChitoFlex, WoundStat, and Combat Gauze Hemostatic Agents Versus Standard Gauze Dressing in Control of Hemorrhage in a Swine Model of Penetrating Trauma. *Academic Emergency Medicine, 18*(4), 340-350.

López-Noriega, A., Arcos, D., Izquierdo-Barba, I., Sakamoto, Y., Terasaki, O., & Vallet-Regí, M. (2006). Ordered mesoporous bioactive glasses for bone tissue regeneration. *Chemistry of Materials, 18*(13), 3137-3144.

Lundblad, R. L., Bradshaw, R. A., Gabriel, D., Ortel, T. L., Lawson, J., & Mann, K. G. (2004). A review of the therapeutic uses of thrombin. *Thrombosis and Haemostasis, 91*(5), 851-860.

Luque, R., Balu, A. M., Campelo, J. M., Gracia, M. D., Losada, E., Pineda, A., . . . Serrano-Ruiz, J. C. (2012). *Catalytic applications of mesoporous silica-based materials* (Vol. 24).

Mackman, N. (2004). Role of tissue factor in hemostasis, thrombosis, and vascular development. *Arteriosclerosis, Thrombosis, and Vascular Biology, 24*(6), 1015-1022.

Mackman, N., Tilley, R. E., & Key, N. S. (2007). Role of the extrinsic pathway of blood coagulation in hemostasis and thrombosis. *Arteriosclerosis, Thrombosis, and Vascular Biology, 27*(8), 1687-1693.

MacLeod, J. B., Lynn, M., McKenney, M. G., Cohn, S. M., & Murtha, M. (2003). Early coagulopathy predicts mortality in trauma. *Journal of Trauma and Acute Care Surgery, 55*(1), 39-44.

Maesen, T. (2007). The zeolite scene-an overview. *Studies in Surface Science and Catalysis, 168*, 1-12.

Mahajna, A., Hirsh, M., & Krausz, M. M. (2007). Use of the hemostatic agent QuikClot® for the treatment of massive splenic injury in a rat model. *European Surgical Research, 39*(4), 251-257.

Makino, T., Jinnin, M., Muchemwa, F., Fukushima, S., Kogushi-Nishi, H., Moriya, C., . . . Ihn, H. (2010). Basic fibroblast growth factor stimulates the proliferation of human dermal fibroblasts via the ERK1/2 and JNK pathways. *British Journal of Dermatology, 162*(4), 717-723.

Malavasi, G., Pedone, A., & Menziani, M. C. (2013). Study of the structural role of gallium and aluminum in 45S5 bioactive glasses by molecular dynamics simulations. *The Journal of Physical Chemistry B, 117*(15), 4142-4150.

Mannucci, P. M., & Levi, M. (2007). Prevention and treatment of major blood loss. *New England Journal of Medicine, 356*(22), 2301-2311.

Mao, C., Chen, X., Miao, G., & Lin, C. (2015). Angiogenesis stimulated by novel nanoscale bioactive glasses. *Biomedical Materials, 10*(2), 025005.

Marder, V. J., Aird, W. C., Bennett, J. S., Schulman, S., & White, G. C. (2012). *Hemostasis and thrombosis: basic principles and clinical practice,* : Lippincott Williams & Wilkins.

Margolis, J. (1958). The kaolin clotting time: a rapid one-stage method for diagnosis of coagulation defects. *Journal of Clinical Pathology, 11*(5), 406.

Margulis, V., Matsumoto, E. D., Svatek, R., Kabbani, W., Cadeddu, J. A., & Lotan, Y. (2005). Application of novel hemostatic agent during laparoscopic partial nephrectomy. *The Journal of urology, 174*(2), 761-764.

Martin, M. J. (2014). Editorial to accompany "A pilot study of the use of kaolin-impregnated gauze (Combat Gauze) for packing high-grade hepatic injuries in a hypothermic coagulopathic swine model". *Journal of Surgical Research, 186*(1), 116-118.

Matsumura, Y., Yoshikata, K., Kunisaki, S.-i., & Tsuchido, T. (2003). Mode of bactericidal action of silver zeolite and its comparison with that of silver nitrate. *Applied and environmental microbiology, 69*(7), 4278-4281.

McManus, J., Hurtado, T., Pusateri, A., & Knoop, K. J. (2007). A case series describing thermal injury resulting from zeolite use for hemorrhage control in combat operations. *Prehospital Emergency Care, 11*(1), 67-71.

Mikaelsson, M. (1991). The role of calcium in coagulation and anticoagulation *Coagulation and blood transfusion* (pp. 29-37): Springer.

Monroe, D. M., Hoffman, M., & Roberts, H. R. (2002). Platelets and thrombin generation. *Arteriosclerosis, Thrombosis, and Vascular Biology, 22*(9), 1381-1389.

Morrissey, J. H. (2001). Tissue factor: an enzyme cofactor and a true receptor. *Thrombosis and Haemostasis, 86*(1), 66-74.

Mortazavi, S., Atefi, A., Roshan-Shomal, P., Raadpey, N., & Mortazavi, G. (2009). Development of a novel mineral based haemostatic agent consisting of a combination of bentonite and zeolite minerals. *Journal of Ayub Medical College, Abbottabad, 21*(1), 3-7.

Mortazavi, S., Tavasoli, A., Atefi, M., Tanide, N., Radpey, N., Roshan-shomal, P., . . . Taeb, S. (2013). CoolClot, a novel hemostatic agent for controlling life-threatening arterial bleeding. *World, 4*(2), 123-127.

Mukherjee, S. (2012). *Applied mineralogy: applications in industry and environment*: Springer.

Mumpton, F. A. (1999). La roca magica: uses of natural zeolites in agriculture and industry. *Proceedings of the National Academy of Sciences, 96*(7), 3463-3470.

Murray, C. K., Roop, S. A., Hospenthal, D. R., Dooley, D. P., Wenner, K., Hammock, J., . . . Gourdine, E. (2006). Bacteriology of war wounds at the time of injury. *Military medicine, 171*(9), 826-829.

Murray, H. H. (1999). Applied clay mineralogy today and tomorrow. *Clay Minerals, 34*(1), 39-39.

Murray, H. H. (2000). Traditional and new applications for kaolin, smectite, and palygorskite: a general overview. *Applied clay science, 17*(5), 207-221.

Naghavi, M., Wang, H., Lozano, R., Davis, A., Liang, X., & Zhou, M. (2015). GBD 2013 Mortality and Causes of Death Collaborators. Global, regional, and national age-sex specific all-cause and cause-specific mortality for 240 causes of death, 1990-2013: a systematic analysis for the Global Burden of Disease Study 2013. *Lancet, 385*(9963), 117-171.

Neuffer, M. C., McDivitt, J., Rose, D., & King, K. (2004). Hemostatic dressings for the first responder: a review. *Military Medicine, 169*(9), 716.

Niles, S. E., McLaughlin, D. F., Perkins, J. G., Wade, C. E., Li, Y., Spinella, P. C., & Holcomb, J. B. (2008). Increased mortality associated with the early coagulopathy of trauma in combat casualties. *Journal of Trauma and Acute Care Surgery, 64*(6), 1459-1465.

Ong, S.-Y., Wu, J., Moochhala, S. M., Tan, M.-H., & Lu, J. (2008). Development of a chitosan-based wound dressing with improved hemostatic and antimicrobial properties. *Biomaterials, 29*(32), 4323-4332.

Ostomel, T. A., Shi, Q., Stoimenov, P. K., & Stucky, G. D. (2007). Metal oxide surface charge mediated hemostasis. *Langmuir, 23*(22), 11233-11238.

Ostomel, T. A., Shi, Q., & Stucky, G. D. (2006). Oxide hemostatic activity. *Journal of the American Chemical Society, 128*(26), 8384-8385.

Ostomel, T. A., Shi, Q., Tsung, C. K., Liang, H., & Stucky, G. D. (2006). Spherical bioactive glass with enhanced rates of hydroxyapatite deposition and hemostatic activity. *Small, 2*(11), 1261-1265.

Otrocka-Domagała, I., Jastrzębski, P., Adamiak, Z., Paździor-Czapula, K., Gesek, M., Mikiewicz, M., & Rotkiewicz, T. (2016). Safety of the long-term application of QuikClot Combat Gauze, ChitoGauze PRO and Celox Gauze in a femoral artery injury model in swine–a preliminary study. *Polish Journal of Veterinary Sciences, 19*(2), 337-343.

Palm, M. D., & Altman, J. S. (2008). Topical hemostatic agents: a review. *Dermatologic Surgery, 34*(4), 431-445.

Parsons, D., Bowler, P., Myles, V., & Jones, S. (2005). Silver antimicrobial dressings in wound management: a comparison of antibacterial, physical, and chemical characteristics. *WOUNDS-A COMPENDIUM OF CLINICAL RESEARCH AND PRACTICE, 17*(8), 222-232.

Patterson, J. A. (2003). Method for applying a blood clotting agent. *U.S. Patent No. US 6521265 B1. Washington, DC: U.S. Patent and Trademark Office.*

Pavelić, K., Hadžija, M., Bedrica, L., Pavelić, J., Đikić, I., Katić, M., . . . Poljak-Blaži, M. (2001). Natural zeolite clinoptilolite: new adjuvant in anticancer therapy. *Journal of Molecular Medicine, 78*(12), 708-720.

Peng, T. (2010). Biomaterials for hemorrhage control. *Trends Biomater Artif Organs, 24*(1), 27-68.

Penn-Barwell, J. G., Brown, K. V., & Fries, C. A. (2015). High velocity gunshot injuries to the extremities: management on and off the battlefield. *Current Reviews in Musculoskeletal Medicine, 8*(3), 312-317.

Philippart, A., Gómez-Cerezo, N., Arcos, D., Salinas, A. J., Boccardi, E., Vallet-Regi, M., & Boccaccini, A. R. (2017). Novel ion-doped mesoporous glasses for bone tissue engineering: Study of their structural characteristics influenced by the presence of phosphorous oxide. *Journal of Non-Crystalline Solids, 455*, 90-97.

Plurad, D., Chandrasoma, S., Best, C., & Rhee, P. (2009). A complication of intracorporeal use of QuikClot for pelvic hemorrhage. *Journal of Trauma and Acute Care Surgery, 66*(5), 1482-1484.

Pretorius, E., Bester, J., Vermeulen, N., & Lipinski, B. (2013). Oxidation inhibits iron-induced blood coagulation. *Current Drug Targets, 14*(1), 13.

Pusateri, A. E., Delgado, A. V., Dick Jr, E. J., Martinez, R. S., Holcomb, J. B., & Ryan, K. L. (2004). Application of a granular mineral-based hemostatic agent (QuikClot) to reduce blood loss after grade V liver injury in swine. *Journal of Trauma and Acute Care Surgery, 57*(3), 555-562.

Pusateri, A. E., Holcomb, J. B., Kheirabadi, B. S., Alam, H. B., Wade, C. E., & Ryan, K. L. (2006). Making sense of the preclinical literature on advanced hemostatic products. *J. Trauma Acute Care Surg., 60*(3), 674-682.

Radin, S., El-Bassyouni, G., Vresilovic, E. J., Schepers, E., & Ducheyne, P. (2005). In vivo tissue response to resorbable silica xerogels as controlled-release materials. *Biomaterials, 26*(9), 1043-1052.

Rahaman, M. N., Day, D. E., Bal, B. S., Fu, Q., Jung, S. B., Bonewald, L. F., & Tomsia, A. P. (2011). Bioactive glass in tissue engineering. *Acta Biomaterialia, 7*(6), 2355-2373.

Rahmat, N., Abdullah, A. Z., & Mohamed, A. R. (2010). A review: mesoporous Santa Barbara amorphous-15, types, synthesis and its applications towards biorefinery production. *American Journal of Applied Sciences, 7*(12), 1579.

Rall, J. M., Cox, J. M., Songer, A. G., Cestero, R. F., & Ross, J. D. (2013). Comparison of novel hemostatic dressings with QuikClot combat gauze in a standardized swine model of uncontrolled hemorrhage. *Journal of Trauma and Acute Care Surgery, 75*(2), S150-S156.

Ran, Y., Hadad, E., Daher, S., Ganor, O., Kohn, J., Yegorov, Y., . . . Hirschhorn, G. (2010). QuikClot Combat Gauze use for hemorrhage control in military trauma: January 2009 Israel Defense Force experience in the Gaza Strip—a preliminary report of 14 cases. *Prehospital and Disaster Medicine, 25*(06), 584-588.

Rao, S. B., & Sharma, C. P. (1997). Use of chitosan as a biomaterial: studies on its safety and hemostatic potential. *J. Biomed. Mater. Res., 34*(1), 21-28.

Ratner, B. D., Hoffman, A. S., Schoen, F. J., & Lemons, J. E. (1996). An introduction to materials in medicine. *Biomaterials Science, 484*.

Renné, T., Schmaier, A. H., Nickel, K. F., Blombäck, M., & Maas, C. (2012). In vivo roles of factor XII. *Blood, 120*(22), 4296-4303.

Rhee, P., Brown, C., Martin, M., Salim, A., Plurad, D., Green, D., . . . Alam, H. (2008). QuikClot use in trauma for hemorrhage control: case series of 103 documented uses. *J. Trauma Acute Care Surg., 64*(4), 1093-1099.

Rimoli, M. G., Rabaioli, M. R., Melisi, D., Curcio, A., Mondello, S., Mirabelli, R., & Abignente, E. (2008). Synthetic zeolites as a new tool for drug delivery. *Journal of Biomedical Materials Research Part A, 87*(1), 156-164.

Robinson, K. (2004). Controlling bleeding in the field: hemostatic powders and dressings debut in the prehospital setting. *Journal of Emergency Nursing, 30*(2), 160-161.

Rodriguez-Fuentes, G., Barrios, M., Iraizoz, A., Perdomo, I., & Cedre, B. (1997). Enterex: Anti-diarrheic drug based on purified natural clinoptilolite. *Zeolites, 19*(5), 441-448.

Rogosnitzky, M. (2014). Method of wound hemostasis using liquid gallium nitrate. *U.S. Patent No. US 8652509 B2. Washington, DC: U.S. Patent and Trademark Office.*

Rosales-Landeros, C., Barrera-Díaz, C. E., Bilyeu, B., Guerrero, V. V., & Núñez, F. U. (2013). A Review on Cr (VI) Adsorption Using Inorganic Materials. *American Journal of Analytical Chemistry, 4*, 8.

Rossaint, R., Bouillon, B., Cerny, V., Coats, T. J., Duranteau, J., Fernández-Mondéjar, E., . . . Nardi, G. (2016). The European guideline on management of major bleeding and coagulopathy following trauma. *J. Crit. Care, 20*(1), 100.

Rouquerol, J., Avnir, D., Fairbridge, C., Everett, D., Haynes, J., Pernicone, N., . . . Unger, K. (1994). Recommendations for the characterization of porous solids (Technical Report). *Pure and Applied Chemistry, 66*(8), 1739-1758.

Russell, A., Path, F., Sl, F. P., & Hugo, W. (1994). 7 Antimicrobial Activity and Action of. *Progress in medicinal chemistry, 31*, 351.

Salinas, A., Shruti, S., Malavasi, G., Menabue, L., & Vallet-Regi, M. (2011). Substitutions of cerium, gallium and zinc in ordered mesoporous bioactive glasses. *Acta Biomater., 7*(9), 3452-3458.

Samudrala, S. (2008). Topical hemostatic agents in surgery: a surgeon's perspective. *AORN Journal, 88*(3), S2-S11.

Sanchez-Salcedo, S., Salinas, A., Vallet-Regi, M., Malavasi, G., Lusvardi, G., & Menabue, L. Development of mesoporous bioactive glasses able to release antibacterial Ga3+ ions.

Schneider, P. (1995). Adsorption isotherms of microporous-mesoporous solids revisited. *Applied Catalysis A: General, 129*(2), 157-165.

Schreiber, M. A., & Neveleff, D. J. (2011). Achieving hemostasis with topical hemostats: making clinically and economically appropriate decisions in the surgical and trauma settings. *AORN Journal, 94*(5), S1-S20.

Schwartz, R. B., Reynolds, B. Z., Shiver, S. A., Lerner, E. B., Greenfield, E. M., Solis, R. A., . . . McManus, J. G. (2011). Comparison of two packable hemostatic Gauze dressings in a porcine hemorrhage model. *Prehospital Emergency Care, 15*(4), 477-482.

Sena, M. J., Douglas, G., Gerlach, T., Grayson, J. K., Pichakron, K. O., & Zierold, D. (2013). A pilot study of the use of kaolin-impregnated gauze (Combat Gauze) for packing high-grade hepatic injuries in a hypothermic coagulopathic swine model. *Journal of Surgical Research, 183*(2), 704-709.

Shah, A. T., Ain, Q., Chaudhry, A. A., Khan, A. F., Iqbal, B., Ahmad, S., . . . ur Rehman, I. (2015). A study of the effect of precursors on physical and biological properties of mesoporous bioactive glass. *Journal of Materials Science, 50*(4), 1794-1804.

Shamosi, A., Farokhi, M., Ai, J., & Sharifi, E. (2015). Induction of spontaneous neo-angiogenesis and tube formation in human endometrial stem cells by bioglass. *Journal of Medical Hypotheses and Ideas, 9*(2), 94-98.

Shanmugam, V., & Robinson, M. (2009). Case report of uncontrollable pelvic bleeding–managed by a previously unreported method (QuikClot®). *Colorectal Disease, 11*(2), 221-222.

Shina, A., Lipsky, A. M., Nadler, R., Levi, M., Benov, A., Ran, Y., . . . Glassberg, E. (2015). Prehospital use of hemostatic dressings by the Israel Defense Forces Medical Corps: A case series of 122 patients. *Journal of Trauma and Acute Care Surgery, 79*(4), S204-S209.

Shruti, S., Salinas, A. J., Ferrari, E., Malavasi, G., Lusvardi, G., Doadrio, A. L., . . . Vallet-Regi, M. (2013). Curcumin release from cerium, gallium and zinc containing mesoporous bioactive glasses. *Microporous Mesoporous Mater., 180*, 92-101.

Shruti, S., Salinas, A. J., Malavasi, G., Lusvardi, G., Menabue, L., Ferrara, C., . . . Vallet-Regì, M. (2012). Structural and in vitro study of cerium, gallium and zinc containing sol–gel bioactive glasses. *Journal of Materials Chemistry, 22*(27), 13698-13706.

Silhavy, T. J., Kahne, D., & Walker, S. (2010). The bacterial cell envelope. *Cold Spring Harbor Perspectives in Biology, 2*(5), a000414.

Slowing, I. I., Trewyn, B. G., Giri, S., & Lin, V. Y. (2007). Mesoporous silica nanoparticles for drug delivery and biosensing applications. *Advanced Functional Materials, 17*(8), 1225-1236.

Smith, A. H., Laird, C., Porter, K., & Bloch, M. (2013). Haemostatic dressings in prehospital care. *Emergency Medicine Journal, 30*(10), 784-789.

Song, Y., Li, Y., Xu, Q., & Liu, Z. (2017). Mesoporous silica nanoparticles for stimuli-responsive controlled drug delivery: advances, challenges, and outlook. *International Journal of Nanomedicine, 12*, 87.

Sperling, C., Fischer, M., Maitz, M. F., & Werner, C. (2009). Blood coagulation on biomaterials requires the combination of distinct activation processes. *Biomaterials, 30*(27), 4447-4456.

Suh, W. H., Suslick, K. S., Stucky, G. D., & Suh, Y.-H. (2009). Nanotechnology, nanotoxicology, and neuroscience. *Progress in Neurobiology, 87*(3), 133-170.

Thomas, S. (2004). MRSA and the use of silver dressings: overcoming bacterial resistance. *World Wide Wounds*.

Trabattoni, D., Gatto, P., & Bartorelli, A. L. (2012). A new kaolin-based hemostatic bandage use after coronary diagnostic and interventional procedures. *International Journal of Cardiology, 156*(1), 53-54.

Tracy, L. E., Minasian, R. A., & Caterson, E. (2016). Extracellular matrix and dermal fibroblast function in the healing wound. *Advances in Wound Care, 5*(3), 119-136.

Travers, S., Lefort, H., Ramdani, E., Lemoine, S., Jost, D., Bignand, M., & Tourtier, J.-P. (2016). Hemostatic dressings in civil prehospital practice: 30 uses of QuikClot Combat Gauze. *European Journal of Emergency Medicine, 23*(5), 391-394.

Vaid, C., Murugavel, S., Kashayap, R., & Tandon, R. P. (2012). Synthesis and in vitro bioactivity of surfactant templated mesoporous sodium silicate glasses. *Microporous and Mesoporous Materials, 159*, 17-23.

Valappil, S. P., Ready, D., Neel, E. A., Pickup, D. M., O'Dell, L. A., Chrzanowski, W., . . . Wilson, M. (2009). Controlled delivery of antimicrobial gallium ions from phosphate-based glasses. *Acta biomaterialia, 5*(4), 1198-1210.

Valappil, S. P., Ready, D., Neel, E. A. A., Pickup, D. M., Chrzanowski, W., O'Dell, L. A., . . . Knowles, J. C. (2008). Antimicrobial gallium-doped phosphate-based glasses. *Advanced Functional Materials, 18*(5), 732-741.

Vallet-Regí, M., Garcia, M. M., & Colilla, M. (2012). *Biomedical applications of mesoporous ceramics: drug delivery, smart materials and bone tissue engineering*: CRC Press.

Vallet-Regí, M., Izquierdo-Barba, I., & Colilla, M. (2012). Structure and functionalization of mesoporous bioceramics for bone tissue regeneration and local drug delivery. *Philosophical Transactions of the Royal Society A, 370*(1963), 1400-1421.

Vallet-Regí, M. (2010). Nanostructured mesoporous silica matrices in nanomedicine. *Journal of Internal Medicine, 267*(1), 22-43.

Vallet-Regí, M., Balas, F., & Arcos, D. (2007). Mesoporous materials for drug delivery. *Angewandte Chemie International Edition, 46*(40), 7548-7558.

Vartuli, J., Kresge, C., Leonowicz, M., Chu, A., McCullen, S., Johnson, I., & Sheppard, E. (1994). Synthesis of mesoporous materials: liquid-crystal templating versus intercalation of layered silicates. *Chemistry of Materials, 6*(11), 2070-2077.

Verron, E., Masson, M., Khoshniat, S., Duplomb, L., Wittrant, Y., Baud'huin, M., . . . Scimeca, J. C. (2010). Gallium modulates osteoclastic bone resorption in vitro without affecting osteoblasts. *British Journal of Pharmacology, 159*(8), 1681-1692.

Walsh, P. (1972). The effects of collagen and kaolin on the intrinsic coagulant activity of platelets. Evidence for an alternative pathway in intrinsic coagulation not requiring factor XII. *British Journal of Haematology, 22*(4), 393-405.

Wang, X., & Li, W. (2016). Biodegradable mesoporous bioactive glass nanospheres for drug delivery and bone tissue regeneration. *Nanotechnology, 27*(22), 225102.

Wang, X., Zhang, Y., Ma, Y., Chen, D., Yang, H., & Li, M. (2016). Selenium–containing mesoporous bioactive glass particles: Physicochemical and drug delivery properties. *Ceramics International, 42*(2), 3609-3617.

Ward, K. R., Tiba, M. H., Holbert, W. H., Blocher, C. R., Draucker, G. T., Proffitt, E. K., . . . Diegelmann, R. F. (2007). Comparison of a new hemostatic agent to current combat hemostatic agents in a swine model of lethal extremity arterial hemorrhage. *Journal of Trauma and Acute Care Surgery, 63*(2), 276-284.

Warren, J. K. (2016). *Evaporites: A geological compendium*: Springer.

Watters, J. M., Van, P. Y., Hamilton, G. J., Sambasivan, C., Differding, J. A., & Schreiber, M. A. (2011). Advanced hemostatic dressings are not superior to gauze for care under fire scenarios. *Journal of Trauma and Acute Care Surgery, 70*(6), 1413-1419.

Wei, F., Daming, W., Tengjiao, M., & Bing, F. (2015). Ag-loaded mesoporous bioactive glasses against Enterococcus faecalis biofilm in root canal of human teeth. *Dental materials journal, 34*(1), 54-60.

White, W. M. (2013). *Geochemistry*: John Wiley & Sons.

Williams, L. B., & Haydel, S. E. (2010). Evaluation of the medicinal use of clay minerals as antibacterial agents. *International geology review, 52*(7-8), 745-770.

Wren, A., Coughlan, A., Placek, L., & Towler, M. (2012). Gallium containing glass polyalkenoate anti-cancerous bone cements: glass characterization and physical properties. *Journal of Materials Science: Materials in Medicine, 23*(8), 1823-1833.

Wright, F. L., Hua, H. T., Velmahos, G., Thoman, D., Demitriades, D., & Rhee, P. M. (2004). Intracorporeal use of the hemostatic agent QuickClot in a coagulopathic patient with combined thoracoabdominal penetrating trauma. *Journal of Trauma and Acute Care Surgery, 56*(1), 205-208.

Wright, J. K., Kalns, J., Wolf, E. A., Traweek, F., Schwarz, S., Loeffler, C. K., . . . Eggers, J. (2004). Thermal injury resulting from application of a granular mineral hemostatic agent. *Journal of Trauma and Acute Care Surgery, 57*(2), 224-230.

Wu, C., & Chang, J. (2012). Mesoporous bioactive glasses: structure characteristics, drug/growth factor delivery and bone regeneration application. *Interface Focus, 2*(3), 292-306.

Wu, C., Miron, R., Sculean, A., Kaskel, S., Doert, T., Schulze, R., & Zhang, Y. (2011). Proliferation, differentiation and gene expression of osteoblasts in boron-containing associated with dexamethasone deliver from mesoporous bioactive glass scaffolds. *Biomaterials, 32*(29), 7068-7078.

Wu, X., Wei, J., Lu, X., Lv, Y., Chen, F., Zhang, Y., & Liu, C. (2010). Chemical characteristics and hemostatic performances of ordered mesoporous calcium-doped silica xerogels. *Biomedical Materials, 5*(3), 035006.

Yan, X., Yu, C., Zhou, X., Tang, J., & Zhao, D. (2004). Highly Ordered Mesoporous Bioactive Glasses with Superior In Vitro Bone-Forming Bioactivities. *Angewandte Chemie International Edition, 43*(44), 5980-5984.

Yim, E. K., & Leong, K. W. (2005). Significance of synthetic nanostructures in dictating cellular response. *Nanomedicine: Nanotechnology, Biology and Medicine, 1*(1), 10-21.

Yu, H., Peng, J., Xu, Y., Chang, J., & Li, H. (2015). Bioglass activated skin tissue engineering constructs for wound healing. *ACS applied materials & interfaces, 8*(1), 703-715.

Zhang, X., Zeng, D., Li, N., Wen, J., Jiang, X., Liu, C., & Li, Y. (2016). Functionalized mesoporous bioactive glass scaffolds for enhanced bone tissue regeneration. *Scientific Reports, 6*.

Zhao, Y., Sun, X., Zhang, G., Trewyn, B. G., Slowing, I. I., & Lin, V. S.-Y. (2011). Interaction of mesoporous silica nanoparticles with human red blood cell membranes: size and surface effects. *ACS nano, 5*(2), 1366-1375.

Zhou, G.-d. (1994). *Fundamentals of structural chemistry*: World Scientific.

Zhou, Y., Shi, M., Jones, J. R., Chen, Z., Chang, J., Wu, C., & Xiao, Y. (2017). Strategies to direct vascularisation using mesoporous bioactive glass-based biomaterials for bone regeneration. *International Materials Reviews*, 1-23.

LIST OF PUBLICATIONS AND PAPERS PRESENTED

❖ Review article

Sara Pourshahrestani, Ehsan Zeimaran, Ivan Djordjevic, Nahrizul Adib Kadri, Mark R. Towler, (2016). Inorganic hemostats: The state-of-the-art and recent advances. Materials Science and Engineering: C, 58, 1255–1268. DOI: 10.1016/j.msec.2015.09.008.

Materials Science and Engineering C 58 (2016) 1255–1268

Contents lists available at ScienceDirect

Materials Science and Engineering C

journal homepage: www.elsevier.com/locate/msec

Inorganic hemostats: The state-of-the-art and recent advances

Sara Pourshahrestani [a], Ehsan Zeimaran [a], Ivan Djordjevic [a], Nahrizul Adib Kadri [a], Mark R. Towler [a,b,*]

[a] Department of Biomedical Engineering, Faculty of Engineering, University of Malaya, Kuala Lumpur 50603, Malaysia
[b] Department of Mechanical & Industrial Engineering, Ryerson University, Toronto M5B 2K3, ON, Canada

ARTICLE INFO

Article history:
Received 28 March 2015
Accepted 3 September 2015
Available online 5 September 2015

Keywords:
Hemorrhage
Hemostasis
Inorganic hemostat
Zeolite
Kaolin
Smectite

ABSTRACT

Hemorrhage is the most common cause of death both in hospitals and on the battlefield. The need for an effective hemostatic agent remains, since all injuries are not amenable to tourniquet use. There are many topical hemostatic agents and dressings available to control severe bleeding. This article reviews the most commonly used inorganic hemostats, subcategorized as zeolite and clay-based hemostats. Their hemostatic functions as well as their structural properties that are believed to induce hemostasis are discussed. The most important findings from *in vitro* and *in vivo* experiments are also covered.

Contents

1. Introduction

Irrepressible bleeding can result in mortality but can also debilitate the process of wound healing and increase the possibility of infection

* Corresponding author at: Department of Mechanical & Industrial Engineering, Ryerson University, Toronto M5B 2K3, ON, Canada.
E-mail address: mtowler@ryerson.ca (M.R. Towler).

http://dx.doi.org/10.1016/j.msec.2015.09.008
0928-4931/

➢ Research articles

Sara Pourshahrestani, Ehsan Zeimaran, Nahrizul Adib Kadri, Nicola Gargiulo, Shani Samuel, Sangeetha Vasudevaraj Naveen, Tunku Kamarulc, Mark R. Towler, (2016). Gallium-containing mesoporous bioactive glass with potent hemostatic activity and antibacterial efficacy. Journal of Materials Chemistry B, 4, 71-86. DOI: 10.1039/C5TB02062J.

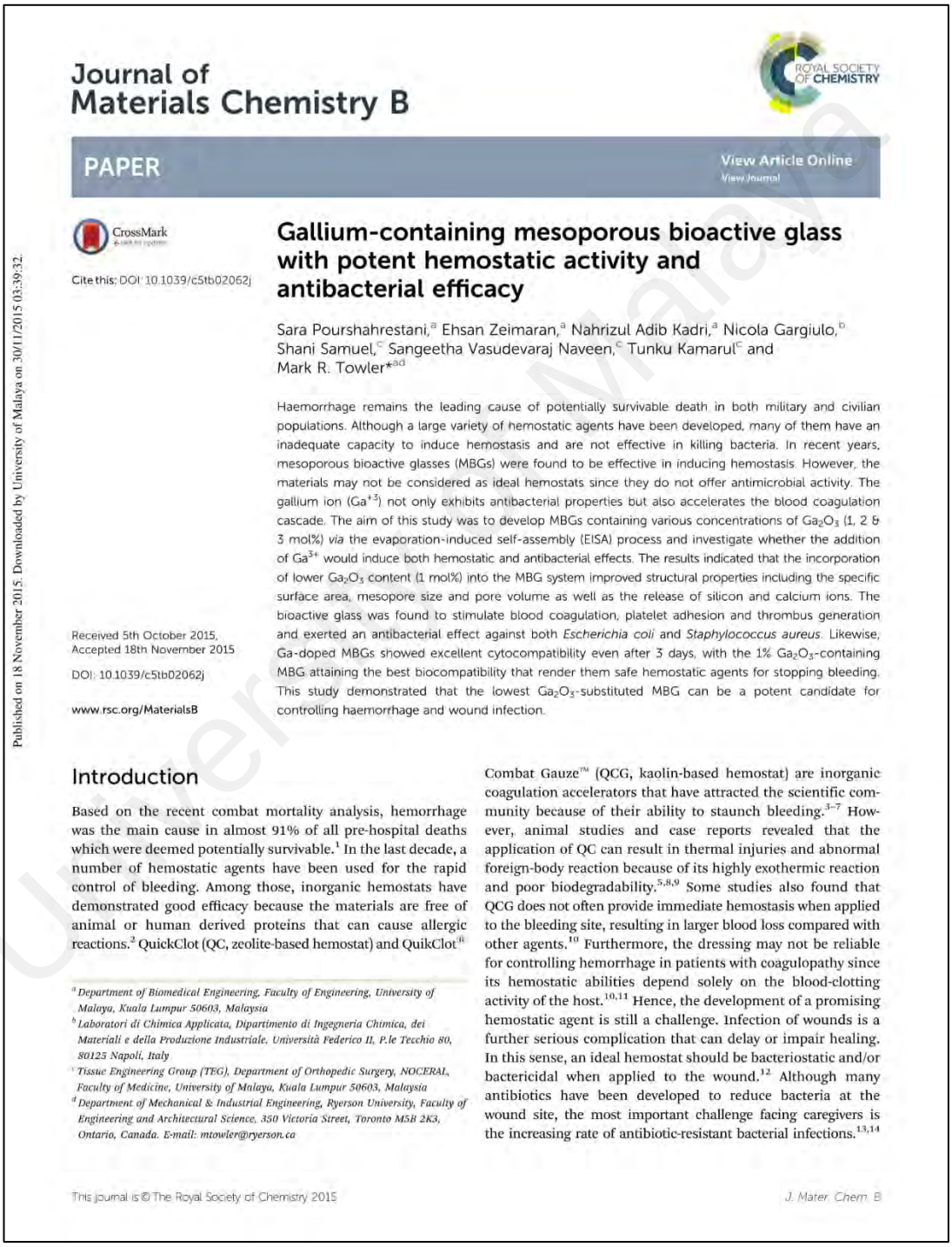

Journal of Materials Chemistry B

PAPER

View Article Online
View Journal

Cite this: DOI: 10.1039/c5tb02062j

Gallium-containing mesoporous bioactive glass with potent hemostatic activity and antibacterial efficacy

Sara Pourshahrestani,[a] Ehsan Zeimaran,[a] Nahrizul Adib Kadri,[a] Nicola Gargiulo,[b] Shani Samuel,[c] Sangeetha Vasudevaraj Naveen,[c] Tunku Kamarul[c] and Mark R. Towler*[ad]

Haemorrhage remains the leading cause of potentially survivable death in both military and civilian populations. Although a large variety of hemostatic agents have been developed, many of them have an inadequate capacity to induce hemostasis and are not effective in killing bacteria. In recent years, mesoporous bioactive glasses (MBGs) were found to be effective in inducing hemostasis. However, the materials may not be considered as ideal hemostats since they do not offer antimicrobial activity. The gallium ion (Ga^{1-3}) not only exhibits antibacterial properties but also accelerates the blood coagulation cascade. The aim of this study was to develop MBGs containing various concentrations of Ga_2O_3 (1, 2 & 3 mol%) *via* the evaporation-induced self-assembly (EISA) process and investigate whether the addition of Ga^{3+} would induce both hemostatic and antibacterial effects. The results indicated that the incorporation of lower Ga_2O_3 content (1 mol%) into the MBG system improved structural properties including the specific surface area, mesopore size and pore volume as well as the release of silicon and calcium ions. The bioactive glass was found to stimulate blood coagulation, platelet adhesion and thrombus generation and exerted an antibacterial effect against both *Escherichia coli* and *Staphylococcus aureus*. Likewise, Ga-doped MBGs showed excellent cytocompatibility even after 3 days, with the 1% Ga_2O_3-containing MBG attaining the best biocompatibility that render them safe hemostatic agents for stopping bleeding. This study demonstrated that the lowest Ga_2O_3-substituted MBG can be a potent candidate for controlling haemorrhage and wound infection.

Received 5th October 2015,
Accepted 18th November 2015

DOI: 10.1039/c5tb02062j

www.rsc.org/MaterialsB

Introduction

Based on the recent combat mortality analysis, hemorrhage was the main cause in almost 91% of all pre-hospital deaths which were deemed potentially survivable.[1] In the last decade, a number of hemostatic agents have been used for the rapid control of bleeding. Among those, inorganic hemostats have demonstrated good efficacy because the materials are free of animal or human derived proteins that can cause allergic reactions.[2] QuickClot (QC, zeolite-based hemostat) and QuikClot Combat Gauze™ (QCG, kaolin-based hemostat) are inorganic coagulation accelerators that have attracted the scientific community because of their ability to staunch bleeding.[3–7] However, animal studies and case reports revealed that the application of QC can result in thermal injuries and abnormal foreign-body reaction because of its highly exothermic reaction and poor biodegradability.[5,8,9] Some studies also found that QCG does not often provide immediate hemostasis when applied to the bleeding site, resulting in larger blood loss compared with other agents.[10] Furthermore, the dressing may not be reliable for controlling hemorrhage in patients with coagulopathy since its hemostatic abilities depend solely on the blood-clotting activity of the host.[10,11] Hence, the development of a promising hemostatic agent is still a challenge. Infection of wounds is a further serious complication that can delay or impair healing. In this sense, an ideal hemostat should be bacteriostatic and/or bactericidal when applied to the wound.[12] Although many antibiotics have been developed to reduce bacteria at the wound site, the most important challenge facing caregivers is the increasing rate of antibiotic-resistant bacterial infections.[13,14]

[a] Department of Biomedical Engineering, Faculty of Engineering, University of Malaya, Kuala Lumpur 50603, Malaysia
[b] Laboratori di Chimica Applicata, Dipartimento di Ingegneria Chimica, dei Materiali e della Produzione Industriale, Università Federico II, P.le Tecchio 80, 80125 Napoli, Italy
[c] Tissue Engineering Group (TEG), Department of Orthopedic Surgery, NOCERAL, Faculty of Medicine, University of Malaya, Kuala Lumpur 50603, Malaysia
[d] Department of Mechanical & Industrial Engineering, Ryerson University, Faculty of Engineering and Architectural Science, 350 Victoria Street, Toronto M5B 2K3, Ontario, Canada. E-mail: mtowler@ryerson.ca

- **Conference paper**

Sara Pourshahrestani, Ehsan Zeimaran, Nahrizul Adib Kadri, Mark R. Towler, (2016). In vitro evaluation of thrombogenicity effect of gallium-containing mesoporous bioactive glass. *10th World Biomaterials Congress*, Canada.

***In vitro* evaluation of thrombogenicity effect of gallium-containing mesoporous bioactive glass**

Sara Pourshahrestani[1], Ehsan Zeimaran[1], Nahrizul Adib Kadri[1], Mark R. Towler[1,2]

[1]Department of Biomedical Engineering, Faculty of Engineering, University of Malaya, Kuala Lumpur 50603, Malaysia.

[2]Department of Mechanical & Industrial Engineering, Ryerson University, Toronto M5B 2K3, ON, Canada.

Introduction: Inorganic hemostats have demonstrated effectiveness in staunching bleed out [1]. Mesoporous bioglasses (MBGs) are promising candidate for hemorrhage control due to their high specific surface area, pore volume and pore size [2]. Gallium nitrate has proven efficacy in stimulation of the early stages of hemostasis (either coagulation, platelet activation, or thrombus formation) [3]. In this paper, MBGs containing three different concentrations of Ga_2O_3 (1, 2 & 3 mol %) were synthesized and the effect of Ga^{3+} addition to the MBG framework on *in vitro* thrombogenicity of MBG was evaluated.

Methods: Three MBGs (80-x) %SiO_2–15%CaO–5%P_2O_5–xGa_2O_3 doped with different content of Ga_2O_3 were synthesized *via* evaporation-induced self-assembly (EISA) process by using Pluronic P123 as a mesostructure former. Briefly, Pluronic P123, tetraethyl orthosilicate (TEOS), Ca $(NO_3)_2.4H_2O$, triethyl phosphate (TEP), Ga $(NO_3)_3$. X H_2O and 0.5 M HNO_3 were dissolved in ethanol and then stirred overnight and the sol underwent the EISA process for one week. The dried gels were calcinated at 600 °C for 5 h. The textural properties of the prepared materials were determined by N2 adsorption/desorption analyses using a Micrometrics ASAP 2020 instrument. The surface area and pore size distribution were determined by applying the Brunauer–Emmett–Teller (BET) the Barret–Joyner–Halenda (BJH) methods respectively. To test the *in vitro* thrombotic effects, the materials were incubated with citrated human blood for 15, 30 and 60 min at 37 °C. The degree of thrombogenicity (DT) of the materials was defined as follows: DT = [(Wt-W0)/W0] × 100%, where W_0 and W_t are the weights of the samples before and after incubation with blood, respectively. Field-emission scanning electron (FESEM: Quanta™ 250 FEG—FEI, USA) micrographs were also obtained to observe the interaction of whole blood with the Ga-MBG materials.

Results and discussion: Table 1 demonstrates the BET, pore volume and pore size of MBG and Ga-MBG samples. Notably, the surface areas and pore volumes of the 1%Ga-MBG were found to be higher than those of other samples.

Table 1. Textural properties of MBG and Ga-MBGs.

Sample code	Ga_2O_3 content (mol %)	(m^2/g)	Average pore diameter (nm)	Pore volume (cm^3/g)
MBG	0	415	5.75	0.55
1%Ga-MBG	1	509	6.34	0.78
2%Ga-MBG	2	396	5.74	0.54
3%Ga-MBG	3	340	6.65	0.52

As can be seen in Figure 1a, with increasing incubation time, the thrombus formation on the surface of 1%Ga-MBG increased greatly with respect to MBG. FESEM images shows that in comparison to MBG (Figure. 1b), more blood cells (RBCs) were aggregated on 1%Ga-MBG surface (Figure. 1c) and coalesced into an erythrocyte plug surrounded by a mesh of cross-linked fibrin strands.

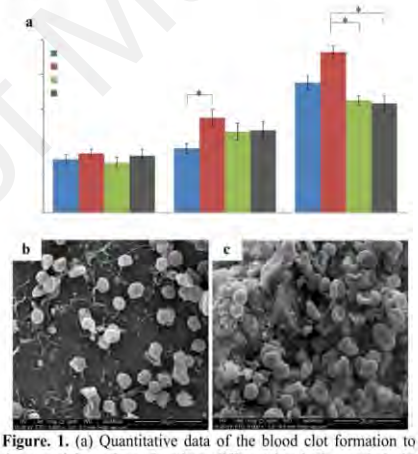

Figure. 1. (a) Quantitative data of the blood clot formation to the materials surface after three different incubation period. (b) FESEM micrographs of RBCs adhered to MBG, (b) and 1%Ga-MBG glasses (c) after 30 min exposure to the whole blood.

The thrombogenic activity of the 1%Ga-MBG could be explained as owing to the synergy of both its higher specific surface area and pore volume that provide more space for trapping blood plasma components combined with the presence of Ga^{3+} which may lead to polymerization of fibrinogen into strong fibrin clots and subsequent stimulation of blood coagulation cascade. The abundant presence of silanol groups on 1%Ga-MBG surface that bind with the phosphatidyl choline-rich RBC membrane, can be also involved in higher thrombogenic potential of 1% Ga-MBG [4].

Conclusion: This study suggests that the MBG with lowest amount of Ga_2O_3 could be considered as a promising candidate for hemostatic application as showed great thrombotic effect *in vitro*. However, there is a growing need to investigate the capability of the materials to produce a stable clot *in vivo*.

Reference:

[1] Pourshahrestani, S., et al., Materials Science and Engineering: C, 2015, doi:10.1016/j.msec.2015.09.008.